2014-09-08

Passive Stabilization of VTOL Aircraft Having Obliquely Tilting Propellers

Gress, Gary

UNIVERSITY OF CALGARY

Passive Stabilization of VTOL Aircraft Having Obliquely Tilting Propellers

by

Gary Robert Gress

A THESIS

SUBMITTED TO THE FACULTY OF GRADUATE STUDIES

IN PARTIAL FULFILMENT OF THE REQUIREMENTS FOR THE

DEGREE OF MASTER OF SCIENCE

DEPARTMENT OF MECHANICAL AND MANUFACTURING ENGINEERING

CALGARY, ALBERTA

SEPTEMBER, 2014

Abstract

This thesis investigates the ability of a hovering bicopter to be self-stabilized in pitch and roll without the use of electronic sensors in those directions. A mathematical model of aircraft dynamics is developed in which the non-cyclic proprotors are allowed to precess freely as gyroscopes since these are known to embody stabilizing elements. In the prior art of bicopter oblique active tilting (OAT), the proprotors generate gyroscopic control moments only when forcibly tilted, and stabilization in pitch and roll requires electronic attitude sensors and actuator servos. A self-stabilized system, however, would reduce cost, stresses and energy consumption, and could be scalable without limit. Through analysis of the characteristic equations it is found that aircraft angular positions cannot be so stabilized, but their velocities can be, maintaining the benefits listed above. This stability is similar to that due the flybar damping system of early Bell helicopters and still useful in small models today.

Acknowledgements

This research project would not have been possible without the kind and ample support of several key individuals.

I would like to thank Dr. Alejandro Ramirez-Serrano for his believing in my ideas and allowing me the opportunity to come to the University of Calgary and continue the research I had begun several years earlier in Ontario.

I cannot help but express also my utmost gratitude to Dr. Theodor Freiheit for his interest, sound advice, and always challenging questions. I am grateful too to my student colleagues Diego Ospina Latorre, Victor H. Guzman and Krispin Davies, for their patience, support and companionship.

I am indebted to my closest friends Robert Chachel and Paul Triska, whose camaraderie since the earliest days in Ontario sustained me during an otherwise lonely quest.

Finally, I would like to express my gratitude to my beloved family, especially my parents. Thank you for loving, and for believing.

Dedication

This thesis is dedicated to my daughter Lisa, and to the memories of Arthur M. Young and S. Domingo Dali.

Table of Contents

List of Tables

List of Figures and Illustrations

List of Symbols, Abbreviations and Nomenclature

Symbol	Definition
$\mathbf{A}$	State-space coefficient matrix
b	Half-span between propeller centers
e	Euler's number, ≅ 2.71828
E	Error, Laplacian of
c_Λ	cosΛ
$\mathbf{C}$	Vector sum of pod corrective moments
C, C_i,	Pod corrective moment, common and individual
$C(s)$	Controller transfer function
$H(s)$	Airframe transfer function
F_x	Axial force on spring-damper
$\mathbf{H}_A$	Angular momentum vector of aircraft
$\mathbf{H}_{Pi}$	Pod i angular momentum due to tilting
H_{Pix}, H_{Piy}, H_{Piz}	Orthogonal components of $\mathbf{H}_{Pi}$
$\mathbf{H}_{P\Omega i}$	Pod i angular momentum due to aircraft motion
$\mathbf{H}_{Ri}$	Angular momentum vector of rotor i
H_{Rix}, H_{Riy}, H_{Riz}	Orthogonal components of $\mathbf{H}_{Ri}$
h	Height of tilt axes above aircraft c of g
i	Rotor or pod number (= 1, 2) , or index number
i, **j**, **k**	Orthogonal unit vectors of inertial reference frame
I	Identity matrix
i_a	Armature current
I_{ax}, I_{ay}, I_{az}	Airframe mass moment of inertia (MMI) about x, y, z respectively (includes masses of pods only)
I_{Ax}, I_{Ay}, I_{Az}	Airframe MMI above plus pod local MMI (I_P)
I_ϕ, I_θ, I_ψ	Airframe MMI plus non-tilting component of I_P
$\mathrm{I_m}$	Imaginary component of root
I_R	Rotor MMI about its spin axis
I_P	Pod mass MMI about its mass center
k_d	Viscous damper damping coefficient
k_{dv}	k_d for vertical-plane rotor axes in steady-state
k^*_{dx}, k^*_{dy}	Non-dimensional k_d, (5.23g), (4.20)
k_q, k_{qd}	Derivative gain, yaw gyro, (5.16), (5.43)
k^*_{qz}, k^*_{qzd}	Non-dimensional k_q, k_{qd} (5.43')

k_{qp}	Proportional gain, yaw gyro, (5.43)
k^*_{qzp}	Non-dimesnional k_{qp}, (5.43')
k_s	Spring coefficient
k^*_{sx}, k^*_{sy}	Non-dimensional spring coefficient, (4.52)
K_m, K_v	Drive motor constants
l	Length of pod control arm and servo arm
L{ }	Laplacian, or Laplace transform of
L_a	Armature winding inductance, drive motor
$\mathbf{M}_a$	Airframe inertial moment vector
$\mathbf{M}_A$	Aircraft inertial moment vector
$\mathbf{M}_e$	Aircraft external disturbing moment
M_{ex}, M_{ey}, M_{ez}	Components of $\mathbf{M}_e$ about respective principal axes
M_{ep}	Pod/rotor external disturbing moment
$\mathbf{M}_{Pi}$	Pod i inertial moment due to tilting
$\mathbf{M}_{Ppi}$	Component of $\mathbf{M}_{Pi}$ perpendicular to $\hat{\mathbf{u}}_i$.
M_{Pui}	Projection of $\mathbf{M}_{Pi}$ along tilt axis ($\hat{\mathbf{u}}_i$)
$\mathbf{M}_{P\Omega i}$	Pod i inertial moment due to aircraft motion
$M_{P\Omega \mathrm{u} i}$	Projection of $\mathbf{M}_{P\Omega i}$ along tilt axis ($\hat{\mathbf{u}}_i$)
$\mathbf{M}_{Ri}$	Inertial moment vector of rotor i
$\mathbf{M}_{Rpi}$	Component of $\mathbf{M}_{Ri}$ perpendicular to $\hat{\mathbf{u}}_i$.
M_{Rsi}	Projection of $\mathbf{M}_{Ri}$ along spin axis ($\hat{\mathbf{s}}_i$)
M_{Rui}	Projection of $\mathbf{M}_{Ri}$ along tilt axis ($\hat{\mathbf{u}}_i$)
$\mathbf{M}_{Ti}$	Aircraft moment vector due to thrust of rotor i
$\mathbf{M}_{Qi}$	Aircraft moment due to drag-torque of rotor i
p_x, p_y	Non-dimensional pod inertia, (5.23a), (4.13a)
$P_\delta(s)$	Pod transfer function, pilot input
$P_\theta(s)$	Pod transfer function, aircraft pitch input
$\mathscr{P}$	$I_P c_\Lambda$
q_x, q_y	Non-dimensional thrust+/-torque, (5.23b), (4.13b)
Q_0	Nominal (hovering) rotor drag-torque
Q_i	Drag-torque of rotor i
$\mathscr{Q}$	Static moment sum, $hT_0 c_\Lambda + Q_0 s_\Lambda$ (2.8) or $hT_0 + Q_0$ (B.5)
r_x, r_y	Non-dimensional rotor inertia, (5.23c), (4.13c)
R	Reference angle, Laplacian of
R_a	Armature winding resistance, drive motor
$\mathrm{R_e}$	Real component of root
$\mathscr{R}$	$I_R \omega_0 s_\Lambda$
s	Laplace operator variable
s_Λ	$\sin\Lambda$
S	Scale factor

$\hat{\mathbf{s}}_i$	Spin axis unit vector of rotor i
t	Time
Δt	Time delay
T_0	Nominal (hovering) rotor thrust
T_i	Thrust of rotor i
$\hat{\mathbf{u}}_i$	Tilt axis unit vector for rotor i
V_a, V_{a0}, V_{ai}	Armature voltage; general, nominal, individual
ΔV_a	Armature voltage difference, from nominal
ϑ_0	Back-EMF effective torque coefficient
ϑ_{0x}^*	Non-dimensional ϑ_0 , (5.23f)
x, y, z	Aircraft principal axes
$\mathbf{x}$	State-space vector variable
$\mathbf{x}_0$	Initial values for $\mathbf{x}$
x_i	Elements of $\mathbf{x}$
Δx	Displacement of linear spring

Λ	Tilt path angle
δ	Pilot control input (servo arm angle)
$\Delta(s)$	Laplacian of δ
Δt	Time delay
Δx	Displacement of linear spring and damper
ΔV_a	Armature voltage difference from nominal
γ, γ_i	Rotor tilt angle, common and individual
$\Gamma(s)$	Laplacian of γ
$\Gamma_\delta(s)$	Pilot-input component of $\Gamma(s)$
$\Gamma_\theta(s)$	Pitch feedback component of $\Gamma(s)$
λ , λ_i	Eigenvalue, i-th eigenvalue
φ	Non-dimensional drag-torque, nominal. (5.23e)
μ	Non-dimensional rotor speed differential (5.1)
ϕ	Aircraft roll angle
ψ	Aircraft yaw angle
θ	Aircraft pitch angle
$\Theta(s)$	Laplacian of θ
ζ	Inertial ratio, I_ψ / I_ϕ
ξ	Aircraft inverse inertia, non-dimensional
ρ	Non-dimensional nominal thrust moment, (5.23d)
σ	Non-dimensional Laplace operator ($= s/\omega_0$)
τ	Non-dimensional time ($= \omega_0 t$)
τ_i	Total torque of rotor i
τ_m	Armature electromagnetic torque, drive motor
ω_0	Nominal (hovering) rotor speed, radians/unit

	time
ω_i	Rotational speed of rotor i, radians/unit time
$\boldsymbol{\Omega}$	Airframe angular velocity vector
$\Omega_x, \Omega_y, \Omega_z$	Orthogonal components of $\boldsymbol{\Omega}$
∞	Infinity. Subscript signifying steady-state

c of g	Center of gravity
EMF	Electro-motive force
IGE	In ground effect
MMI	Mass moment of inertia
OAT	Oblique active tilting
OGE	Out of ground effect
SAS	Stability augmentation system
SCAS	Stability and control augmentation system
VTOL	Vertical take-off and landing
V/STOL	Vertical/short take-off and landing

Epigraph

"If I were to build a flying machine I would plan to sustain it by means of a number of rapidly revolving inclined planes… Such a machine would rise from the ground as a bird rises. Then I would drive the machine ahead with a propeller."

Thomas A. Edison, 1909

Inventor

"Edison invents, while I discover what is already there to be uncovered."

Nikola Tesla, 1891

Engineer, Inventor

Chapter One: Introduction

1.1 Introduction

This work concerns the improvement of aircraft called convertiplanes which can take off vertically, hover, and then fly horizontally at high speed. In particular, it is part of an ongoing effort directed towards uncovering and developing a convertiplane type which inherently belongs to both flight realms, consisting as such of congruous dual-use components of minimal number.

In this thesis a bicopter hover control system normally associated with electronic stability augmentation is investigated for its natural stabilization capability. Using linearized mathematical models, pitch stability is proven analytically and roll-yaw stability is established for a range of parameter values. It is found that such a system will automatically incorporate dynamic control elements (gyroscopic and momentum wheel) in hover – thereby increasing control effectiveness in that mode – and static airplane-like elements about the same axes in fast forward flight using the same control components. This behaviour can be emulated using electronics so is not restricted to just naturally stabilized systems. It is also found that this dual phase control – termed here biphasic control – voids the need for control swapping during transition; roll control in hover is obtained by the same device and its operation as roll control in fast forward flight. The same is true of yaw. So, though natural or self-stabilization may or may not be useful on its own, its investigation has produced a control prescription for effective operation in the two flight realms.

1.2 Background

1.2.1 Gyroscopic Bicopters: Oblique Active Tilting (OAT)

In 1999 the author began experimenting with electric-powered, radio-controlled vertical take-off and landing (VTOL) aircraft models, which – as a challenge – were restricted to a configuration of two rigid, laterally displaced and tiltable proprotors (non-cyclic rotors and propellers will be referred to as proprotors in this thesis). The attraction of these aircraft, called bicopters, is their conduciveness to transitioning to and flying in airplane mode.

It was obvious that stability of a bicopter was achievable using cyclic helicopter rotors (the bicopter essentially becoming two helicopters attached together), but the goal was to first explore it without this complication and understand why such aircraft were not operational. Control of these models in hover was initially planned as follows:

1. pitch via collective longitudinal tilting of the proprotors
2. yaw via differential longitudinal tilting
3. altitude via collective speed control of the prop motors
4. roll via differential speed control

However, the models were unstable in pitch, even with the assistance of proportional and derivative feedback sensors of the model's attitude (Gress, 2002, 2007). There was no apparent damping, and airframe pitching in an opposite direction to proprotor longitudinal tilting dominated the behaviour.

But in 2001 pitch stability was finally achieved by having the proprotors tilt obliquely, that is, in (symmetric) directions part-way between longitudinal and lateral. In conjunction with a proportional pitch sensor, the lateral tilting component introduced a

gyroscopic pitching moment which damped the aircraft's oscillations. And intentional oblique tilting by the pilot increased the control power immensely; it generated gyroscopically-amplified pitching moments, adding to the conventional thrust vectored ones.

By eliminating cyclic this new stabilization system – termed oblique active tilting (OAT) – greatly simplified the rotor heads. It also allowed the proprotor diameters to be reduced and their speeds increased relative to helicopter rotors, thereby eliminating the reduction gearboxes as well. In terms of the number of parts, the models were now much closer to airplanes than helicopters.

1.2.2 Pitch Stabilization in OAT

The OAT system uses two gyroscopes types to stabilize aircraft pitch. The first is the electronic pitch sensor, generally referred to as a "gyro" in the hobby industry – as it will be here – but in reality is an oscillating piezo crystal which generates measurable coriolis forces when rotated. Included with it will be a feedback control algorithm, usually derivative or proportional – or a combination of both – by which it sends corrective instructions to the tilt servos based on the aircraft pitch rate that it measures (and angle that it calculates).

The second is the mechanical actuator gyroscope – or control effector – which consists collectively of the two proprotor tilt servos which receive the instructions sent by the piezo gyro, and the prop-motors and proprotors that they tilt. However, this arrangement is somewhat redundant and perhaps unnecessary, as will be discussed in the next section.

1.3 Self-Stabilization of Bicopters

1.3.1 The Potential for Self-stabilization

It is well known that a mechanical gyroscope can act as a sensor as well as an actuator. Forcibly tilt a gyroscope about an axis (perpendicular to its spin axis) and it will generate a moment about a third axis perpendicular to the first two. This is the actuator feature of a gyroscope, utilized by several stabilization devices, including OAT.

But apply a moment to a gyroscope about an axis perpendicular to its spin axis and it will precess or tilt – if it is free to do so – about a third axis which is perpendicular to the first two. This is the sensor feature of a gyroscope, the precession in turn generating a new moment which opposes the originally applied one. It is only approximated in OAT since the proprotor is never free to tilt on its own.

It was with this understanding that the author questioned the need for the electronic piezo gyro, and whether the spinning proprotors couldn't be used as both actuators and sensors. Perhaps the proprotors could tilt by themselves and stabilize the aircraft. In 2009 an OAT model was modified by disconnecting the (roll and pitch) piezo gyros and replacing the rigid servo linkages with flexible ones, allowing the proprotors to tilt on their own. Holding the model in hand – with proprotors spinning – a resistance to rolling and pitching was observed which increased with proprotor speed. Though the model could not be flown as such (it was difficult to stabilize yaw because of the freely-tilting proprotors), roll and pitch stabilization were clearly discernable – and the ramifications very encouraging. If this behaviour could be harnessed in practice then the proprotors would no longer have to be actively tilted for stabilization, and the only tilting

would be for intentional, directional control. Such a change could make the control method more suitable for full-size aircraft, and perhaps be even beneficial for hobby models; it could eliminate the electronic attitude sensors, and reduce stresses, energy consumption and associated costs. It was with these possibilities in mind that the author decided to investigate self-stabilization analytically, and to determine the conditions under which it may be utilized and implemented.

1.3.2 Merits of Self-stabilization

More fully, a self-stabilized system could be:

1. be free of time delays, making for potentially better flight characteristics.
2. be free of the large stresses associated with forced, active tilting of rigid proprotors. In self-stabilization, by definition, the proprotors tilt by themselves.
3. be lower in energy consumption.
4. be self-adapting to varying flying conditions such as aircraft weight and air density.
5. be lower in cost. The electronic controller constitutes about half the cost of a hobby bicopter such as the Nymbus, with the ratio increasing as the model becomes smaller.
6. be automatically scalable. There are limits to scale reduction with electronics because of the higher frequencies involved.

As will be seen in later chapters there are further merits; the self-stabilized system is self-decoupling in roll and yaw and is stable in fast forward flight.

1.3.3 Parallels to Helicopter with Flybar

It is worth noting that a conventional R/C helicopter with a Bell-Hiller rotor head (Figure 1-1) – usually identified by the presence of a flybar - does not require electronic attitude sensors and programmed control algorithms for stabilization in pitch and roll.

Figure 1-1. Bell-Hiller helicopter rotor head showing flybar. (Hirobo)

The flybar does not stabilize pitch and roll of the helicopter, however. It provides damping of their motions, slowing them down such that they become manageable by the human pilot (Daughady, 1955, Kim, 2004). The Bell-Hiller system, therefore, is an angular velocity stabilization mechanism (Cunha, 2003, Barczyk 2013), and the human pilot is an essential element in the stabilization of the pitch and roll *angles*.

Other VTOL UAVs types – such as quadcopters or multicopters with unarticulated, non-tilting proprotors – do require active electronic stabilization, even for just roll and pitch angular velocities. So, if there was any stabilization system that could be considered passive or "natural", it would be the helicopter's Bell-Hiller mechanism.

Its existence was partly the inspiration and benchmark for this thesis. It was one goal of the author to determine if a bicopter – a vehicle more conducive than a helicopter to hovering in confined areas and to fast forward flight – could possess at least the equivalent natural stability of a helicopter.

1.3.4 Initial Embodiment and Self-stabilization in Pitch

The self-stabilized bicopter concept's basic elements are depicted in Figure 1-2 and consist of a hypothetical hovering aircraft equipped with rotors which can tilt freely about oblique axes.

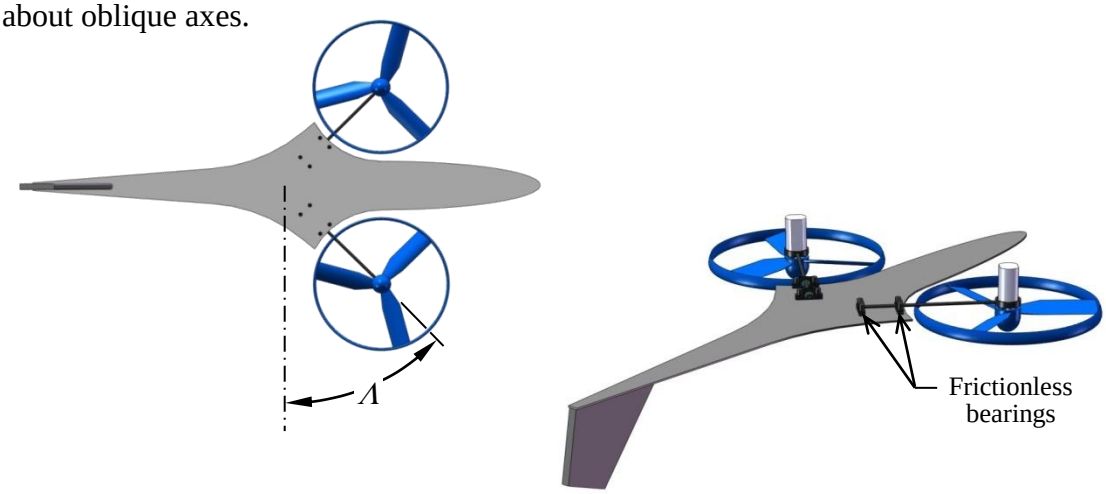

Figure 1-2. Free-tilt aircraft top and underside views.

External pitch disturbances applied to a hovering bicopter will cause its spinning proprotors to precess laterally if they are allowed to do so. In turn, a gyroscopic moment is created that opposes the original pitching. If the proprotors are restricted to tilt in oblique directions instead – as they are in Figure 1-2 – they will still precess, but now in those oblique directions.

Applying a nose-up pitching moment to the aircraft as shown in Figure 1-3 will cause the proprotors to tilt both inward and forward – for the spin directions shown. This not only creates gyroscopic moments which resist the pitch disturbance, but complementary thrust and drag-torque moments that do as well.

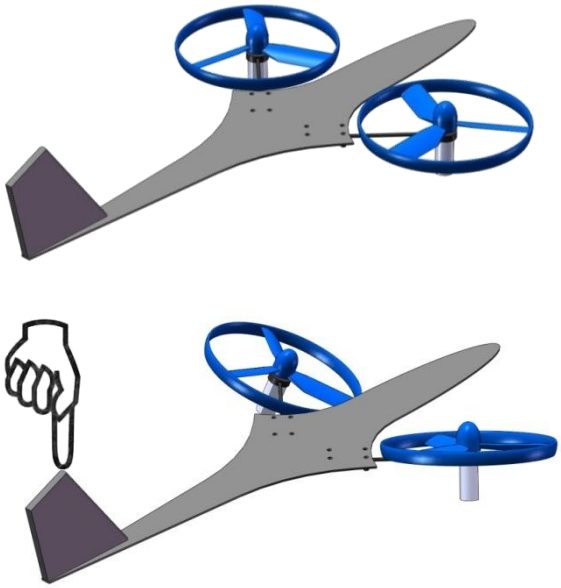

Figure 1-3. *Top*: Free-tilt aircraft hovering undisturbed with rotors level. *Bottom*: Rotors precessing inward and consequently forward due to externally applied moment.

The gyroscopic resisting moments are generated only during the tilting, whereas the thrust and drag-torque moments are functions of the tilt angles. These latter moments are here termed the *static* moments. For this discussion it is assumed that the aircraft's center of mass is located below the tilt axes such that the thrust moment is in the proper, corrective direction.

For as long as the disturbance is applied, the rotors will continue to precess until the static moments counteract it. At that point a new equilibrium, with the aircraft pitched, will be reached.

The challenges are to determine if this characteristic can be harnessed to enable self-stabilization of the aircraft, and whether the pilot can still effect intentional control without interfering with this stabilization.

1.3.5 Self-stabilization in Roll

Here the sequence of events following a roll disturbance is analyzed, and from it roll stability is surmised qualitatively.

If the aircraft with freely tilting proprotors is suddenly subjected to an external rolling moment $M_{ex}$the proprotors will respond by tilting (precessing) in the directions shown in Figure 1-4. This tilting of course generates gyroscopic moments on the aircraft which tend to resist or oppose the rolling moment.

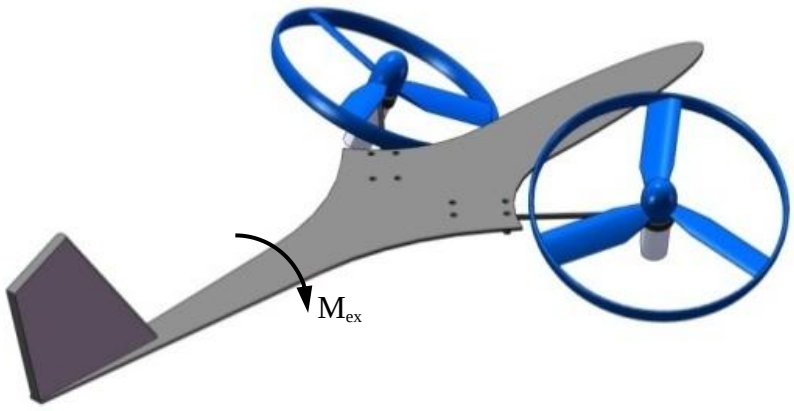

Figure 1-4. Applied external rolling moment M_{ex} and resulting proprotor tilting.

If the aircraft had a conventionally low center of mass, then, in terms of thrust vectoring, these tilt directions would be wrong – they would exacerbate the rolling of the vehicle. With the center of mass raised as shown in Figure 1-5, however, the thrust vector moments would tend to oppose the original roll disturbance.

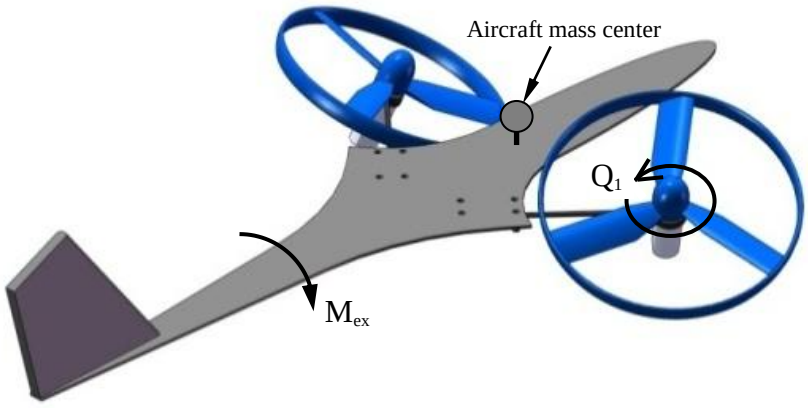

Figure 1-5. Static roll stability requires a raised center of mass, the amount of which is reduced by the presence of proprotor drag-torques Q_i (Q_1 shown).

In actuality, the requirement for a high mass center is not quite so extreme as it is tempered by the presence of the proprotor drag torques Q_i. Their components about the aircraft longitudinal axis both oppose the disturbing moment M_{ex} – the opposition by Q_1 is readily visualized from Figure 1-5. Therefore the aircraft mass center does not need to be raised above the proprotor tilt axes to enable static stability, and therefore the aircraft can still be statically stable in pitch per the previous section.

As a result of the differential tilting initiated by the roll disturbance, the proprotor thrust vectors will also begin to yaw the aircraft in the positive direction as shown in Figure 1-6

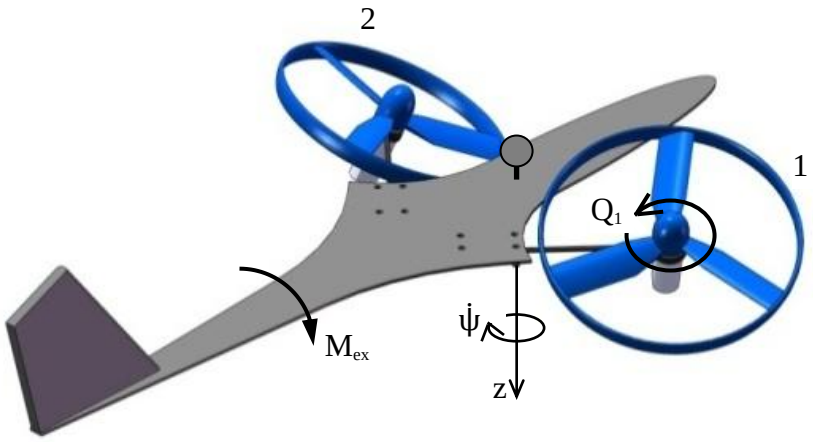

Figure 1-6. Differential tilting initiated by roll disturbance begins to yaw the aircraft.

It is assumed here that the bicopter contains an onboard yaw gyro, just as radio-controlled conventional and coaxial helicopters do. It is also assumed that the gyro operates the proprotor speed controls differentially. Justification for inclusion of the gyro while maintaining that the aircraft is self-stabilized will be made Chapter 6.

The gyro, sensing this yawing of the aircraft, will signal drive-motor 1 to speed up and 2 to slow down, thereby increasing Q_1 and lowering Q_2 . As intended, the resulting net torque opposes the yawing motion. But a consequence of the ensuing speed difference is that proprotor thrust T_1 increases and T_2 decreases, which of course opposes the original roll disturbance. Therefore, one can surmise that, with the aid of the electronic yaw gyro, roll can be stabilized.

In summary, the events following a roll disturbance are:

1. Differential precession of proprotors and generation of gyroscopic moments opposing roll disturbance. (This is the dynamic response).

2. From the above tilting, the generation of thrust vector moments and drag-torque components that oppose roll disturbance. The former require a raised aircraft mass center. (these are static stability response).
3. Yawing of the aircraft due to differential tilts.
4. Yaw gyro signaling differential motor speeds, thereby generating a net torque repressing the yaw.
5. Consequent generation of thrust differential, which also opposes roll disturbance.

1.3.6 Sequence of Events Following a Yaw Disturbance

The events following a positive yaw disturbance would be:

1. Yaw gyro signalling differential motor speeds, thereby generating a net torque opposing the yaw disturbance.
2. Consequent generation of a thrust differential, which creates a (negative) rolling moment.
3. Differential precession of proprotors (in opposite direction to that shown in previous section), caused by and opposing the rolling moment in 2.
4. From tilting in 3, generation of thrust-vector moments and drag-torque components opposing rolling moment in 2.
5. Also from tilting in 3, creation of yawing moment opposing the original yaw disturbance.

1.4 Objectives

The objectives of the research presented in this thesis document are to: investigate self-stabilization of bicopters analytically and prove it mathematically wherever possible; substantiate these proofs with simulations, and to; determine the conditions under which self-stabilization may be utilized and implemented. Of equal importance is determining how control of the aircraft by the pilot can be implemented without interfering with – or being interfered by – the self-stabilization system.

1.5 Organization

This dissertation is organized as follows: Chapter 2 contains a literature review of VTOL aircraft control and stabilization, especially in regards to their simplicity and effectiveness in the context of convertiplanes (which can transition to fast forward flight). It discusses gyroscopics as a means of providing such control and stabilization, and contains a background of the author's relevant work with OAT. Chapter 2 also contains a description of one other known implementation in history of passive stabilization using gyroscopics: the Fieux passive ship stabilizer of the 1930s.

Chapter 3 develops the mathematical model of a bicopter's angular motion in three-dimensional (3D) space. It provides for the free tilting - or any other tilting prescription - of the proprotors relative to the airframe. This model is then linearized so that equations of angular motion in one dimension may be extracted – and characteristic equations developed - in subsequent chapters.

Chapter 4 analyzes hover pitch stability of the bicopter through inspection of the characteristic equation. Passive dampers and springs are subsequently added between

airframe and proprotor tilting, and a Simulink model is constructed to corroborate the mathematical results A root locus plot (vs. spring constant) of the aircraft response is drawn and compared to handling quality boundaries specified for US military VTOL aircraft. A flow chart of this work is shown in Figure 1-7.

Chapter 5, after having established that the roll and yaw motions are interdependent and cannot be separated, analyzes their stability by inspection of the characteristic equation. A Simulink model is run to corroborate the results. These tasks are depicted in the flow chart of Figure 1-8.

In Chapter 6 sample runs from a SimMechanics three-dimensional, non-linear model reveal the limitations of linear analysis.

Chapter 7 contains the Conclusions.

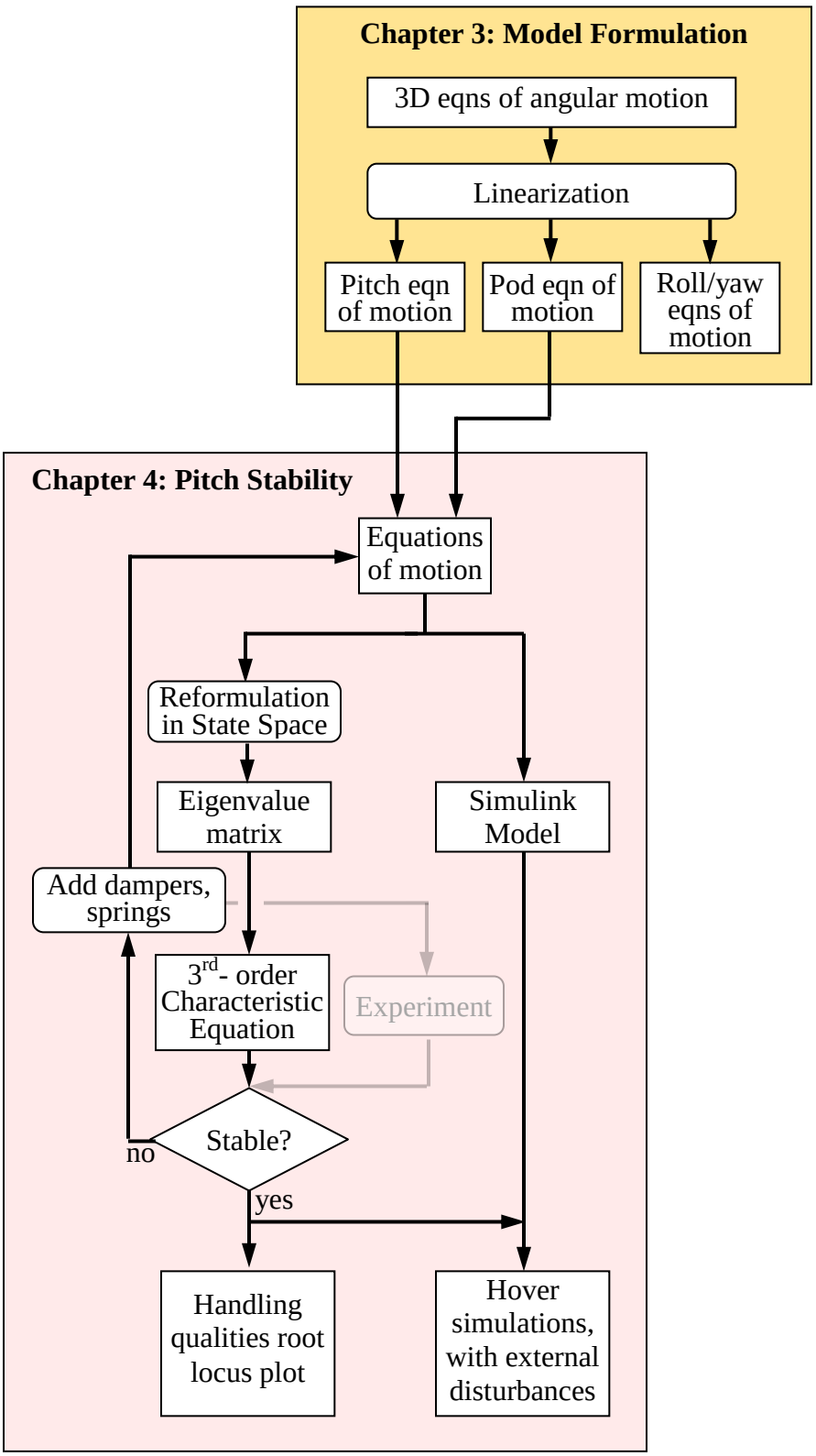

Figure 1-7. Flow chart of Chapters 3 and 4

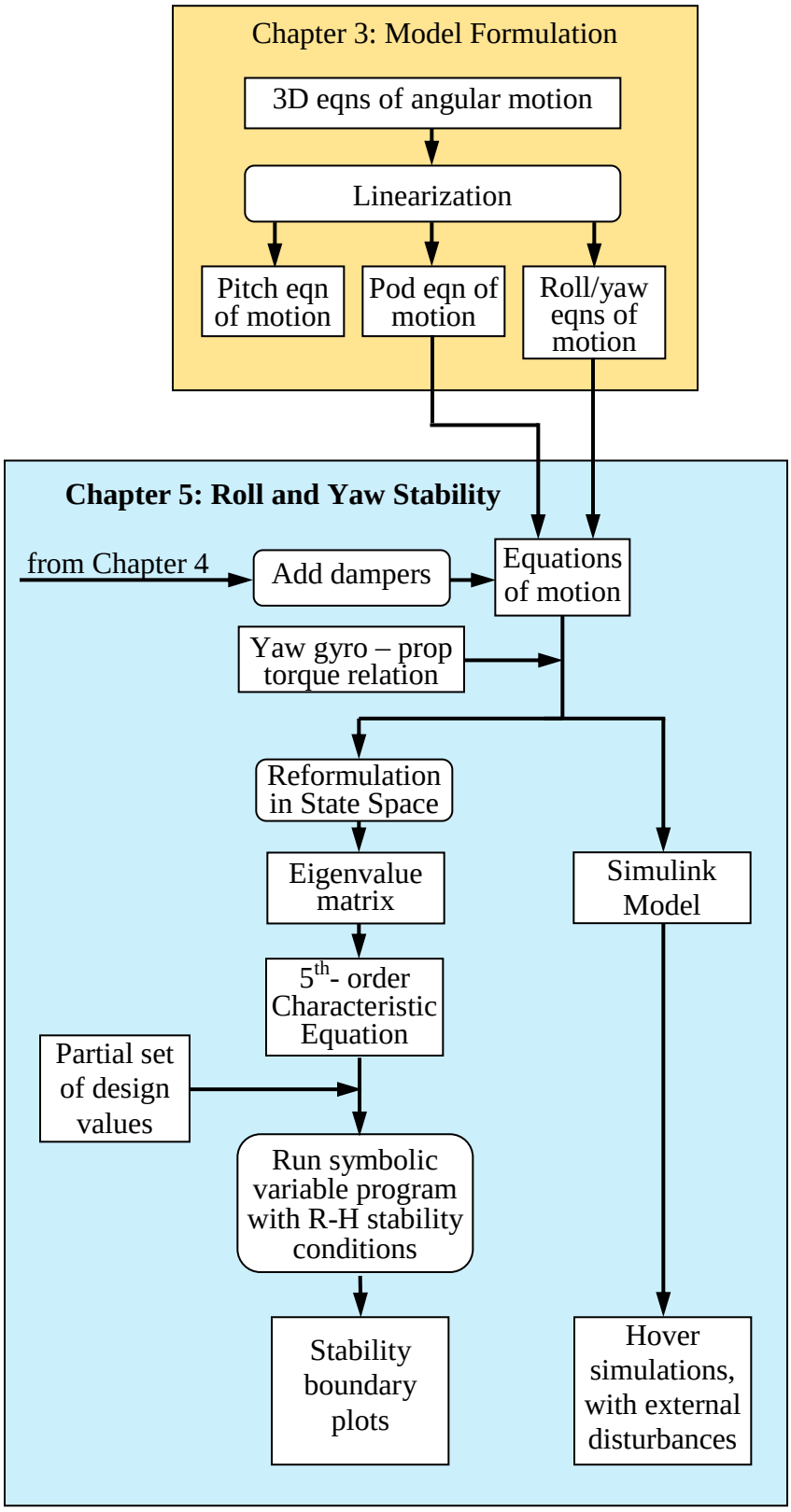

Figure 1-8. Flow chart of Chapters 3 and 5

Chapter Two: Literature Review

2.1 Introduction

This chapter reviews the history and state of the art of convertiplanes, those aircraft which can take off and land vertically, hover and then fly horizontally at high speed. It discusses the inherent difficulties such aircraft are faced with, and identifies the shortcomings of conventional solutions. Subsequent sections list the features of a more ideal convertiplane and describe in more detail the OAT bicopter and its gyroscopics which were developed to furnish some of these features. Other instances of active stabilization of vehicles using gyroscopics are also reviewed. The chapter ends with a description of passive and active ship stabilizers, the former being the only other known implementation of transport self-stabilization using gyroscopes.

2.2 The Quest for Aircraft that Hover and can fly at High Speed

In the field of aviation a largely still-unanswered pursuit is the development of a convertiplane whose design for operation in the two regimes entails no substantial compromises in either regime (DARPA, 2013). Some examples of such aircraft that do have substantial compromises are:

- Winged quadcopters whose four lift-propellers do not tilt forward for flying in airplane mode. Propulsion in airplane mode is by a fifth propeller, which of course is not necessary for hovering. Examples of this aircraft type are the Hybrid Quadrotor by Latitude Engineering (www.latitudeengineering.net, 2014) and the Quadcruiser by Airbus Group (www.airbus-group.com, 2014)

- Tailsitter aircraft which rotate 90 degrees to transition from hover to airplane mode. The two major compromises here are the perpendicular exposure of the wing surface to gusts in hover, and the arduous transition sequence – especially the airplane to hover one
- Tilt rotor aircraft having cyclic rotors. In hover the downwash of the large rotors is partially masked by the wing. In airplane mode the cyclic controls are locked and the aircraft is controlled by deflection of conventional surfaces.

The advent of the helicopter, with its disappointingly low speeds and short ranges, was soon followed by the optimistic and prolific development of various alternate VTOL aircraft in the 1950s and 1960s, most for the purpose of flying faster than a helicopter (Campbell, 1963, McCormick, 1967).

2.2.1 A Matter of Stability and Control (in Hover)

However, all of the projects suffered problems (Anderson, 1981) and, after reviewing historical surveys of VTOL development (Hirschberg, 1997, 2002) , it appears that all but a few of the original 60 VTOL aircraft types ultimately failed due to the incongruous hover stability and control devices they used - mostly for aircraft pitch. Most such devices were either

- ineffective or lacking in control power
- too complex and failure-prone, or
- liabilities in forward flight.

Examples were: moveable vanes in the main rotors' intake or downwash; the powering and control of four lifting propellers (or ducted fans) instead of two, and; a vertical-axis exhaust nozzle or propeller at the tail of the aircraft.

The one rotorcraft convertiplane project which succeeded and led to eventual and present production was the Bell XV-3 tilt rotor (1955), distant precursor to the experimental XV-15 of 1977, and the Bell-Boeing V-22 Osprey (Figure 2-1) placed into service in 2007 (Whittle, 2010). Effective attitude control in hover is via helicopter-style cyclic and collective blade pitch. Control in airplane mode is by conventional control surfaces.

Figure 2-1. Production V-22 Osprey Tiltrotor.

A large part of the development difficulty of the V-22 then lay in making these rotors congruent with the full task at hand, i.e., more efficient and structurally suitable for operation in airplane mode (Martin, 2000).

2.3 Faster, Simpler and More Efficient

With the promise and successes of the tilt rotor – and the realization of just how difficult the field of VTOL was – there was almost no official development of alternate

types after the project abandonments in the 1960s. From then until recently, any new concept proposals were met with skepticism by the established players. However, there was a belief by some (Leishman, 2007) that the tilt rotor – with its dual, cyclic, and large-diameter rotors – was still an overly complex, costly and restrictive solution.

This heritage is reflected in the aircraft's performance. The Osprey's maximum forward speed of 262 knots (NAVAIR, 2011) at sea level is considerably greater than a helicopter's – due to the flow through the rotor no longer being edge-wise – but it is still not exceptional considering the installed power (Leishman, 2007). It is not surprising, then, that official dissention has emerged as well. A recent (2013) US government solicitation (see DARPA BAA-13-19) states:

"The current inventory of vertical flight machines … is inadequate for flight at high speeds to cover long ranges and hovering under extreme conditions…. "

The agency also recognized that improved performance can no longer be obtained by resorting to convolution, for in the same solicitation it specifies:

"It is highly desirable that simplicity and elegance be incorporated into the design space at a fundamental level, and that the technological solutions produced result in increased net effectiveness (efficiency), preferably with reduced system complexity.."

It would seem, then, that the future development path must combine higher performance with greater simplicity. The latter quite assuredly implies that most or all of the elements of the aircraft provide some benefit in both flight modes.

2.3.1 Reducing Proprotor Diameter

Reducing the proprotor's diameter (and increasing its rotational speed) allows it to be encased in a protective shroud, which may increase the thrust of the proprotor and also develop a thrust itself (McCormick, 1967, pg. 232). Together with the elimination of the tiltrotors's wing-masking effect and also some or all of its reduction gearing, these will help recover the efficiency lost in hover due to the reduced diameter. Proprotor shrouds or ducts can also produce substantial aerodynamic lift in forward flight (Hirschberg, 1997).

In the past, cyclic-pitch rotors could not be substantially reduced in diameter because cyclic was not compatible with the consequent higher rotational speeds (Daley, 2001). However, this limitation may be fading, for Augusta Westland's experimental convertiplane "Project Zero", a sketch of which is shown in Figure 2-2, has a wingspan of approximately 43 ft., cyclic pitch proprotors of 10 ft. diameter, and has successfully hovered (Hirschberg, 2013). Rather than swashplates, it uses electromechanical actuators to cyclically vary the blades' pitch angles (Wang, 2013), a method similar to those of some proposed marine propulsion systems (Wham, 1987).

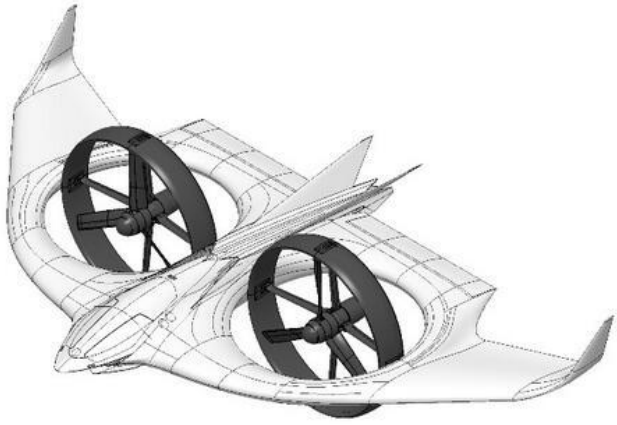

Figure 2-2: Sketch of Augusta-Westland 'Project Zero' aircraft (2013)

For all of its inherent complexity, cyclic has probably been the most effective method of hover control, and to do without it (in rotorcraft) has in the past invited even more complexity. Without cyclic the V-22 Osprey and the Project Zero aircraft would have needed more proprotors, such as the failed 4-propeller 1963 Curtiss-Wright X-19A tilt prop (Figure 2-3) did, with its extensive cross-shafting, gearboxes and drag-inducing downwash at the rear wing in forward flight (Borst, 1990). This aircraft would have hovered well except for very poor mechanical control implementation (Anderson, 1981).

Figure 2-3: Curtiss-Wright X-19A tilt prop (1963)

But it is noteworthy that one exception to the project abandonment rule of the 1960s was the non-cyclic Bell X-22A tilt duct (Figure 2-4), which had four ducted, collective-pitch proprotors and hovered better than most helicopters (Marquardi, 1970).

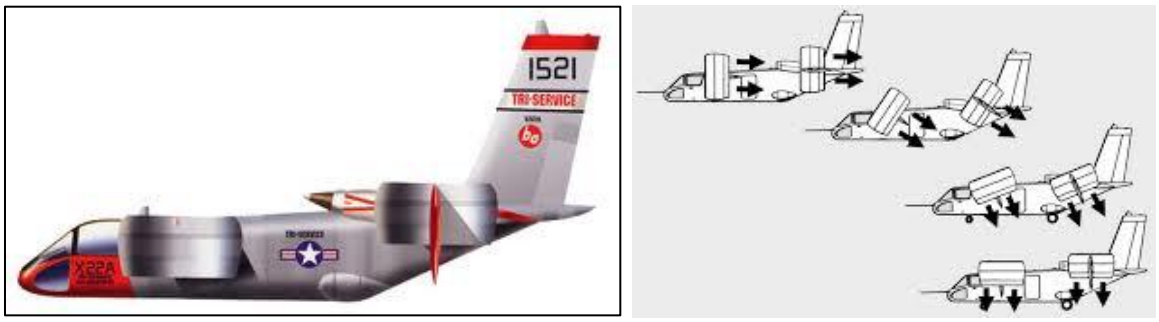

Figure 2-4: Side view and operation of the X-22A

The X-22A garnered extensive data, remaining operational until 1984, and had excellent hover stability out of ground effect (Marquardi, 1970). Anderson (1981), however, had stated that wind effects were considerable because of the side forces on the ducts. Campbell (1963) also noted another adverse characteristic, the upwash between the front and rear ducts near the sides of the fuselage. It could cause large amounts of debris to be thrown above the fuselage and re-ingested by the proprotors.

2.3.2 Eliminating Cyclic and the Reliance on Thrust Manipulation, and Introducing Gyroscopics

The tilt rotor's complexity and cost have relegated it to exclusive markets such as the military and commuter airlines, leaving a large VTOL void in general aviation.

Consequently, over the past couple of decades or so, some individuals and small companies have begun exploring alternate VTOL concepts. Most, like the Moller SkyCar 400 (moller.com, 2014) and the Urban Aeronautics AirMule (www.urbanaero.com), are variants of the abandoned projects of the 1950s and 1960s, and involve manipulation of the proprotors' thrusts vectors for attitude (and altitude) control in hover. However, the limitations of those early concepts of course still apply. They are best epitomized by Anderson's (1981) observation:

"…V/STOL aircraft impose several unique control system requirements beyond those associated with conventional aircraft. The lack of any significant dynamic pressures [normally] associated with forward flight precludes any inherent stability"

But after many unfruitful experiments attempting to stabilize radio-controlled models using similar methods, the author finally achieved success in 2001 using an additional, enabling control element: the gyroscopic moment resulting from forced precession of a rigid lift-propeller (Gress, 2002). Aircraft pitch, for instance, was now partly controlled by the lateral component of the precession or tilting. This is the OAT method referred to in the Introduction, which allowed stable hovers with just two airplane propellers (or fans), and whose gyroscopic control moments were independent of distances to the aircraft center of gravity. It also allowed the use of propeller shrouds or ringed propellers – thereby potentially reducing the X-22A's (and the Moller Skycar's) problematic four-duct configuration to just two. Before describing this system in more detail, it is now possible to conjecture a more ideal convertiplane, which is done in the next section.

2.3.3 A More Ideal Convertiplane

Based on most of the observations garnered in previous sections of this chapter – along with a few others which are elicited here – the author surmised that a faster, simpler and more efficient convertiplane, shown in Figure 2-5, is one that:

- has only two proprotors
- does not mask the efflux of its proprotors (as the wing does in the V-22)
- is as stable in hover as a helicopter – or better.
- does not require substantial moment arm lengths to effect control in hover
- is controlled by the same device(s) in the two flight modes

Figure 2-5: A more ideal convertiplane

2.4 Oblique Active Tilting (OAT)

2.4.1 Gyroscopics in OAT, Orbital Satellite Attitude Control and Ground Vehicle/Ship Stabilization

In work prior to this thesis the author extensively investigated OAT, including performing a theoretical analysis of pitch stability and experimentation using radio-controlled (R/C) models (Gress, 2002, 2003, 2007, 2008). Figure 2-6 shows the Nymbus 650 (referred to here as simply the Nymbus), designed in 2011 and which is the latest incarnation of aircraft employing OAT. Its data and specifications, contained in Appendix B, will be used extensively in this thesis.

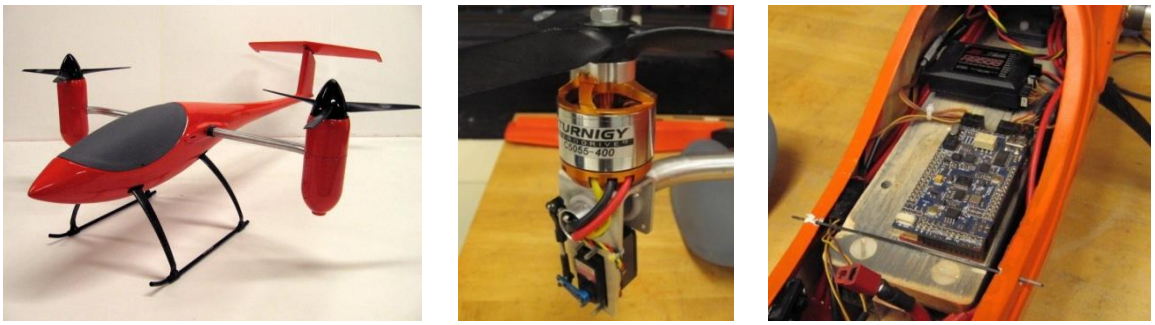

(a) **(b)** **(c)**

Figure 2-6 (a) Nymbus OAT radio-controlled VTOL model aircraft by the author. (b) Propeller pod closeup showing how oblique tilting arises from bent spar-end. (c) Canopy removed, showing Arduino electronic attitude sensor/controller.

The primary function of the lateral component of oblique tilting is to generate gyroscopic pitch-control moments which dynamically assist conventional thrust vectoring arising from the longitudinal component. This generation has parallels in the use of control moment gyroscopes (CMGs) for the attitude control of orbital satellites, the Hubble Space Telescope and the International Space Station (ISS) as shown in Figure 2-7.

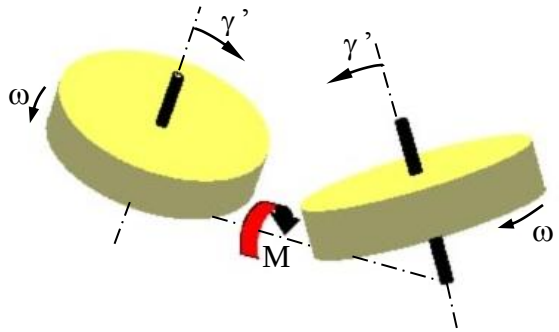

Figure 2-7. Oppositely spinning control moment gyroscopes of orbital satellite. Each is tilted towards the other at rate γ', together generating net moment M on vehicle (from Gress, 2007).

(Jacot, 1966) is a good early description of the use of CMGs for attitude control in space. (Gurrisi, 2010) discusses the practical operation of CMGs aboard the ISS. Since the first appearance of CMGs and up to the present time, there has been considerable research on the design of their feedback control laws; some of these are surveyed in (Kurokawa, 2007). Considerable work has also been done regarding the avoidance of singularities and saturation in CMGs (e.g., Yoon, 2004).

CMGs in orbital satellites are a prominent and successful example of the use of gyroscopics for attitude control and stabilization of vehicles. But there have been many other proposed and implemented applications, especially in the roll stabilization of mono-rail trains (Brennan, 1905, Shivoliskii, 1924), two-wheeled ground vehicles (Karnopp,

2002, Spry, 2008), and of ships (Ferry, 1933, Adams, 2005). In all of the ground vehicles, attitude sensing (of the vehicle) has been by means other than the gyroscopes themselves, and stabilization is effected by the forced precession of the gyroscopes. A passive stabilization system for these vehicle types is usually not possible because a perturbed roll angle from the vertical implies a lower energy state. Only in the case of ships has there been use of gyroscopes in a passive way, where the gyroscope becomes both attitude sensor and control effector, these actions usually being moderated by springs and dampers. This is because the vessel is continually receiving energy in the form of waves. Passive ship stabilization will be discussed in more detail in Section 2.4.3 since it applies directly to the subject of this thesis.

2.4.2 Gyroscopics for Control and Stabilization of Aircraft: Internal CMGs vs. External Propellers

Research into using internal CMGs to augment the control of aircraft has also been conducted. Of them Lim (2007) stated their useful torque is very transient, and that there is no net change in vehicle angular momentum. Any bias will result in the CMGs storing angular momentum, reducing gimbal mobility. To restore high-frequency control the CMGs must be desaturated by applying an external torque, usually through a lower frequency aerodynamic control effector.

In OAT the propellers are both the CMGs and the aerodynamic control effectors, constantly interacting with the environment and imparting an external torque. The lateral tilt component creates a drag-torque pitching moment, complementing the conventional thrust vectoring from the longitudinal component. Figure 2-8 shows how the propellers'

spin directions and tilt paths must be oriented. Gyroscopic rolling moments will cancel one another when they are tilted equally and collectively in the forward or rearward oblique directions. The same is true of the gyroscopic pitching moments when the propellers are tilted equally but differentially.

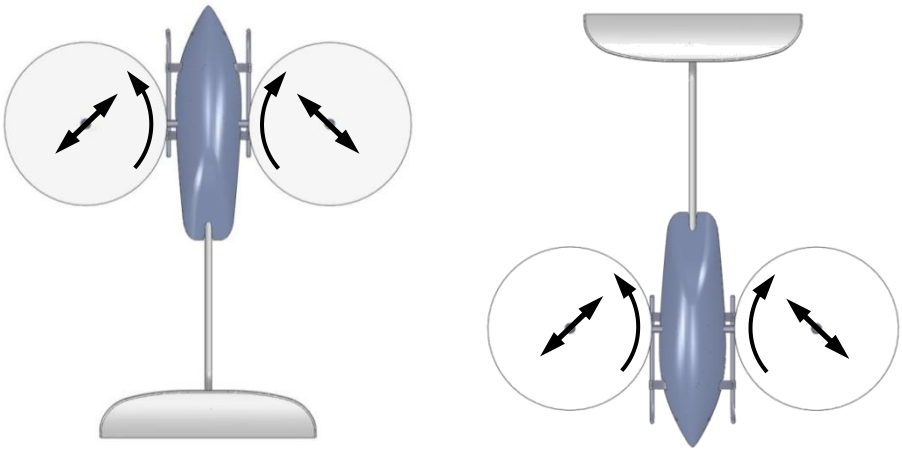

Figure 2-8. Top views of OAT aircraft showing the two possible spin directions relative to aircraft, and the associated proper tilt directions for generating the reinforcing gyroscopic and drag-torque control moments.

The oblique direction of the tilting – usually 45 degrees from either longitudinal or lateral – is of course a compromise. For control of aircraft pitch, effective thrust vectoring favours purely longitudinal tilting, whereas the gyroscopic and drag-torque pitching moments are zero for this direction but maximum for purely lateral tilting.

2.4.3 Active Tilting Baseline for Comparison

Building upon the concepts developed in OAT by the author (and referenced previously), other researchers have investigated propeller gyroscopics for augmenting VTOL aircraft control (Kendoul, 2005, Thorne, 2012, Al-Rihani, 2012, Gasco, 2013). In all of these and the author's prior work, aircraft stability was achieved by the forced precession of the propellers using servos commanded by electronic aircraft attitude

sensors. This is the active method of stabilization. Though this thesis investigates passive stabilization in hovering aircraft, the following sections examine the active method - specifically OAT - in more detail and represent it mathematically. This will be the baseline with which the passive or self-stabilized system will be compared.

2.4.4 OAT aircraft pitch model

Figure 2-9 shows the OAT aircraft schematic of Gress (2007) which accompanies its formulation of the aircraft pitch model or equation. The proprotors in this model are confined to tilt simultaneously and equally as shown in the figure. The model assumes that electromechanical servos – governed by a pitch feedback algorithm accompanying an electronic pitch sensor– exactly prescribe the tilt angle of the proprotors.

.

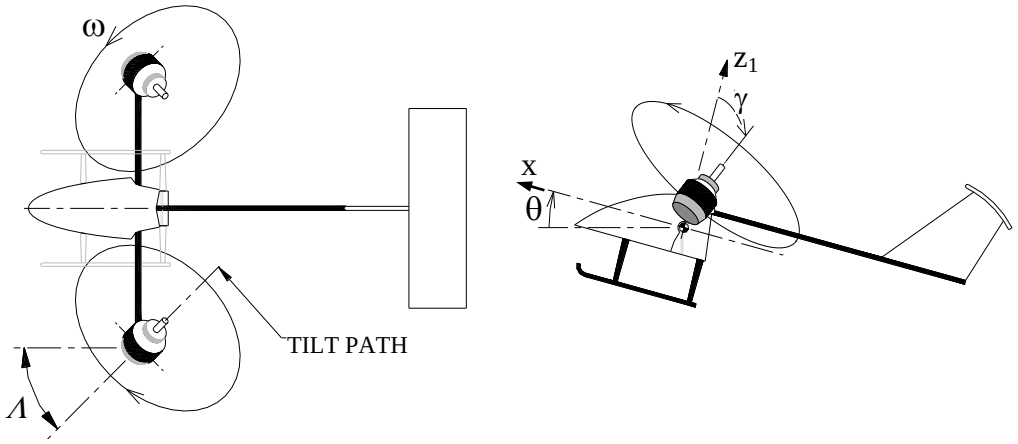

Figure 2-9. OAT stick aircraft. Pitch angle θ and tilt angles γ both shown positive. From (Gress, 2007).

In terms of the symbols used in this thesis, and using the short forms $s_\Lambda \equiv \sin\Lambda$ and $c_\Lambda \equiv \cos\Lambda$, this linearized (small angle) model is

$$½I_{Ay}\frac{d^2\theta}{dt^2} + I_P c_\Lambda \frac{d^2\gamma}{dt^2} - I_R\omega_0 s_\Lambda \frac{d\gamma}{dt} - (hT_0 c_\Lambda + Q_0 s_\Lambda)\gamma = 0 \qquad (2.1)$$

where γ is the proprotor tilt angle from the aircraft vertical (in oblique direction Λ), θ is the aircraft pitch angle. I_{Ay} , I_P and I_R are the airframe, propeller pod and propeller mass moment of inertias about the pitch, tilt and spin axes respectively. T_0 is the propeller thrust, Q_0 its drag torque, and h is the height of the tilt axes above the aircraft center of mass. Equation (2.1) applies to a balanced aircraft having no externally applied pitching moments. As expected, it shows that the adverse pod inertial effect – represented by the second-order tilt term – is most severe for longitudinal tilting, $\Lambda = 0$, and that the beneficial gyroscopic pitching moment (the first-order tilt term) vanishes for this tilt direction.

2.4.5 Stabilization of OAT aircraft

2.4.5.1 P-controller for Pitch

In Gress (2007) the author uses a simple proportional controller – or P-controller – for proprotor tilt as a function of aircraft pitch, without time delay:

$$\gamma = -k_p\theta \qquad (2.2)$$

Equation (2.2) represents an ideal sensor-actuator, or proportional piezo gyro with connected tilt servos. Eliminating γ in (2.1) using (2.2) yields the aircraft equation of motion solely in terms of pitch θ

$$\left(\frac{I_{Ay}}{2k_p} - I_P c_\Lambda\right)\frac{d^2\theta}{dt^2} \;+\; I_R\omega_0 s_\Lambda \frac{d\theta}{dt} \;+\; (hT_0 c_\Lambda + Q_0 s_\Lambda)\theta \;=\; 0 \qquad (2.3)$$

which is also the system's implicit characteristic equation. Considering its second-order coefficient, it is once more evident that pod inertia is a potential destabilizer.

It is desirable that pitching of the aircraft in hover (say, due to an unspecified disturbance) does not cause it to translate horizontally. For such a condition to be satisfied the propeller axes must remain in a vertical plane, which is ensured by the following approximate relationship, valid for small angles (see (4.30) and (4.31) of this thesis):

$$\gamma \;=\; -\frac{1}{\cos\Lambda}\cdot\theta \qquad (2.4)$$

Equating (2.4) and (2.2) specifies the necessary gain for the proportional controller:

$$k_p \;=\; \frac{1}{\cos\Lambda} \qquad (2.5)$$

Note that introducing a derivative component into the controller would have created a negative third-order term in the equation of motion (2-3) and destabilized the aircraft. Even without this problem, it would have not allowed the vertical-plane condition (2.4).

An integral controller component will cause difficulty as well. Whereas an imbalanced P-controlled aircraft will simply hover at the pitch angle that counteracts the imbalance, an integral controller will continually try to reduce the error and increase the

propeller tilt angle further past the vertical, thereby accelerating the aircraft horizontally instead.

2.4.5.2 P-controller with time delay: Humans cannot fly present bicopters without electronic assistance.

In practice the control of propeller tilt angle based on the feedback of aircraft pitch angle will involve a time delay, which can be attributed to either or both the sensor and actuator. If this delay is constant and represented as Δt, introducing it into the proportional control model (2.2) yields

$$\gamma(t) \;=\; -\,k_p\theta(t-\Delta t) \tag{2.6}$$

Assuming θ to be linear over the interval Δt, the control model can be written as

$$\gamma(t) \;=\; -\,k_p[\theta(t)-\Delta t\cdot\theta'(t)] \;=\; -\,k_p\theta(t) \;+\; k_p\Delta t\cdot\theta'(t) \tag{2.7}$$

which of course is also a first-order Taylor series approximation if θ is not linear. Eliminating $\gamma(t)$ in (2.1) using (2.7) yields the new characteristic equation

$$\mathcal{P}\Delta t\frac{d^3\theta}{dt^3} \;+\; \left(\frac{I_{Ay}}{2k_p}-\mathcal{P}-\mathcal{R}\Delta t\right)\frac{d^2\theta}{dt^2} \;+\; [\mathcal{R}-\mathcal{Q}\Delta t]\frac{d\theta}{dt} \;+\; \mathcal{Q}\theta \;=\; 0 \tag{2.8}$$

where $\mathcal{P}=I_P c_\Lambda$, $\mathcal{R}=I_R\omega_0 s_\Lambda$ and $\mathcal{Q}=hT_0c_\Lambda+Q_0s_\Lambda$. The new, negative terms in (2.8) demonstrate the destabilizing effect of time delay. For the coefficients to be

positive and the system stable - and assuming the controller is attempting to keep the propeller axes in the earth-vertical plane per (2.5) - Δt must satisfy:

$$\Delta t \;<\; \frac{\frac{I_{Ay}}{2k_p} - \mathscr{P}}{\mathscr{R}} \;=\; \frac{\left(\frac{1}{2} I_{Ay} - I_P\right) c_{\Lambda}}{\mathscr{R}} \tag{2.9}$$

and

$$\Delta t \;<\; \frac{\mathscr{R}}{\mathscr{Q}} \tag{2.10}$$

For the Nymbus data of Appendix B the maximum time delays according to (2.9) and (2.10) are 0.114 sec. and 0.229 sec. respectively.

These conditions are easily satisfied by hobby attitude sensors (gyros) and digital actuator servos, which typically have operating frequencies ranging from 50 to 400Hz depending on the model. So (2.9) and (2.10) show that OAT aircraft can be stabilized in pitch by electronics, which of course has been confirmed in practice.

The time delay relations also show that a human pilot cannot control an OAT model aircraft without electronic stability augmentation. Many studies on human response times have been performed, and the results are in fair agreement that human transport delay (associated with visual observation and mental processing of the information) is of the order of 0.2 sec., and that time lag (representing human muscle structure's inability to respond instantaneously to commands to move) is approximately 0.1 sec (MIL-F-83300, 1970, Key 1971, Franklin, 2002). The sum of these two values is greater than either of the maximum allowable delays for the Nymbus above. So, based on this analysis and many experimental tests in the past, it is safe to surmise that a human operator cannot pilot an OAT model aircraft without assistance. It can also be seen that -

upon inspection of (2.9) and (2.10) - this situation cannot be improved much by changing the gyroscopic properties of the propellers; raising the value of $\mathcal{R}$, for example, will increase one maximum time delay but decrease the other. There is, therefore, no need to investigate further the handling qualities of the unassisted system as such.

There is one further (Routh-Hurwitz) condition for the stability of a third-order system (Franklin, 2010, pg. 133), which is

$$a_1 a_2 > a_3 \tag{2.11}$$

for a general third-order polynomial in x written as

$$x^3 + a_1 x^2 + a_2 x + a_3 = 0 \tag{2.12}$$

Applying this condition to characteristic equation (2.8) gives a maximum allowable time delay of 0.102 sec, which is similar to the first two values and therefore does not change the deductions above.

2.4.5.3 Electronic stabilization of roll and yaw in OAT bicopters

Of the standard control algorithms, the author found PD-control (proportional derivative) to be the most effective for stabilizing roll and yaw of OAT bicopters. In those implementations the roll sensor (gyro) sent corrective signals to the propeller speed controls to differentially change the thrust magnitudes, and the yaw sensor corrective signals to the servos to differentially tilt the propellers. However, such roll control will cause the aircraft to yaw because of the resulting propeller torque differences – and yaw control as such will cause the aircraft to roll because of the gyroscopic moments generated – and therefore each sub-system must continuously work to compensate the

effects of the other. The net result, surprisingly, is control and stability enhancement, but this can be improved further by changing the control strategy as outlined in Section 2.4.8.

2.4.6 Pilot Pitch Control in OAT

The pilot's control of pitch in OAT bicopters is achieved by collectively tilting the propellers using the same servos which implement the electronic controller's stabilization algorithm, the latter allowing "pass-through" of the pilot's commands. Figure 2-10 shows the bicopter's pitch response improving as the tilt-path direction becomes more lateral.

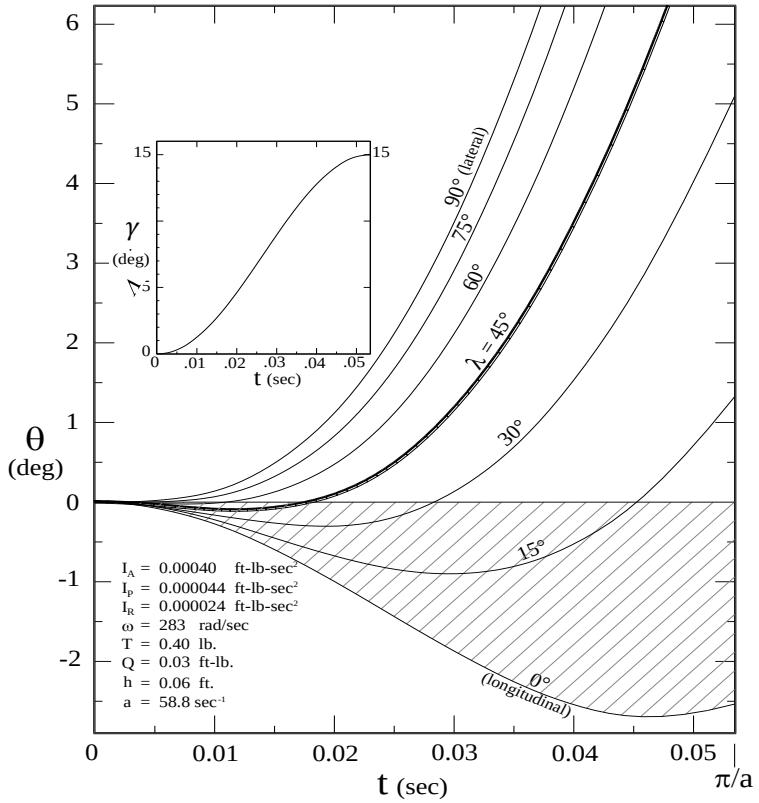

Figure 2-10. Predicted OAT aircraft pitch response to control input $\gamma(t)$ (inset) for various tilt-path angles Λ. Adapted from Gress (2007)

2.4.7 Fieux passive Ship Stabilizer and Parallels to Aircraft Self-stabilization

The inactive (or "passive" in present terminology) Fieux ship stabilizer described in (Ferry, 1933), and dating to circa 1924, is the only known device that operates in a similar fashion to the one proposed in this thesis. Referring to Fig 2-11, it consists of two large gyroscopes driven by electric motors in opposite directions about horizontal axes. The two gyro casings are able to precess about vertical axes and are geared together so that their precession velocities are equal and in opposite direction. This arrangement prevents inadvertent pitching of the ship, and conversely prevents pitching of the ship from affecting precession. Rolling of the ship, on the other hand, causes the gyroscopes to precess equally and oppositely – which is allowed by the gearing – thereby generating same-direction resisting (stabilizing) moments about the roll axis,

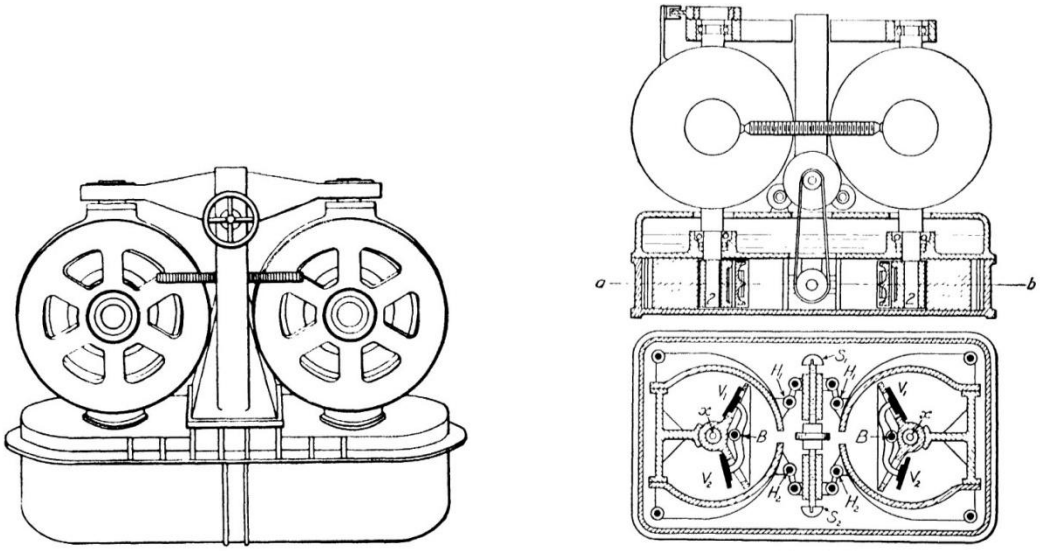

(a) **(b)**

Figure 2-11. (a) Ship anti-roll gyroscopes, athwartship view. (b) *Top*: cutaway view of same, revealing 'hydraulic brakes' or dampers below the gyroscopes. *Bottom*: cutaway top view of damper fluid tank, showing vanes therein which rotate when the gyroscopes precess. from (Ferry, 1933).

A unique feature of the Fieux stabilizer is the viscous fluid damper used to absorb the energy of the ship's roll. Vanes rotate within the damper tank when the gyroscopes precess, offering a resisting moment proportional to the rate of precession

Because the precession of its gyroscopes' was roughly in phase with the rolling of the ship, the Fieux device did a poor job of minimizing the roll angle. This synchronicity meant that the precession rate – and therefore the gyroscopic resisting moment to roll – was greatest when the roll rate was at its maximum, and therefore when a substantial roll angle had already been established.

Such synchronous behaviour is necessary for aircraft stabilization because, as discussed previously, the propeller axes need to remain near or in the vertical plane during its pitching. But a ship with internal gyroscopes has no such requirement, and therefore improvements over the Fieux system were sought.

2.4.8 Sperry Active Ship Stabilizer and Parallels to OAT

The Sperry system (Figure 2-12) was comprised primarily of a small control gyroscope having three degrees of rotational freedom, a large moment-generator gyroscope of two degrees freedom, and a precession motor that could force the latter's precession. A slight roll of the ship (by even a small angle) would cause the control gyro to precess, closing the precession motor circuit and thereby forcing precession of the large gyroscope. In this way very large control moments could be generated at small roll angles, thereby preventing them from increasing further.

Parallels with aircraft OAT are obvious in that both systems consist of a control gyro and a moment-generator gyro (piezo pitch gyro and propellers, respectively, in OAT). And the precession motor in the Sperry system is simply the tilt servo of OAT; each requires or absorbs energy in the forcing or arresting of the moment-generator

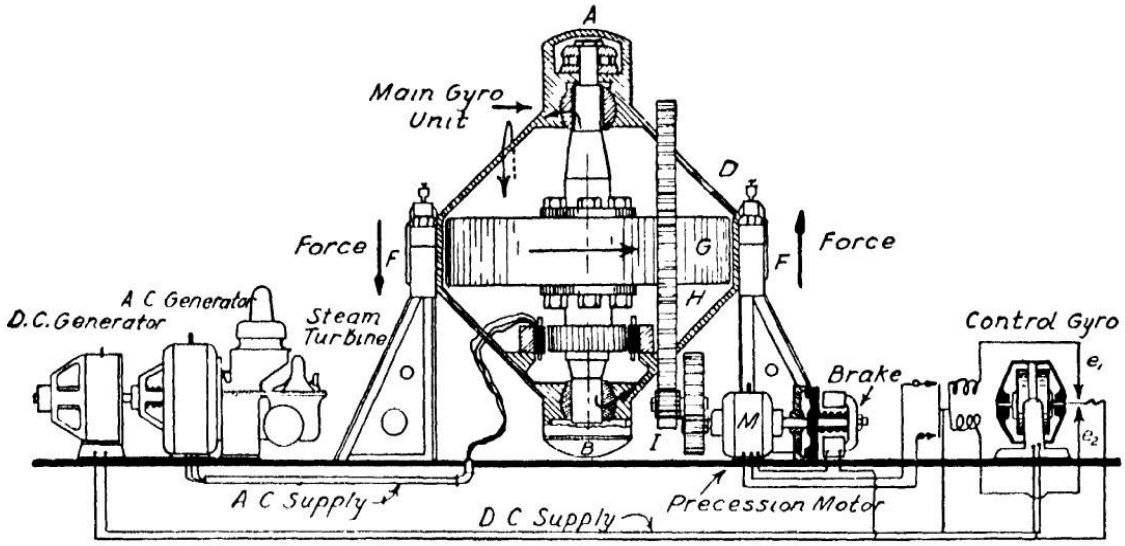

Figure 2-12. Sperry active ship stabilizer. from (Ferry, 1933)

However, by this means the ship-borne system effectively became a derivative or rate-type controller – quite different from its passive counterpart – whereas OAT must of necessity utilize an essentially proportional controller, thereby emulating the passive, self-stabilized system. There appears, therefore, nothing advantageous about the electronic system in terms of the control moments generated and their timing. On the contrary, because of time delays inherent to control electronics, the self-stabilizing system would be the preferred one.

Chapter Three: Mathematical Model of Hovering Bicopter

3.1 Introduction

In this chapter the three-dimensional equations of angular motion of a hovering bicopter with freely tilting proprotors are derived in order to determine its attitudinal stability. Its translational equations of motion of the mass center are not derived since angles and attitudinal stability are independent of them at low speeds (where aerodynamic-surface forces are not prevalent).

The angular motion equations are then linearized using small perturbation theory, and the equation of motion about each of the three major axes is extracted using the superposition principle. In this form the equations are ready to be used in subsequent chapters to determine stability about each of the axes independently.

Concurrently the proprotor *pod* (see Figure 3-1) equations of tilting motion – relative to the airframe – are also derived and similarly prepared here for use in the subsequent stability chapters.

3.2 Modelling Assumptions, Conventions and Conditions

This section defines the assumptions used in constructing the mathematical model of the hovering aircraft and the conditions for determining the aircraft's hover stability. A schematic of the aircraft with component names is shown in Figure 3-1.

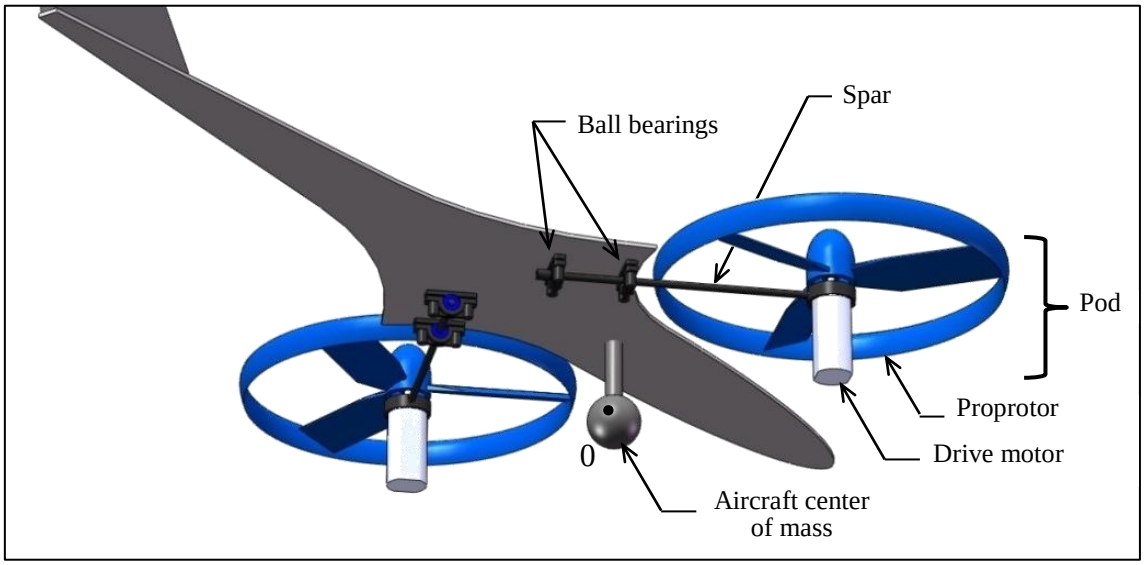

Figure 3-1. Underside of schematic aircraft showing major elements.

3.2.1 *Assumptions*

The assumptions used in formulating the model are:

1. Aircraft stability in hover is synonymous with its attitudinal or angular (or rates thereof) stability; any translational motion (of the aircraft centre of mass) is ignored and considered not to affect said stability.
2. The two proprotors spin in opposite directions.
3. Proprotors are rigid, unarticulated within themselves, and their planes of rotation are perpendicular to their respective spin axes.
4. Proprotor speeds are constant unless controlled otherwise.
5. Proprotor thrust and drag-torque magnitudes are functions of proprotor rotational speed only, calculated in each instance as if in the steady state; their vectors are always coincident with the proprotor spin axes.

6. Center of masses of pods lie at the intersection of their associated pivot axes and proprotor spin axes.
7. Aircraft center of mass, and inertias about its principle axes, are constant and independent of proprotor tilt.
8. There is no aerodynamic damping of the aircraft angular motion, and there are no aerodynamic effects resulting from aircraft motion in general.
9. There are no transient aerodynamic effects.
10. Proprotor mass moment of inertia I_R includes rotating part of drive motor.

3.2.2 Conventions

The geometry and positive-tilt (about unit axes $\hat{\mathbf{u}}_i$) conventions of the model are shown in Figure 3-2.

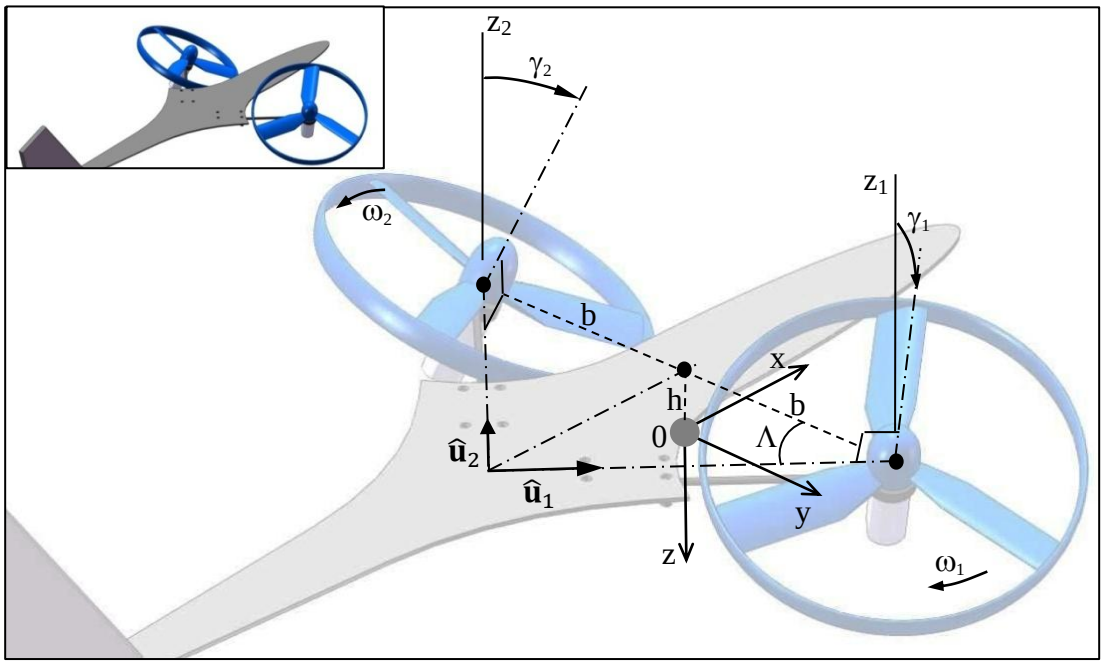

Figure 3-2. Schematic with local coordinates and relevant geometric variables.

In conventional aerospace practice the aircraft angular velocity relative to inertial space is usually expressed as

$$\boldsymbol{\omega} = \begin{bmatrix} p \\ q \\ r \end{bmatrix}$$

However, in this work $\omega_{i=1,2}$ represents the rotational speeds of the two proprotors, and variables $p_{x,y}$, $q_{x,y}$ and $r_{x,y}$ represent the three coefficient groups in the equations of motion. So, instead, the angular velocity of the aircraft frame relative to inertial space is written here as

$$\boldsymbol{\Omega} = \begin{bmatrix} \Omega_x \\ \Omega_y \\ \Omega_z \end{bmatrix}$$

3.2.3 Conditions for Stability

The determinations of aircraft hover stability in subsequent chapters are made only for the linearized system, which is also time-invariant and therefore an LTI (linear time-invariant) system. At various times either bounded-input bounded-output (BIBO) stability or zero-input (asymptotic) stability are here investigated, and both are satisfied for LTI systems if the roots of the characteristic equation (or transfer function denominator polynomial) all have negative real parts (Franklin, 2010, Kuo, 1995). This condition is determined here by applying the Routh-Hurwitz stability criterion (Franklin 2010, which refers to it as Routh's stability criterion). An exception to this condition exists if the system is a velocity controller (Kuo, 1995, pg. 332); the system would have

root(s) at the origin and would be considered stable. This exception applies to the aircraft with centering springs analyzed in Section 4.6.

In the Simulink simulations of Chapters 4 and 5 the initial condition for the aircraft is it hovering level with zero angular velocity and acceleration in all directions. Being a linear system the magnitudes of applied external disturbing moments M_e are arbitrary, but in this analysis they are kept to relatively small values, usually 10% of the proprotor drag torque Q_o.

3.3 Inertial Moments due to Spinning Proprotors

3.3.1 Effect on airframe and on pod tilting

Referring to Figure 3-3, the unit vectors coinciding with the proprotor axes are:

$$\hat{\mathbf{s}}_1 = \begin{bmatrix} -\cos\Lambda \cdot \sin\gamma_1 \\ \sin\Lambda \cdot \sin\gamma_1 \\ -\cos\gamma_1 \end{bmatrix} \tag{3.1a}$$

and

$$\hat{\mathbf{s}}_2 = \begin{bmatrix} \cos\Lambda \cdot \sin\gamma_2 \\ \sin\Lambda \cdot \sin\gamma_2 \\ -\cos\gamma_2 \end{bmatrix} \tag{3.1b}$$

The angular momentum vectors (expressed in the aircraft reference frame) due to spinning of the two proprotors are

$$\mathbf{H}_{R1} = -I_R\omega_1\hat{\mathbf{s}}_1 \equiv \begin{bmatrix} H_{R1x} \\ H_{R1y} \\ H_{R1z} \end{bmatrix} \tag{3.2a}$$

$$\mathbf{H}_{R2} = I_R\omega_2\hat{\mathbf{s}}_2 \equiv \begin{bmatrix} H_{R2x} \\ H_{R2y} \\ H_{R2z} \end{bmatrix} \tag{3.2b}$$

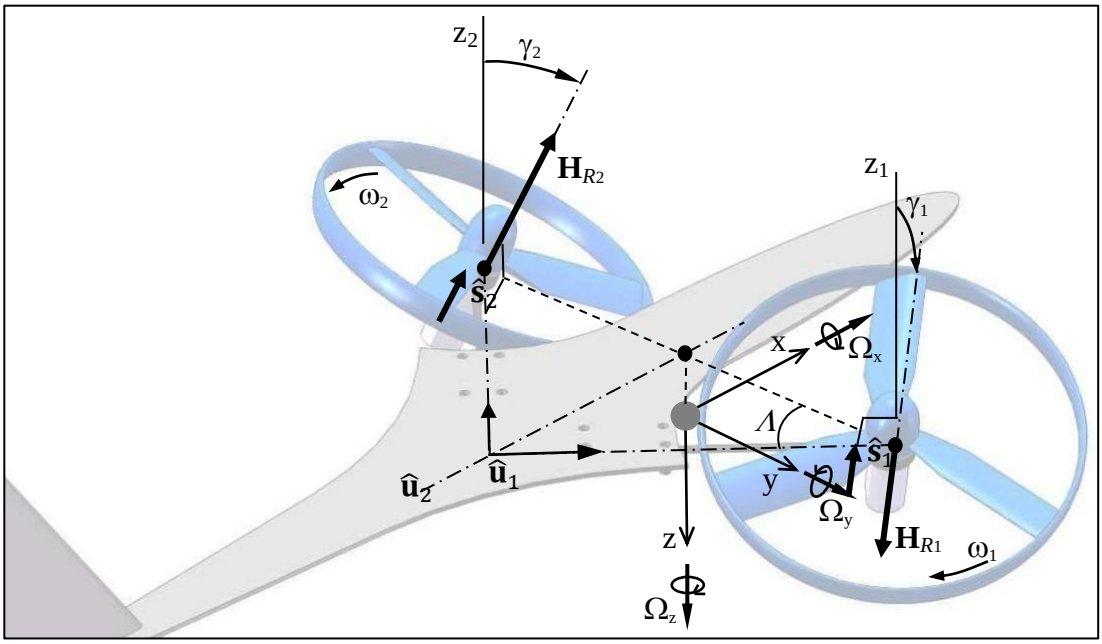

Figure 3-3. Proprotor angular momentum vectors $\mathbf{H}_{Ri}$ (relative to airframe).

The time derivative of a vector **B**, referenced to a frame rotating with angular velocity **Ω** (relative to inertial space), is

$$\frac{d\mathbf{B}}{dt} = \frac{\delta\mathbf{B}}{\delta t} + \boldsymbol{\Omega} \times \mathbf{B} \tag{3.3a}$$

where

$$\frac{\delta\mathbf{B}}{\delta t} = \frac{dB_x}{dt}\mathbf{i} + \frac{dB_y}{dt}\mathbf{j} + \frac{dB_z}{dt}\mathbf{k} \tag{3.3b}$$

Using this relation, the proprotor inertial moment vectors $\mathbf{M}_{Ri}$ can then be obtained from the proprotors' angular momentum rates of change (due to proprotor speed and tilt changes, and the aircraft's angular motion):

$$-\mathbf{M}_{Ri}|_{i=1,2} = \left.\frac{d\mathbf{H}_{Ri}}{dt}\right|_{i=1,2} = \frac{dH_{Rix}}{dt}\mathbf{i} + \frac{dH_{Riy}}{dt}\mathbf{j} + \frac{dH_{Riz}}{dt}\mathbf{k} + \left(\Omega_y H_{Riz} - \Omega_z H_{Riy}\right)\mathbf{i} + \left(\Omega_z H_{Rix} - \Omega_x H_{Riz}\right)\mathbf{j} + \left(\Omega_x H_{Riy} - \Omega_y H_{Rix}\right)\mathbf{k} \tag{3.4}$$

Substituting the H_R coefficients from (3.2) into (3.4):

$$\begin{aligned}\frac{-\mathbf{M}_{R1}}{I_R} &= \left[\cos\Lambda\frac{d}{dt}(\omega_1\sin\gamma_1) + \Omega_y\omega_1\cos\gamma_1 + \Omega_z\sin\Lambda\,\omega_1\sin\gamma_1\right]\mathbf{i} \\ &+ \left[-\sin\Lambda\frac{d}{dt}(\omega_1\sin\gamma_1) - \Omega_x\omega_1\cos\gamma_1 + \Omega_z\cos\Lambda\,\omega_1\sin\gamma_1\right]\mathbf{j} \\ &+ \left[\frac{d}{dt}(\omega_1\cos\gamma_1) - \left(\Omega_x\sin\Lambda + \Omega_y\cos\Lambda\right)\omega_1\sin\gamma_1\right]\mathbf{k} \qquad (3.5a)\end{aligned}$$

and

$$\begin{aligned}\frac{-\mathbf{M}_{R2}}{I_R} &= \left[\cos\Lambda\frac{d}{dt}(\omega_2\sin\gamma_2) - \Omega_y\omega_2\cos\gamma_2 - \Omega_z\sin\Lambda\,\omega_2\sin\gamma_2\right]\mathbf{i} \\ &+ \left[\sin\Lambda\frac{d}{dt}(\omega_2\sin\gamma_2) + \Omega_x\omega_2\cos\gamma_2 + \Omega_z\cos\Lambda\,\omega_2\sin\gamma_2\right]\mathbf{j} \\ &+ \left[-\frac{d}{dt}(\omega_2\cos\gamma_2) + \left(\Omega_x\sin\Lambda - \Omega_y\cos\Lambda\right)\omega_2\sin\gamma_2\right]\mathbf{k} \qquad (3.5b)\end{aligned}$$

Moments $\mathbf{M}_{Ri}$ act on the proprotors' respective drive motors and consequently their mountings. In order to determine the individual motions of the rotor pods and airframe, these moments need to be divided into orthogonal components, one acting about the pivot axis $\hat{\mathbf{u}}_i$ of the respective pod (and therefore tending to tilt the pod), and the other acting perpendicular to the first and conveyed directly to the airframe.

The projection of a vector $\mathbf{a}$ onto another vector $\mathbf{b}$ is:

$$\mathbf{a}_b = a_b\hat{\mathbf{b}} \qquad (3.6)$$

where $\hat{\mathbf{b}}$ is the unit vector in the direction of $\mathbf{b}$, and a_b is a scalar given by the dot product:

$$a_b = \mathbf{a}\cdot\hat{\mathbf{b}} \qquad (3.7)$$

Defining M_{Rui} as the (scalar) magnitude of $\mathbf{M}_{Ri}$ in the direction of (i.e., about) tilt axis $\hat{\mathbf{u}}_i$, from (3.7) it is:

$$M_{Rui} = \mathbf{M}_{Ri} \cdot \hat{\mathbf{u}}_i \tag{3.8}$$

The unit tilt axis vectors are:

$$\hat{\mathbf{u}}_1 = \begin{bmatrix} \sin \Lambda \\ \cos \Lambda \\ 0 \end{bmatrix}, \quad \hat{\mathbf{u}}_2 = \begin{bmatrix} \sin \Lambda \\ -\cos \Lambda \\ 0 \end{bmatrix} \tag{3.9a, b}$$

or, in generalized form:

$$\hat{\mathbf{u}}_i = \begin{bmatrix} \sin \Lambda \\ (-1)^{i-1} \cos \Lambda \\ 0 \end{bmatrix} \tag{3.9c}$$

Inserting (3.5) and (3.9) into (3.8), the proprotor inertial moments M_{Rui} acting on the pods about their respective tilt axes are then:

$$M_{Ru1} = I_R \omega_1 \left[\left(\Omega_x \cos \Lambda - \Omega_y \sin \Lambda \right) \cos \gamma_1 - \Omega_z \sin \gamma_1 \right] \tag{3.10a}$$

$$M_{Ru2} = I_R \omega_2 \left[\left(\Omega_x \cos \Lambda + \Omega_y \sin \Lambda \right) \cos \gamma_2 + \Omega_z \sin \gamma_2 \right] \tag{3.10b}$$

Figure 3-4 shows moment M_{Ru1} tending to tilt pod 1 about its pivot axis.

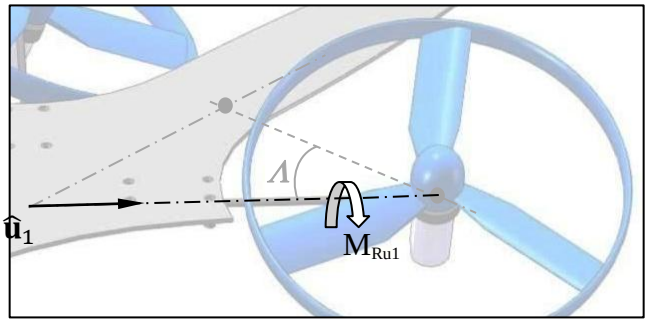

Figure 3-4. M_{Ru1} acting on pod 1 about its pivot axis.

From geometry $\mathbf{M}_{Rpi}$, the component of $\mathbf{M}_{Ri}$ perpendicular to $\hat{\mathbf{u}}_i$, is just $\mathbf{M}_{Ri}$ minus the parallel component:

$$\mathbf{M}_{Rpi} = \mathbf{M}_{Ri} - M_{Rui}\hat{\mathbf{u}}_i \tag{3.11}$$

Moments $\mathbf{M}_{Rpi}$ act on the airframe (through radial forces on the pivot bearings) only, i.e., they cannot tilt the rotor pods. Expanding (3.11) for the two pods gives:

$$\mathbf{M}_{Rp1} = I_R \begin{bmatrix} -\left[\frac{d}{dt}(\omega_1 \sin\gamma_1) + \omega_1\left(\Omega_x \sin\Lambda + \Omega_y \cos\Lambda\right)\cos\gamma_1\right]\cos\Lambda \\ \left[\frac{d}{dt}(\omega_1 \sin\gamma_1) + \omega_1\left(\Omega_x \sin\Lambda + \Omega_y \cos\Lambda\right)\cos\gamma_1\right]\sin\Lambda \\ -\frac{d}{dt}(\omega_1 \cos\gamma_1) + \omega_1\left(\Omega_x \sin\Lambda + \Omega_y \cos\Lambda\right)\sin\gamma_1 \end{bmatrix} \tag{3.12a}$$

$$\mathbf{M}_{Rp2} = I_R \begin{bmatrix} -\left[\frac{d}{dt}(\omega_2 \sin\gamma_2) + \omega_2\left(\Omega_x \sin\Lambda - \Omega_y \cos\Lambda\right)\cos\gamma_2\right]\cos\Lambda \\ -\left[\frac{d}{dt}(\omega_2 \sin\gamma_2) + \omega_2\left(\Omega_x \sin\Lambda - \Omega_y \cos\Lambda\right)\cos\gamma_2\right]\sin\Lambda \\ \frac{d}{dt}(\omega_2 \cos\gamma_2) - \omega_2\left(\Omega_x \sin\Lambda - \Omega_y \cos\Lambda\right)\sin\gamma_2 \end{bmatrix} \tag{3.12b}$$

3.3.2 Effect of Tilting and Aircraft Motion on Proprotor Spins

Any moment acting to change the spin speed of a proprotor itself can be obtained by projecting $\mathbf{M}_{Ri}$ onto the respective shaft axis. Using an "s" subscript to denote action about the shaft, this moment is

$$M_{Rsi} = \mathbf{M}_{Ri} \cdot \hat{\mathbf{s}}_i$$

which, for pod 1, upon substitution of (3.1) and (3.5a), becomes

$$\frac{M_{Rs1}}{I_R} = \sin\gamma_1 \frac{d}{dt}(\omega_1 \sin\gamma_1) + \cos\gamma_1 \frac{d}{dt}(\omega_1 \cos\gamma_1)$$

$$= \quad \sin^2\gamma_1 \frac{d\omega_1}{dt} + \cos^2\gamma_1 \frac{d\omega_1}{dt} \qquad = \quad \frac{d\omega_1}{dt}$$

which shows there is only an inertial moment acting on the proprotor about its axis if it is accelerating about that axis; there are no other such moments due to rotor tilting or aircraft motion. This result shows that $\mathbf{M}_{Rp1}$ is perpendicular to both the tilt and spin axes. The same result, of course, is obtained for rotor 2.

3.4 Inertial Moments due to Tilting Pods

When the pods are tilting they possess angular momentum relative to the aircraft frame of reference. As shown in Fig. 3-5 the corresponding angular momentum vectors $\mathbf{H}_{Pi}$ are coincident with the respective tilt axes $\hat{\mathbf{u}}_i$, and are given by

$$\mathbf{H}_{Pi} = I_P \frac{d\gamma_i}{dt} \hat{\mathbf{u}}_i \tag{3.13}$$

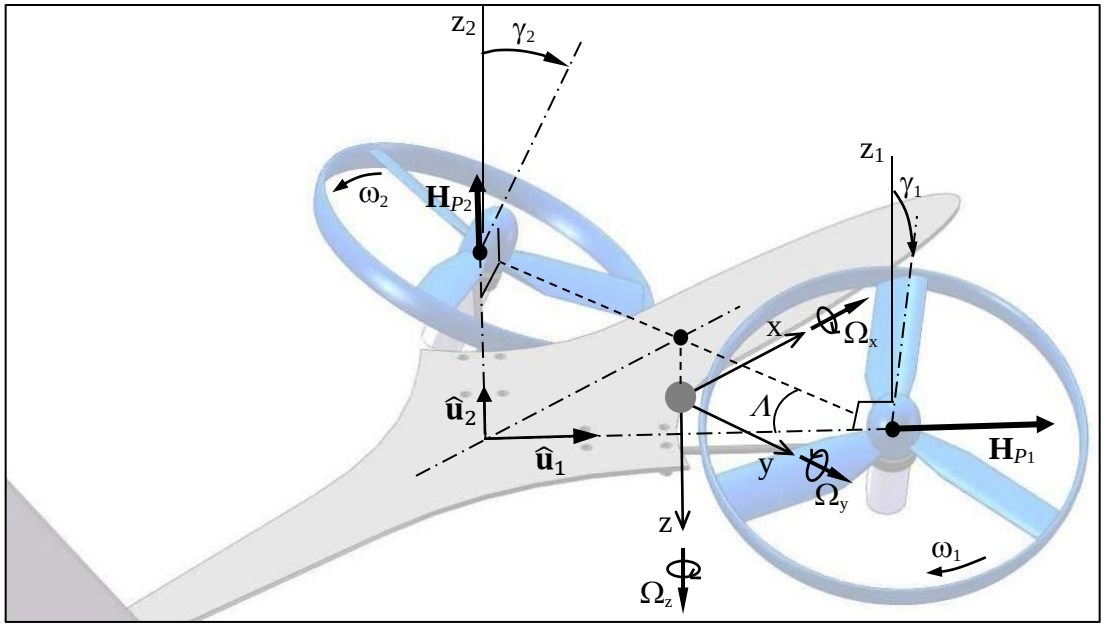

Figure 3-5. Relative angular momentum vectors $\mathbf{H}_{Pi}$ due to pod tilting.

Substituting $\hat{\mathbf{u}}_i$ in (3.13) with (3.9c) gives:

$$\mathbf{H}_{Pi}|_{i=1,2} \;=\; I_P \frac{d\gamma_i}{dt}\begin{bmatrix} \sin\Lambda \\ (-1)^{i-1}\cos\Lambda \\ 0 \end{bmatrix} \;\equiv\; \begin{bmatrix} H_{Pix} \\ H_{Piy} \\ H_{Piz} \end{bmatrix} \tag{3.14}$$

Following the method of section 3.2, the pod inertial moments $\mathbf{M}_{Pi}$ are obtained from their rates of change of angular momentum:

$$\begin{aligned} \left.\frac{-\mathbf{M}_{Pi}}{I_P}\right|_{i=1,2} &= \left.\frac{1}{I_P}\frac{d\mathbf{H}_{Pi}}{dt}\right|_{i=1,2} \\ &= \left[\sin\Lambda\,\frac{d^2\gamma_i}{dt^2} + (-1)^i\,\Omega_z\cos\Lambda\,\frac{d\gamma_i}{dt}\right]\mathbf{i} \\ &\quad + \left[(-1)^{i-1}\cos\Lambda\,\frac{d^2\gamma_i}{dt^2} + \Omega_z\sin\Lambda\,\frac{d\gamma_i}{dt}\right]\mathbf{j} \\ &\quad + \left[(-1)^{i-1}\Omega_x\cos\Lambda - \Omega_y\sin\Lambda\right]\frac{d\gamma_i}{dt}\mathbf{k} \end{aligned} \tag{3.15}$$

Similar to that derived in the previous section, the components M_{Pui} of $\mathbf{M}_{Pi}$ about the pivot axes $\hat{\mathbf{u}}_i$ are simply the dot products of $\mathbf{M}_{Pi}$ and $\hat{\mathbf{u}}_i$, giving

$$M_{Pui} \;=\; -\,I_P\frac{d^2\gamma_i}{dt^2} \tag{3.16}$$

Figure 3-6 shows M_{Pu1} shows acting on pod 1.

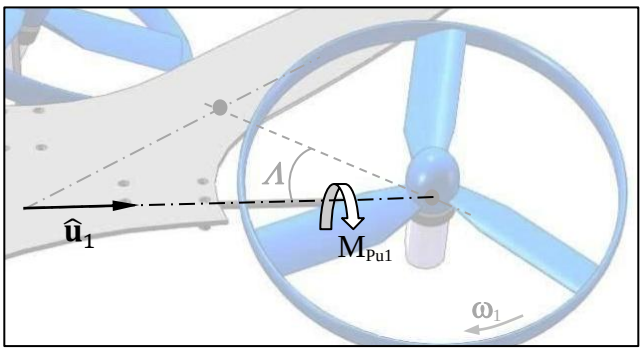

Figure 3-6. M_{Pu1} acting on pod 1 about its pivot axis.

As in the method of Section 3.2, the components of $\mathbf{M}_{Pi}$ perpendicular to the pivot axes are $\mathbf{M}_{Pi}$ minus the parallel component:

$$\mathbf{M}_{Ppi} = -I_P \frac{d\gamma_i}{dt} \begin{bmatrix} (-1)^i \Omega_z \cos \Lambda \\ \Omega_z \sin \Lambda \\ (-1)^{i-1} \Omega_x \cos \Lambda - \Omega_y \sin \Lambda \end{bmatrix} \tag{3.17}$$

These are gyroscopic moments acting on the aircraft, not due to tilting of spinning propellers, but to tilting of pods in conjunction with airframe rotation. The pod inertia I_P about the pivot axis will include that of the rotor.

3.5 Airframe Inertial Moments

Referring to Figure 3-7, if the aircraft is assumed to be symmetrical about the *0xz* plane, then its products of inertia, I_{Axy} and I_{Ayz}, become zero (Etkin, 1996, pg. 102). Also, if the *0x* and *0z* axes are coincident with the principal axes of the aircraft then the remaining product of inertia, I_{Azx}, vanishes as well. In the following derivation it is also assumed that the principal inertias of the airframe are constant and independent of pod tilt.

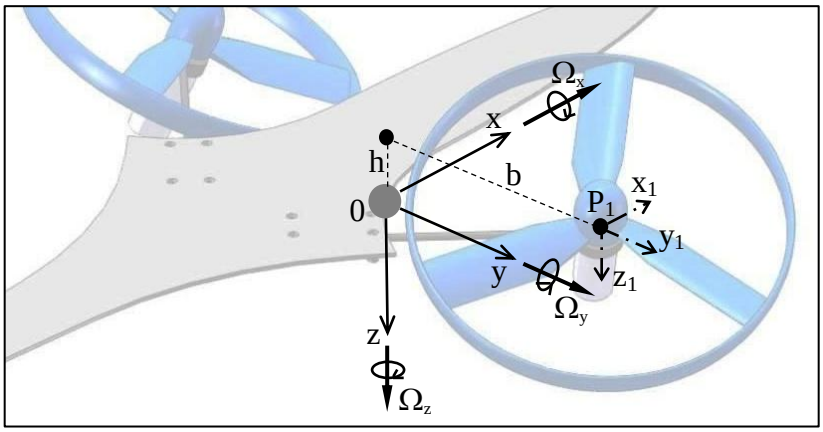

Figure 3-7. Aircraft principal axes and angular velocities, and location of pod center P_1 relative to aircraft center of mass 0.

With these simplifications the aircraft inertial moment derives from its rate of change of angular momentum in the world reference as

$$-\mathbf{M}_A \;=\; \frac{\mathrm{d}\mathbf{H}_A}{\mathrm{dt}} \;=\; \begin{bmatrix} I_{Ax}\dot{\Omega}_x + \left(I_{Az} - I_{Ay}\right)\Omega_y\Omega_z \\ I_{Ay}\dot{\Omega}_y + \left(I_{Ax} - I_{Az}\right)\Omega_x\Omega_z \\ I_{Az}\dot{\Omega}_z + \left(I_{Ay} - I_{Ax}\right)\Omega_x\Omega_y \end{bmatrix} \tag{3.18}$$

Equation (3.18) does not account for moments generated by the spinning of proprotors and tilting of pods. These moments are dealt with in Sections 3.2 and 3.3. However, (3.18) does include the masses and inertias of these items. Because of the latter there will be moments acting on the pods resulting from aircraft motion, tending to tilt them about their pivot axes. Since it will be necessary to eventually sum all the moments that cause the pods to tilt (Section 3.8), equation (3.18) must be separated into components which act directly upon the rigid airframe and those pod moments which act about their pivot axes.

It is assumed that a pod's inertia I_P about its pivot axis is also the moment of inertias about its local orthogonal axes $P_i x_i$, $P_i y_i$ and $P_i z_i$ (and the value being independent of the pod tilt angle, γ_i). The moment $\mathbf{M}_{P\Omega i}$ acting on each pod due to motion of the aircraft is then

$$\left.\frac{-\mathbf{M}_{P\Omega i}}{I_P}\right|_{i=1,2} = \quad \frac{1}{I_P}\,\frac{d\mathbf{H}_{P\Omega i}}{dt}$$

$$= \quad \dot{\Omega}_x\mathbf{i} \;+\; \dot{\Omega}_y\mathbf{j} \;+\; \dot{\Omega}_z\mathbf{k} \tag{3.19}$$

which, because of the assumption of the same pod inertia about all axes, is considerably simpler than (3.18). Using the methods of Section 3.2, the projection of these on the respective pivot axes are

$$\left.\frac{M_{P\Omega ui}}{I_P}\right|_{i=1,2} = -\dot{\Omega}_x \sin \Lambda + (-1)^i \dot{\Omega}_y \cos \Lambda \tag{3.20}$$

which, of course, are the inertial moments acting to tilt the rotor pods. In vector form in the aircraft frame of reference, they are

$$\left.\frac{\mathbf{M}_{P\Omega ui}}{I_P}\right|_{i=1,2} = \frac{M_{P\Omega ui}}{I_P}\,\hat{\mathbf{u}}_i \tag{3.21}$$

Using (3.9c) and (3.20), in full they become

$$\left.\frac{\mathbf{M}_{P\Omega ui}}{I_P}\right|_{i=1,2} = \begin{bmatrix} -\dot{\Omega}_x \sin^2 \Lambda + (-1)^i \dot{\Omega}_y \sin \Lambda \cos \Lambda \\ (-1)^i \dot{\Omega}_x \sin \Lambda \cos \Lambda - \dot{\Omega}_y \cos^2 \Lambda \\ 0 \end{bmatrix} \tag{3.22}$$

Since these moments act to tilt the rotor pods about their frictionless bearings, they cannot be acting on the remainder of the airframe (except through the control system, which is accounted for in the formulation of that system). Therefore they must be subtracted from the aircraft moment in (3.18) in order to determine the moment on the airframe. Summing the pod tilting moments in (3.22) gives

$$\frac{1}{I_P}\sum_{i=1}^{2} \mathbf{M}_{P\Omega ui} = -2\begin{bmatrix} \dot{\Omega}_x \sin^2 \Lambda \\ \dot{\Omega}_y \cos^2 \Lambda \\ 0 \end{bmatrix} \tag{3.23}$$

The net inertial airframe moment is then

$$\mathbf{M}_a \;=\; \mathbf{M}_A - \;\sum_{i=1}^{2} \mathbf{M}_{P\Omega ui} \tag{3.24}$$

which, from (3.18) and (3.23), is written in full as

$$\mathbf{M}_a \;=\; -\begin{bmatrix} I_{Ax}\dot{\Omega}_x + \left(I_{Az} - I_{Ay}\right)\Omega_y\Omega_z \\ I_{Ay}\dot{\Omega}_y + \left(I_{Ax} - I_{Az}\right)\Omega_x\Omega_z \\ I_{Az}\dot{\Omega}_z \;+ \left(I_{Ay} - I_{Ax}\right)\Omega_x\Omega_y \end{bmatrix} \;+\; 2I_P \begin{bmatrix} \dot{\Omega}_x \sin^2\Lambda \\ \dot{\Omega}_y \cos^2\Lambda \\ 0 \end{bmatrix} \tag{3.25}$$

Using an alternate convention of writing each of the aircraft principal inertias I_{Ax} , I_{Ay} , I_{Az} as the sum of the respective airframe inertia I_{ax} , I_{ay} or I_{az} and pod inertias (about their own local axes), gives

$$\left.\begin{aligned} I_{Ax} \;&=\; I_{ax} \;+\; 2I_P \\ I_{Ay} \;&=\; I_{ay} \;+\; 2I_P \\ I_{Az} \;&=\; I_{az} \;+\; 2I_P \end{aligned}\right\} \tag{3.26}$$

Note, however, that the airframe inertias still include the pods as point masses. For reference, from Figure 3-7, the airframe inertias can be broken down further, to

$$\left.\begin{aligned} I_{ax} \;&=\; I_{asx} \;+\; 2m_P(b^2 + h^2) \\ I_{ay} \;&=\; I_{asy} \;+\; 2m_P h^2 \\ I_{az} \;&=\; I_{asz} \;+\; 2m_P b^2 \end{aligned}\right\} \tag{3.27}$$

where I_{asx} , I_{asy} , I_{asz} are the inertias of the aircraft structure without pods, and m_P is the mass of a pod. However, for purposes of this chapter, (3.26) will suffice. Chapters 4 and 5 will introduce another simplifying convention for representing aircraft inertias. Substituting (3.26) into (3.25) then puts the aircraft inertial moment in terms of airframe inertias

$$\mathbf{M}_a = -\begin{bmatrix} I_{ax}\dot{\Omega}_x + (I_{az} - I_{ay})\Omega_y\Omega_z \\ I_{ay}\dot{\Omega}_y + (I_{ax} - I_{az})\Omega_x\Omega_z \\ I_{az}\dot{\Omega}_z + (I_{ay} - I_{ax})\Omega_x\Omega_y \end{bmatrix} - 2I_P\begin{bmatrix} \dot{\Omega}_x\cos^2\Lambda \\ \dot{\Omega}_y\sin^2\Lambda \\ \dot{\Omega}_z \end{bmatrix} \qquad (3.28)$$

3.6 Moments due to Propeller Thrusts and Drag Torques

3.6.1 General Thrusts and Drag Torques

General moment relations due to the proprotor thrusts and drag torques can be written for the aircraft without requiring knowledge of how they are generated or what their relationship is to one another. For the aircraft under investigation these are specified in the next sub-section. Referring to Figure 3-8, the proprotor thrust vectors $\mathbf{T}_i$ are assumed to be collinear with their respective spin axes, therefore intersecting the pivot axes and not causing the proprotor pods to tilt. But they do act radially through their respective pivot bearings to generate a net moment on the aircraft. Writing the thrust vectors in terms of thrust magnitudes T_i and pod tilt angles γ_i, this moment is:

$$\mathbf{M}_{Ti}|_{i=1,2} = \begin{bmatrix} (-1)^i bT_i\cos\gamma_i + hT_i\sin\Lambda\sin\gamma_i \\ -(-1)^i hT_i\cos\Lambda\sin\gamma_i \\ bT_i\cos\Lambda\sin\gamma_i \end{bmatrix} \qquad (3.29)$$

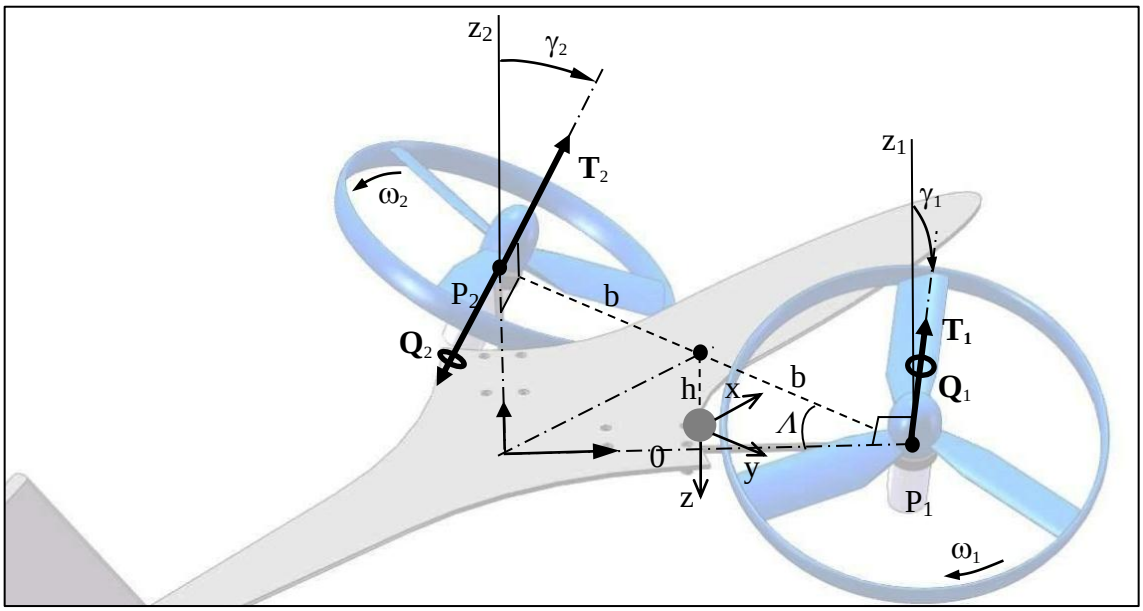

Figure 3-8. Proprotor thrust and drag-torque vectors

The proprotor drag-torque vectors are treated in the exact same way. The aircraft moment due to them is:

$$\mathbf{M}_{Qi}\big|_{i=1,2} = \begin{bmatrix} -Q_i \cos\Lambda \sin\gamma_i \\ -(-1)^i Q_i \sin\Lambda \sin\gamma_i \\ (-1)^i Q_i \cos\gamma_i \end{bmatrix} \tag{3.30}$$

3.6.2 Thrusts and Drag Torques as Linearized Functions of Prop Rotor Speeds

The aircraft under investigation uses fixed-pitch proprotors whose speeds are changed to vary their thrusts. The thrust and the drag torque of a given proprotor i in OGE (out of ground effect) hover can be written in terms of its variation from the nominal rotational speed ω_0 as

$$T_i = \left(\frac{\omega_i}{\omega_0}\right)^2 T_0\,, \qquad Q_i = \left(\frac{\omega_i}{\omega_0}\right)^2 Q_0 \tag{3.31}$$

where T_0 and Q_0 are the nominal thrust and aerodynamic drag torque, respectively, measured at the nominal speed ω_0 (usually the hover speed). These relations can be approximated by linear ones by noting that the first two terms of a Taylor series representation of $f\left(\frac{\omega_i}{\omega_0}\right) = \left(\frac{\omega_i}{\omega_0}\right)^2$ about the nominal value 1 is:

$$f(1) + \frac{f'(1)}{1!}\left(\frac{\omega_i}{\omega_0} - 1\right) = 2\frac{\omega_i}{\omega_0} - 1$$

The linear approximations of relations (3.31) then are

$$T_i \cong \left(2\frac{\omega_i}{\omega_0} - 1\right)T_0\,, \qquad Q_i \cong \left(2\frac{\omega_i}{\omega_0} - 1\right)Q_0 \tag{3.32}$$

3.7 External Disturbance

Referring to Figure 3-9, disturbing moment $\mathbf{M}_e$ represents any unbalance due to external elements, such as wind gusts, and is given by

$$\mathbf{M}_e = \begin{bmatrix} M_{ex} \\ M_{ey} \\ M_{ez} \end{bmatrix} \tag{3.33}$$

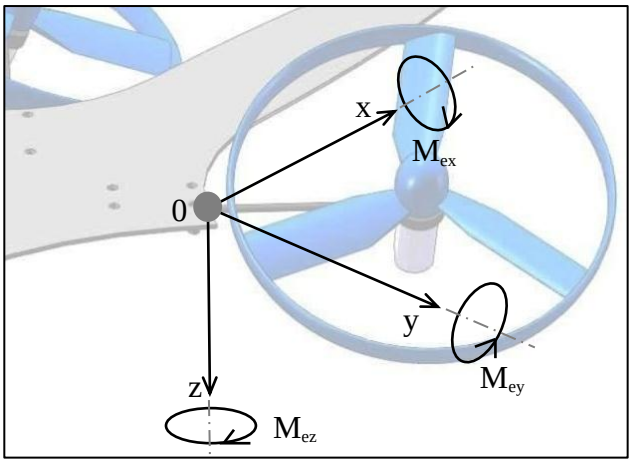

Figure 3-9. External disturbing moment's three orthogonal components.

There can also be external disturbing moments acting on the pods (and tending to tilt them). These are formally added to the pitch equations in Chapter 4.

3.8 Pod Equations of Motion about their Pivot Axes

The sum of the moments obtained from previous sections of this chapter about each pod axis – along with an as-yet-unspecified corrective or control moment C_i – is:

$$M_{Pui} + M_{P\Omega ui} + M_{Rui} - C_i = 0 \tag{3.34}$$

Letting $\sin\Lambda = s_\Lambda$ and $\cos\Lambda = c_\Lambda$ and writing (A6.1) in full for each pod:

$$I_P \frac{d^2\gamma_1}{dt^2} + I_P\left(\dot{\Omega}_x s_\Lambda + \dot{\Omega}_y c_\Lambda\right) + I_R\omega_1\left[\left(-\Omega_x c_\Lambda + \Omega_y s_\Lambda\right)\cos\gamma_1 + \Omega_z \sin\gamma_1\right] + C_i = 0 \tag{3.35a}$$

$$I_P \frac{d^2\gamma_2}{dt^2} + I_P\left(\dot{\Omega}_x s_\Lambda - \dot{\Omega}_y c_\Lambda\right) - I_R\omega_2\left[\left(\Omega_x c_\Lambda + \Omega_y s_\Lambda\right)\cos\gamma_2 + \Omega_z \sin\gamma_2\right] + C_i = 0 \tag{3.35b}$$

Assuming small proprotor tilt angles such that $\sin\gamma_i \cong \gamma_i$ and $\cos\gamma_i \cong 1$, these simplify to

$$I_P \frac{d^2\gamma_1}{dt^2} + I_P\left(\dot{\Omega}_x s_\Lambda + \dot{\Omega}_y c_\Lambda\right) + I_R\omega_1\left[-\Omega_x c_\Lambda + \Omega_y s_\Lambda + \Omega_z\gamma_1\right] + C_1 = 0 \tag{3.36a}$$

$$I_P \frac{d^2\gamma_2}{dt^2} + I_P\left(\dot{\Omega}_x s_\Lambda - \dot{\Omega}_y c_\Lambda\right) - I_R\omega_2\left[\Omega_x c_\Lambda + \Omega_y s_\Lambda + \Omega_z\gamma_2\right] + C_2 = 0 \tag{3.36b}$$

3.9 Airframe 3D Equation of Angular Motion and its Linearization/Simplification

3.9.1 Complete Non-linear Equation

To obtain the equation of motion of the aircraft, the moments acting on it and derived in previous sections are summed and the result equated to zero:

$$\mathbf{M}_a + \mathbf{C} + \sum_{i=1}^{2}\left(\mathbf{M}_{Ppi} + \mathbf{M}_{Rpi} + \mathbf{M}_{Ti} + \mathbf{M}_{Qi}\right) + \mathbf{M}_e = 0 \tag{3.39}$$

where $\boldsymbol{C}$ is the airframe moment subject to and opposing the pod correction/control moments C_i of section 3.7, and is given by

$$\begin{aligned}\mathbf{C} &= C_1\hat{\mathbf{u}}_1 + C_2\hat{\mathbf{u}}_2 \\ &= C_1\begin{bmatrix}\sin\Lambda\\ \cos\Lambda\\ 0\end{bmatrix} + C_2\begin{bmatrix}\sin\Lambda\\ -\cos\Lambda\\ 0\end{bmatrix} \qquad \text{(from (3.9a, b))} \\ &= \begin{bmatrix}s_\Lambda(C_1+C_2)\\ c_\Lambda(C_1-C_2)\\ 0\end{bmatrix} \qquad (3.40)\end{aligned}$$

Abbreviating the trigonometric functions in Λ as $\sin\Lambda = s_\Lambda$ and $\cos\Lambda = c_\Lambda$, and referencing the relevant previous sections in this chapter, (3.39) written in full is

$$\begin{bmatrix}I_{ax}\dot{\Omega}_x + (I_{az}-I_{ay})\Omega_y\Omega_z\\ I_{ay}\dot{\Omega}_y + (I_{ax}-I_{az})\Omega_x\Omega_z\\ I_{az}\dot{\Omega}_z + (I_{ay}-I_{ax})\Omega_x\Omega_y\end{bmatrix} + 2I_P\begin{bmatrix}\dot{\Omega}_x {c_\Lambda}^2\\ \dot{\Omega}_y {s_\Lambda}^2\\ \dot{\Omega}_z\end{bmatrix} - \begin{bmatrix}s_\Lambda(C_1+C_2)\\ c_\Lambda(C_1-C_2)\\ 0\end{bmatrix} - I_P\begin{bmatrix}\Omega_z c_\Lambda(-\dot{\gamma}_1+\dot{\gamma}_2)\\ \Omega_z s_\Lambda(\ \dot{\gamma}_1+\dot{\gamma}_2)\\ \Omega_x c_\Lambda(\dot{\gamma}_1-\dot{\gamma}_2) - \Omega_y s_\Lambda(\dot{\gamma}_1+\dot{\gamma}_2)\end{bmatrix}$$

$$+ I_R\begin{bmatrix}\left[\frac{d}{dt}(\ \omega_1\sin\gamma_1+\omega_2\sin\gamma_2) + \Omega_x s_\Lambda(\ \omega_1\cos\gamma_1+\omega_2\cos\gamma_2) + \Omega_y c_\Lambda(\omega_1\cos\gamma_1-\omega_2\cos\gamma_2)\right]c_\Lambda\\ \left[\frac{d}{dt}(-\omega_1\sin\gamma_1+\omega_2\sin\gamma_2) + \Omega_x s_\Lambda(-\omega_1\cos\gamma_1+\omega_2\cos\gamma_2) - \Omega_y c_\Lambda(\omega_1\cos\gamma_1+\omega_2\cos\gamma_2)\right]s_\Lambda\\ \frac{d}{dt}(\ \omega_1\cos\gamma_1-\omega_2\cos\gamma_2) + \Omega_x s_\Lambda(-\omega_1\sin\gamma_1+\omega_2\sin\gamma_2) - \Omega_y c_\Lambda(\omega_1\sin\gamma_1+\ \omega_2\sin\gamma_2)\end{bmatrix}$$

$$- \begin{bmatrix}b(-T_1\cos\gamma_1+T_2\cos\gamma_2) + h\,s_\Lambda(T_1\sin\gamma_1+T_2\sin\gamma_2)\\ h\,c_\Lambda(T_1\sin\gamma_1-\ T_2\sin\gamma_2)\\ b\,c_\Lambda(T_1\sin\gamma_1+\ T_2\sin\gamma_2)\end{bmatrix} - \begin{bmatrix}-c_\Lambda(Q_1\sin\gamma_1+Q_2\sin\gamma_2)\\ s_\Lambda(Q_1\sin\gamma_1-Q_2\sin\gamma_2)\\ -\ Q_1\cos\gamma_1+Q_2\cos\gamma_2\end{bmatrix} = \begin{bmatrix}M_{ex}\\ M_{ey}\\ M_{ez}\end{bmatrix} \tag{3.41}$$

3.9.2 Simplified and Linearized Equation

The first step in simplifying (3.41) is to assume small propeller tilt angles such that $\sin\gamma_i \cong \gamma_i$ and $\cos\gamma_i \cong 1$. Substituting these approximations into (3.41) gives

$$\begin{bmatrix} I_{ax}\dot{\Omega}_x + (I_{az} - I_{ay})\Omega_y\Omega_z \\ I_{ay}\dot{\Omega}_y + (I_{ax} - I_{az})\Omega_x\Omega_z \\ I_{az}\dot{\Omega}_z + (I_{ay} - I_{ax})\Omega_x\Omega_y \end{bmatrix} + 2I_P \begin{bmatrix} \dot{\Omega}_x c_\Lambda{}^2 \\ \dot{\Omega}_y s_\Lambda{}^2 \\ \dot{\Omega}_z \end{bmatrix} - \begin{bmatrix} s_\Lambda(C_1 + C_2) \\ c_\Lambda(C_1 - C_2) \\ 0 \end{bmatrix} - I_P \begin{bmatrix} \Omega_z c_\Lambda(-\dot{\gamma}_1 + \dot{\gamma}_2) \\ \Omega_z s_\Lambda(\ \dot{\gamma}_1 + \dot{\gamma}_2) \\ \Omega_x c_\Lambda(\dot{\gamma}_1 - \dot{\gamma}_2) - \Omega_y s_\Lambda(\dot{\gamma}_1 + \dot{\gamma}_2) \end{bmatrix}$$

$$+ I_R \begin{bmatrix} \left[\frac{d}{dt}(\ \omega_1\gamma_1 + \omega_2\gamma_2) + \Omega_x s_\Lambda(\ \omega_1 + \omega_2) + \Omega_y c_\Lambda(\omega_1 - \omega_2)\right] c_\Lambda \\ \left[\frac{d}{dt}(-\omega_1\gamma_1 + \omega_2\gamma_2) + \Omega_x s_\Lambda(-\omega_1 + \omega_2) - \Omega_y c_\Lambda(\omega_1 + \omega_2)\right] s_\Lambda \\ \frac{d}{dt}(\omega_1 - \omega_1) + \Omega_x s_\Lambda(-\omega_1\gamma_1 + \omega_2\gamma_2) - \Omega_y c_\Lambda(\omega_1\gamma_1 + \omega_2\gamma_2) \end{bmatrix}$$

$$- \begin{bmatrix} b(-T_1 + T_1) + h\, s_\Lambda(T_1\gamma_1 + T_2\gamma_2) \\ h\, c_\Lambda(T_1\gamma_1 - T_2\gamma_2) \\ b\, c_\Lambda(T_1\gamma_1 + T_2\gamma_2) \end{bmatrix} - \begin{bmatrix} -c_\Lambda(Q_1\gamma_1 + Q_2\gamma_2) \\ s_\Lambda(Q_1\gamma_1 - Q_2\gamma_2) \\ -Q_1 + Q_2 \end{bmatrix} = \begin{bmatrix} M_{ex} \\ M_{ey} \\ M_{ez} \end{bmatrix} \qquad (3.42)$$

The equation of motion can be simplified further using small disturbance theory, which assumes that the aircraft angular velocities are small, so that their squares and products are negligible compared to first-order quantities (Etkin, 1996).

This theory can be directly applied to the airframe gyroscopics of the first matrix in (3.42), thereby eliminating all of its ΩΩ products. However, rather than applying this theory to the remainder of the equation indiscriminately, it is necessary to determine which terms in (3.42) should be eliminated through an understanding of the processes they represent.

Of first note is that the sum of the proprotor speeds $\omega_1 + \omega_2$ will be roughly constant for hovering flight and approximately equal to $2\omega_0$, where ω_0 is the nominal hover proprotor speed. Therefore the sum $\omega_1 + \omega_2$ can be replaced by $2\omega_0$ wherever it occurs in (3.42).

In comparison to their sum, the proprotor speed difference $\omega_1 - \omega_2$ is small, and can assumed to be zero wherever it forms a product with an aircraft angular velocity Ω in (3.42).

The gyroscopic pod terms of the fourth matrix will be substantially smaller than the gyroscopic propeller terms of the fifth matrix since $\Omega \ll \omega$. Also, during predominantly rolling motion the two proprotor tilt angles will be approximately equal in magnitude and of the same sign, and therefore the first- and third-row roll terms of the fourth matrix will vanish. Similarly, during predominantly pitching motion the tilt angles will be nearly equal but of opposite sign, and therefore the second- and third-row pitch terms will disappear. With all the above arguments it is justifiable to eliminate the fourth matrix in (3.42) for the stability analysis.

In the case of sums of products involving ω such as $\omega_1\gamma_1 + \omega_2\gamma_2$ or $\omega_1\gamma_1 - \omega_2\gamma_2$, it is assumed that during normal maneuvers ω_1 and ω_2 deviate from ω_0 only relatively slightly, and that the variance in these sums will be largely due to variations in γ_1 and γ_2. With this assumption the speeds can be safely replaced by the nominal ω_0.

However, the small disturbance theory is applied directly to – and sets to zero - any such sum which results in a product of tilt angle γ_i and airframe angular velocity Ω (which would otherwise create a non-linear situation of a product in two unknowns). With the above changes the equation of motion becomes

$$\begin{bmatrix} (I_{ax} + 2I_P c_\Lambda{}^2)\dot{\Omega}_x \\ (I_{ay} + 2I_P s_\Lambda{}^2)\dot{\Omega}_y \\ (I_{az} + 2I_P)\dot{\Omega}_z \end{bmatrix} - \begin{bmatrix} s_\Lambda(C_1 + C_2) \\ c_\Lambda(C_1 - C_2) \\ 0 \end{bmatrix} + I_R \begin{bmatrix} \omega_0 c_\Lambda[(\dot{\gamma}_1 + \dot{\gamma}_2) + 2\Omega_x s_\Lambda] \\ \omega_0 s_\Lambda[(-\dot{\gamma}_1 + \dot{\gamma}_2) - 2\Omega_y c_\Lambda] \\ \dot{\omega}_1 - \dot{\omega}_2 \end{bmatrix}$$

$$- \begin{bmatrix} b(-T_1 + T_2) + h\, s_\Lambda(T_1\gamma_1 + T_2\gamma_2) \\ h\, c_\Lambda(T_1\gamma_1 - T_2\gamma_2) \\ b\, c_\Lambda(T_1\gamma_1 + T_2\gamma_2) \end{bmatrix} - \begin{bmatrix} -c_\Lambda(Q_1\gamma_1 + Q_2\gamma_2) \\ s_\Lambda(Q_1\gamma_1 - Q_2\gamma_2) \\ -Q_1 + Q_2 \end{bmatrix} = \begin{bmatrix} M_{ex} \\ M_{ey} \\ M_{ez} \end{bmatrix} \quad (3.43)$$

3.9.3 Linearized equation with rotor speed-thrust model

For thrust and aerodynamic torques that are a function only of the proprotor speeds, replacing T_i and Q_i in (3.43) with their linear ω_i-functions (3.32) – and treating the resulting products of ω_i and γ_i as before – gives:

$$\begin{bmatrix} (I_{ax} + 2I_P c_\Lambda{}^2)\dot{\Omega}_x \\ (I_{ay} + 2I_P s_\Lambda{}^2)\dot{\Omega}_y \\ (I_{az} + 2I_P)\dot{\Omega}_z \end{bmatrix} - \begin{bmatrix} s_\Lambda(C_1 + C_2) \\ c_\Lambda(C_1 - C_2) \\ 0 \end{bmatrix} + I_R \begin{bmatrix} \omega_0 c_\Lambda[(\dot{\gamma}_1 + \dot{\gamma}_2) + 2\Omega_x s_\Lambda] \\ \omega_0 s_\Lambda[(-\dot{\gamma}_1 + \dot{\gamma}_2) - 2\Omega_y c_\Lambda] \\ \dot{\omega}_1 - \dot{\omega}_2 \end{bmatrix}$$

$$- T_0 \begin{bmatrix} 2b(-\omega_1 + \omega_2)/\omega_0 + hs_\Lambda(\gamma_1 + \gamma_2) \\ h\, c_\Lambda(\gamma_1 - \gamma_2) \\ b\, c_\Lambda(\gamma_1 + \gamma_2) \end{bmatrix} - Q_0 \begin{bmatrix} -c_\Lambda(\gamma_1 + \gamma_2) \\ s_\Lambda(\gamma_1 - \gamma_2) \\ 2(-\omega_1 + \omega_2)/\omega_0 \end{bmatrix} = \begin{bmatrix} M_{ex} \\ M_{ey} \\ M_{ez} \end{bmatrix} \quad (3.44)$$

3.10 Euler Angles

In the aircraft reference frame aligned with its principal axes, the aircraft roll, pitch and yaw rates are then, respectively (Etkin, 1996, pg. 104):

$$\frac{d\phi}{dt} = \Omega_x + (\Omega_y \sin\phi + \Omega_z \cos\phi)\tan\theta \quad (3.45)$$

$$\frac{d\theta}{dt} = \Omega_y \cos\phi - \Omega_z \sin\phi \quad (3.46)$$

$$\frac{d\psi}{dt} = (\Omega_y \sin\phi + \Omega_z \cos\phi)\sec\theta \quad (3.47)$$

These angles will be used extensively in the following Chapters.

3.11 Conclusion

This chapter has developed the linearized and separated equations of angular motion (3.44) for the airframe, and for the pods relative to the airframe (3.36). The latter equations will be necessary for both of the following stability chapters. The highlighted line in (3.44) is the pitch equation of motion. It will be used in Chapter 4 to determine aircraft pitch stability while legitimately ignoring (setting to zero) motion of the aircraft in the other directions.

The line above the highlighted one in (3.44) is the roll equation of motion, and the one below it is the yaw equation of motion. They will be used simultaneously in Chapter 5 to determine the coupled stability of the aircraft in these directions while justifiably ignoring pitch.

Chapter Four: Pitch Stability

4.1 Introduction

The equations derived in the previous chapter are used here to analytically determine whether a hovering bicopter with freely (or semi-freely) tilting proprotors can be self-stabilized in pitch.

4.1.1 Parameter Constraints and Pitch-only Equations of Motion

The moments on the airframe about the pitch axis are highlighted in (3.44). Because of the use of the small disturbance theorem, there are no rolling or yawing motion terms in this line. It is also apparent from (3.44) that the means by which roll and yaw are controlled, namely differential tilting ($\Delta\gamma_2 = \Delta\gamma_1$) and differential speed changes ($\Delta\omega_2 = -\Delta\omega_1$), have no effect on aircraft pitch.

These facts mean that, for the linearized system, pitching motion – and, more specifically, pitch stability – is independent of yaw and roll. Therefore, the pitch stability of this system can be legitimately investigated while specifying that roll and yaw remain zero, that proprotor tilting is equal and *collective* only, and that proprotor speeds are equal and constant. Consistent with the superposition principle for linear systems, the results can then be superimposed upon the case of general motion. Using $\Omega_x = \Omega_z = 0$, its operation will be symmetric about the x-z plane and have the following constraints:

$$\gamma_2 = -\gamma_1 \equiv -\gamma\,, \qquad \omega_2 = \omega_1 = \omega_0\,, \qquad C_2 = -C_1 \equiv -C \tag{4.1}$$

Since the proprotor speeds are fixed at their nominal value, their thrusts and drag torques will also be constant at their nominal hover values T_0 and Q_0 respectively.

From Section 3.9 the pitch rate of the aircraft is $\frac{d\theta}{dt} = \Omega_y$. These constraints are depicted in Figure 4-1. Substituting them into the pitch portion of (3.44) yields:

$$½I_\theta \frac{d^2\theta}{dt^2} - I_R\omega_0 s_\Lambda \left(c_\Lambda \frac{d\theta}{dt} + \frac{d\gamma}{dt}\right) - (hT_0 c_\Lambda + Q_0 s_\Lambda)\gamma - c_\Lambda C = \frac{1}{2} M_{ey} \tag{4.2}$$

where $½I_\theta = \frac{1}{2} I_{ay} + I_P s_\Lambda^2$. Substituting the constraints into either pod equation (3.36a) or (3.36b) with $\Omega_x = \Omega_z = 0$, and including an external disturbing moment M_{ep} for both, results in the same single equation:

$$I_P c_\Lambda \frac{d^2\theta}{dt^2} + I_P \frac{d^2\gamma}{dt^2} + I_R\omega_0 s_\Lambda \frac{d\theta}{dt} + C = M_{ep} \tag{4.3}$$

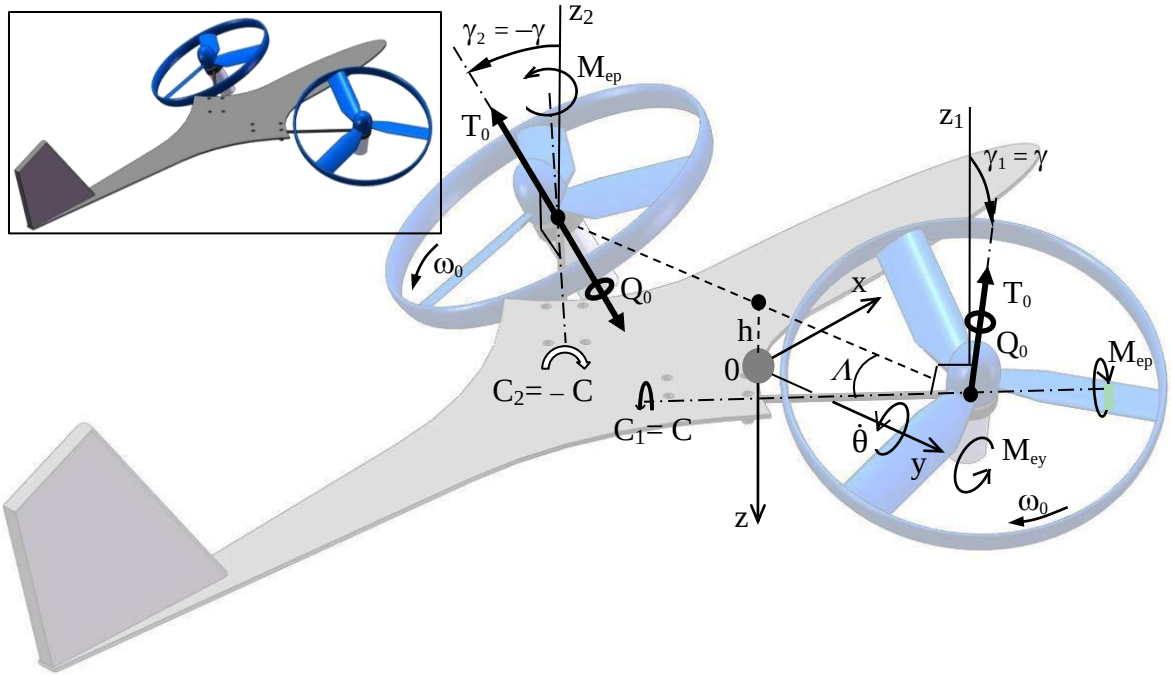

Figure 4-1. Pitch-only schematic showing constraints on proprotor variables. Rotors always tilt collectively by same amount. Rotor speeds are equal and constant and therefore so are thrusts and drag torques.

Equations (4.2) and (4.3) fully describe the system in pitch, and determine the pod tilt angle γ and aircraft pitch angle θ as functions of time t.

4.1.2 Equations of motion in terms of non-dimensional time τ

To make the analysis universal it will be convenient to express the equations of motion non-dimensionally. The first step in this direction is to define a non-dimensional time $\tau = \omega_0 t$ and replace t with τ/ω_0 in the equations, yielding:

$$½I_\theta\omega_0^2\frac{d^2\theta}{d\tau^2} - I_R\omega_0^2 s_\Lambda\left(c_\Lambda\frac{d\theta}{d\tau}+\frac{d\gamma}{d\tau}\right) - (hT_0c_\Lambda + Q_0 s_\Lambda)\gamma - c_\Lambda C = ½M_{ey} \quad (4.2')$$

$$I_P\omega_0^2 c_\Lambda\frac{d^2\theta}{d\tau^2} + I_P\omega_0^2\frac{d^2\gamma}{d\tau^2} + I_R\omega_0^2 s_\Lambda\frac{d\theta}{d\tau} + C = M_{ep} \quad (4.3')$$

The use of ω_0 in this fashion is not arbitrary; as Appendix A shows, ω_0 and the aircraft's natural frequency of oscillation change in the same proportion as the scale of the aircraft is changed. Therefore, with this transformation, geometrically similar aircraft of different sizes will have the same τ-response. The transformation also allows the remaining coefficients to be properly non-dimensionalized in subsequent sections.

4.2 State-space Eigenvalues: Unstable Aircraft with Freely Tilting Pods.

Stability of the system is determined here using the natural frequency approach of state-space analysis (Franklin, 2010, pp. 438-439). External disturbances M_{ey} and M_{ep} are set to zero and, though doing so allows the rotor pods to freely rotate without restraint, control/corrective input C is made zero for now as well. Coupled equations (4.2) and (4.3) can then be written in the state-space form as

$$\dot{\mathbf{x}} = \mathbf{A}\mathbf{x} \tag{4.4}$$

Assuming some initial conditions $\mathbf{x}(0) = \mathbf{x}_0$, and that the resulting responses of the entire system are at the same natural frequency, the state can then be written as

$$\mathbf{x}(\tau) = e^{\lambda_i \tau}\mathbf{x}_0 \tag{4.5}$$

where the coefficients λ_i are to be determined. Differentiating (4.5) and substituting it and the result into (4.4) yields

$$\lambda_i e^{\lambda_i \tau}\mathbf{x}_0 = \mathbf{A}e^{\lambda_i \tau}\mathbf{x}_0 \tag{4.6}$$

or

$$\lambda_i \mathbf{x}_0 = \mathbf{A}\mathbf{x}_0 \tag{4.7}$$

Equation (4.7) can be rewritten as

$$(\mathbf{A} - \lambda_i \mathbf{I})\mathbf{x}_0 = 0 \tag{4.8}$$

which constitutes the conventional eigenvalue problem. For a non-zero $\mathbf{x}_0$, (4.8) has a solution if and only if

$$\det(\mathbf{A} - \lambda_i \mathbf{I}) = 0 \tag{4.9}$$

which is a polynomial in the eigenvalues λ_i, known as the characteristic equation. The system unknowns can be written in state-space form as:

$$x_1 = \gamma \tag{4.10a}$$

$$x_2 = \dot{\gamma} = \dot{x}_1 \tag{4.10b}$$

$$\dot{x}_2 = \ddot{\gamma} \tag{4.10c}$$

$$x_3 = \dot{\theta} \tag{4.10d}$$

$$\dot{x}_3 = \ddot{\theta} \tag{4.10e}$$

where it is noted that the pitch angle θ is not represented since only its derivatives appear in equations of motion (4.2') and (4.3'). This means that only the stability of the pitch *rate* can be established in this analysis, and not that of the pitch *angle*. Substituting definitions (4.10) into the equations of motion, with $C = 0$ and $M_{ey} = M_{ep} = 0$, yields

$$\dot{x}_3 - r_y s_\Lambda (c_\Lambda x_3 + x_2) - q_y x_1 = 0 \tag{4.11}$$

$$c_\Lambda \dot{x}_3 + \dot{x}_2 + \frac{r_y}{p_y} s_\Lambda x_3 = 0 \tag{4.12}$$

where

$$p_y = \frac{I_P}{½I_\theta} \tag{4.13a}$$

$$q_y = \frac{hT_0 c_\Lambda + Q_0 s_\Lambda}{½I_\theta \omega_0^2} \tag{4.13b}$$

$$r_y = \frac{I_R}{½I_\theta} \tag{4.13c}$$

Note that all of these new variables are independent of scale. That is, they will have the same values for geometrically similar aircraft of different size.

Eliminating $\dot{x}_3$ between (4.11) and (4.12) gives a state equation in derivative $\dot{x}_2$ alone:

$$\dot{x}_2 + r_y s_\Lambda c_\Lambda x_2 + r_y s_\Lambda \left(c_\Lambda^2 + \frac{1}{p_y} \right) x_3 + q_y c_\Lambda x_1 = 0 \tag{4.14}$$

Collecting and writing state equations (4.10b), (4.11) and (4.14) in the matrix form of (4.4) produces

$$\begin{bmatrix} \dot{x}_1 \\ \dot{x}_2 \\ \dot{x}_3 \end{bmatrix} = \underbrace{\begin{bmatrix} 0 & 1 & 0 \\ -q_y c_\Lambda & -r_y s_\Lambda c_\Lambda & -r_y s_\Lambda \left(c_\Lambda^2 + \frac{1}{p_y} \right) \\ q_y & r_y s_\Lambda & r_y s_\Lambda c_\Lambda \end{bmatrix}}_{\mathbf{A}} \begin{bmatrix} x_1 \\ x_2 \\ x_3 \end{bmatrix} \tag{4.15}$$

Therefore, from (4.9), the characteristic equation is obtained from the solution of

$$\det\begin{bmatrix} -\lambda & 1 & 0 \\ -q_y c_\Lambda & -r_y s_\Lambda c_\Lambda - \lambda & -r_y s_\Lambda \left(c_\Lambda^2 + \frac{1}{p_y}\right) \\ q_y & r_y s_\Lambda & r_y s_\Lambda c_\Lambda - \lambda \end{bmatrix} = 0 \tag{4.16}$$

which is

$$\lambda^3 + \left[\frac{(r_y s_\Lambda)^2}{p_y} + q_y c_\Lambda\right]\lambda + \frac{q_y r_y s_\Lambda}{p_y} = 0 \tag{4.17}$$

According to the Routh-Hurwitz stability criterion (Franklin, 2010, pp. 132-134), all coefficients of the characteristic equation must be positive and therefore they must exist. However, the second-order term in (4.17) is missing and therefore the system as defined is unstable. This is supported by the Simulink model of Section 4.7; in it the amplitude of the pitch oscillations increases continuously with time after a pulse or step pitch disturbance.

4.3 Dampers between pods and airframe

The fact that moment C was set to zero for the analysis, thereby allowing the proprotor pods to tilt freely without restraint, offers a clue to the cause of this instability. The pitch disturbing moment causes tilting of the proprotors which, in turn, provides resistance to that moment. But at some point the motion must be abated and energy absorbed.

With nothing in the system as defined so far which accomplished this, it was surmised by the author that viscous dampers might be suitable. This choice was later

substantiated by knowledge of the ship anti-roll device shown in Section 2.2.3. Such dampers, illustrated in Figure 4-2, were therefore installed between the pods and airframe in the mathematical model. The interface moment C is then given by:

$$C = k_d \frac{d\gamma}{dt} \qquad \left(= k_d \omega_0 \frac{d\gamma}{d\tau}\right) \tag{4.18}$$

where k_d is an as-yet unspecified damping coefficient. Equation (4.18) typically represents a rotary viscous fluid-type damper with internal rotor and stator (Fig. 4-2a), but also can be used to approximate a linear damper connected to a control arm (Fig. 4-2b). The introduction of a damper also provides a means by which the pilot can control the tilting of the pods while still allowing self-stabilization, as shown in Fig. 4-2c.

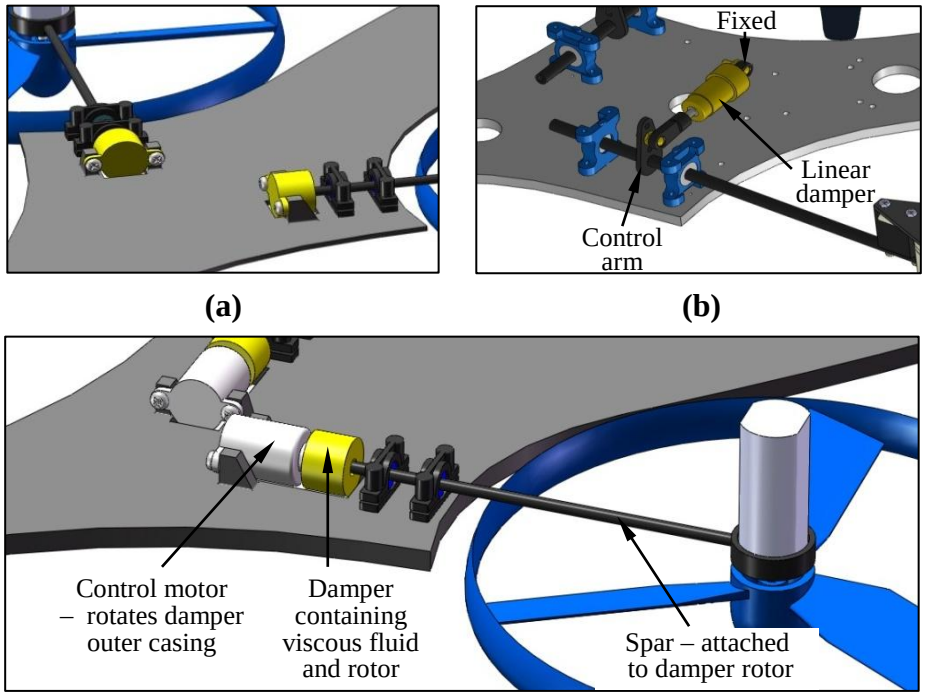

Figure 4-2. a) Aircraft underside with rotational dampers (yellow) installed between rotor pods and airframe. b) Alternate design using linear damper (one of two shown). Free end is fixed to airframe. c) Means by which the pilot can control pod while still allowing self-stabilization. In the case of the linear damper the pilot would control the motion of the damper end.

4.3.1 New characteristic equation

Substituting this new definition for C into equations of motion (4.2') and (4.3'), and applying the state-space methods of the preceding section to them yields the new condition

$$\det\begin{bmatrix} -\lambda & 1 & 0 \\ -q_y c_\Lambda & -r_y s_\Lambda c_\Lambda - k_{dy}^*\left(c_\Lambda^2 + \frac{1}{p_y}\right) - \lambda & -r_y s_\Lambda\left(c_\Lambda^2 + \frac{1}{p_y}\right) \\ q_y & r_y s_\Lambda + c_\Lambda k_{dy}^* & r_y s_\Lambda c_\Lambda - \lambda \end{bmatrix} = 0 \qquad (4.19)$$

where

$$k_{dy}^* = \frac{k_d}{\frac{1}{2} I_\theta \omega_0} \qquad (4.20)$$

The solution of (4.19) yields the new characteristic equation

$$\lambda^3 + k_{dy}^*\left(\frac{1}{p_y} + c_\Lambda^2\right)\lambda^2 + \left[\frac{\left(r_y s_\Lambda\right)^2}{p_y} + q_y c_\Lambda\right]\lambda + \frac{q_y r_y s_\Lambda}{p_y} = 0 \qquad (4.21)$$

with the rotational damper providing the missing second-order term, and therefore the system can be stable since all coefficients are now positive.

There are further requirements for the system to be stable, but before investigating these it is worth noting that (4.21) immediately shows the system to be unstable if:

1. the tilting is purely longitudinal ($\sin \Lambda = 0$).
2. the proprotor is massless or has no inertia ($I_R = 0$).
3. there are no proprotor aerodynamic vectoring components ($q_y = 0$).

Upon multiplication of (4.21) by p_y, it is also readily apparent that the characteristic equation is third-order solely because of pod inertia. However, unlike for non-proportionally controlled OAT bicopters (Section 2.1.3.1), the third-order term here is not destabilizing.

4.3.2 Further Routh-Hurwitz criteria for stability

The additional Routh-Hurwitz condition for stability of a third-order system, introduced in Section 2.3.5.2, is repeated here, where the polynomial

$$x^3 + a_1x^2 + a_2x + a_3 = 0 \tag{4.22}$$

must satisfy

$$a_1a_2 > a_3 \tag{4.23}$$

Applying this condition to the characteristic equation (4.21) shows that k_{dy}^* must be greater than a certain positive value for stability, the marginal-stability value k_{dys}^*:

$$k_{dy}^* > \frac{q_y r_y s_\Lambda}{\left(1 + p_y c_\Lambda^2\right)\left[\frac{\left(r_y s_\Lambda\right)^2}{p_y} + q_y c_\Lambda\right]} \equiv k_{dys}^* \tag{4.24}$$

The Simulink model responses of Section 4.7 confirm this result, with oscillations at constant amplitude for $k_{dy}^* = k_{dys}^*$. From Appendix B data, k_{dys}^* for the Nymbus is 0.000902. For the case of purely lateral tilting, $\Lambda = 90$ degrees, (4.24) reduces to

$$k_{dy90}^* > \frac{q_y}{p_y} \equiv k_{dys90}^* \tag{4.25}$$

4.3.3 Steady-state Tilt Angle γ and Pitch Angle θ after a Step Disturbance

Here only the effect of the airframe disturbing moment M_{ey} is considered. If it is constant after its initial application (and therefore a step disturbance), then for a steady state to exist the thrust and drag-torque vectors must exactly counter that disturbing moment. Setting all of the derivatives in (4.2) to zero uniquely determines the rotor tilt angle tilt angle in the steady state:

$$\gamma_\infty \;=\; \frac{-½M_{ey}}{hT_0c_\Lambda + Q_0s_\Lambda} \;=\; -\frac{M^*_{ey}}{2q_y} \tag{4.26}$$

where

$$M^*_{ey} \;=\; \frac{M_{ey}}{½I_\theta\omega_0^2}$$

To find the corresponding steady-state pitch angle of the aircraft, equation (4.3) can be integrated (after replacing C with (4.18) and ignoring the integration constant, i.e., assuming the initial values are zero), yielding:

$$I_Pc_\Lambda\frac{d\theta}{d\tau} \;+\; I_Rs_\Lambda\theta \;=\; -I_P\frac{d\gamma}{d\tau} \;-\; \frac{k_d}{\omega_0}\gamma \tag{4.27}$$

or

$$\frac{d\theta}{d\tau} \;+\; \frac{I_Rs_\Lambda}{I_Pc_\Lambda}\theta \;=\; -\frac{1}{c_\Lambda}\left[\frac{d\gamma}{d\tau} + \frac{k_d}{I_P\omega_0}\gamma\right] \tag{4.27′}$$

Setting the derivatives in (4.27) to zero gives the steady-state pitch angle:

$$\theta_\infty \;=\; -\frac{k_d}{I_R\omega_0s_\Lambda}\,\gamma_\infty \;=\; -\frac{k^*_{dy}}{r_ys_\Lambda}\,\gamma_\infty \tag{4.28}$$

Eliminating γ_∞ in (4.28) using (4.26) gives the steady-state pitch angle in terms of M^*_{ey} :

$$\theta_\infty \;=\; \frac{½k_d\,M_{ey}}{I_R\omega_0s_\Lambda(hT_0c_\Lambda + Q_0s_\Lambda)} \;=\; \frac{k^*_{dy}M^*_{ey}}{2r_yq_ys_\Lambda} \tag{4.29}$$

4.3.4 Proprotor Axes in Vertical Plane in Steady-state (but not during transient)

Generally, for the aircraft not to translate horizontally during pitching, it is desirable that the proprotor axes remain in the vertical plane. From geometry, the angle relationship ensuring this is

$$\tan\theta \;=\; -\,c_{\Lambda}\cdot\tan\gamma \tag{4.30}$$

which, for small θ and γ, can be approximated as:

$$\theta \;=\; -\,c_{\Lambda}\cdot\gamma \tag{4.31}$$

Comparing (4.31) with (4.28) produces the relations that make the prop axes coincident with the vertical plane in the steady state as shown in Figure 4-3:

$$k_d \;=\; I_R\,\omega_0 s_{\Lambda} c_{\Lambda} \;=\; \frac{1}{2} I_R\,\omega_0 \sin 2\Lambda \;\equiv\; k_{dv} \tag{4.32}$$

or

$$k^*_{dy} \;=\; \frac{1}{2} r_y s_{2\Lambda} \;\equiv\; k^*_{dyv} \tag{4.32'}$$

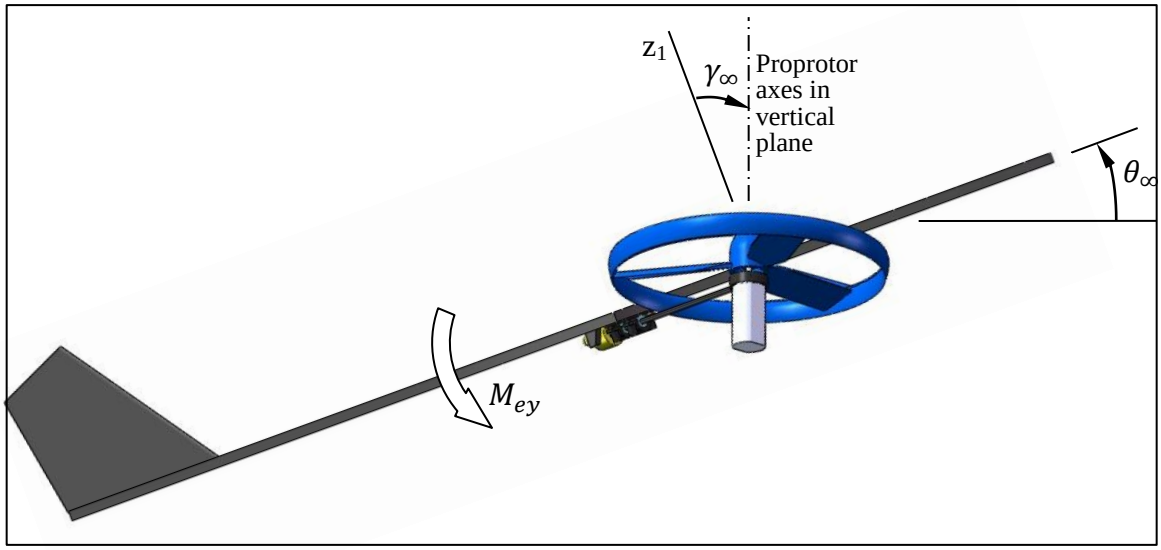

Figure 4-3. Stead-state proprotor axes can lie in vertical plane per (4.32)

However, satisfying this condition does not mean that the proprotor axes will stay in the vertical plane during the transient part of the response. This would require (4.31) to be satisfied for all times τ, which of course not only implies synchronous tilting – i.e., the tilt angle being in phase with the pitch angle (actually 180 degrees out of phase because they are of opposite sign) – but also that the tilting is of sufficient magnitude. Satisfying both conditions is physically impossible with the present system, as is shown in the next section.

4.3.5 Synchronous tilting

From inspection of (4.27 and (4.27'), synchronous or in-phase tilting can only occur when either $I_P = 0$ or

$$\frac{I_R s_\Lambda}{c_\Lambda} = \frac{k_d}{\omega_0} \tag{4.33}$$

with the latter being the more realistic condition. Rearranging it gives

$$k_d = I_R \omega_0 \frac{s_\Lambda}{c_\Lambda} \equiv k_{dsyn} \tag{4.33'}$$

$$k_{dy}^* = r_y \frac{s_\Lambda}{c_\Lambda} \equiv k_{dysyn}^* \tag{4.33''}$$

From (4.27') the resulting proportional relationship between pitch and tilt for this damping coefficient is:

$$\theta(\tau) = -\frac{1}{c_\Lambda}\gamma(\tau) \tag{4.34}$$

which gives a magnitude for tilt angle that is less than that required for vertical-plane proprotor axes, given by (4.31).

4.3.6 Effect of Increasing Payload Mass on Aircraft Stability

Adding a point mass payload at the aircraft center of mass will not increase the airframe inertia I_θ , and so the parameters p_y , q_y and r_y defined in (4.13) will not change either. The characteristic equation (4.21) will then remain unchanged if the non-dimensional damping coefficient k_{dy}^* is kept constant (by maintaining ratio $\frac{k_d}{\omega_0}$), and the aircraft will have the same hover stability characteristics as before.

However, in a more realistic scenario, the payload will have dimensions and not be located at the aircraft center of mass. In the general case, then, I_θ and ω_0 will both increase with added payload. Multiplying (4.21) through by p_y gives

$$p_y \lambda^3 + k_{dy}^*\left(1 + p_y c_\Lambda^2\right)\lambda^2 + \left[\left(r_y s_\Lambda\right)^2 + p_y q_y c_\Lambda\right]\lambda + q_y r_y s_\Lambda = 0 \qquad (4.21')$$

The two lowest order coefficients of (4.21') will decrease in magnitude with increasing I_θ^2, indicating reduced relative effectiveness of the gyroscopic and thrust-torque terms. However, k_{dy}^* predominates the second-order coefficient and, for a given k_d , it decreases with increasing $I_\theta \omega_0$. Whether or not $I_\theta \omega_0$ increases faster than I_θ^2 (and therefore whether ω_0 increases faster than I_θ) will depend on how the additional payload is distributed in the aircraft. If they increase at the same rate then the system behaviour in non-dimensional time - except for third-order effects due to (non-dim.) pod inertia p_y - will be independent of payload mass.

In any case the coefficients of (4.21') will always remain positive when increasing payload mass, but it is the additional third-order stability requirement (4.24) that raises the lower limit for k_d as ω_0 and I_θ are increased.

4.3.7 Comparison to Stability of OAT Aircraft for Zero Pod Inertia

Rewriting the equation of pitching motion (2.3) for an OAT aircraft equipped with proportional controller (without time delay), and using

- non-dimensional time, $\tau = \omega_0 t$, and parameter definitions (4.13)
- controller gain k_p from (2.5)
- I_θ in place of I_{Ay}, using (3.26) and the definition following (4.2)
- a solution for θ of $\theta_0 e^{\lambda\tau}$

it becomes the explicit characteristic equation

$$c_\Lambda\left(1 - p_y\, s_\Lambda^2\right)\lambda^2 \;+\; r_y\, s_\Lambda\, \lambda \;+\; q_y \;=\; 0 \qquad (2.3')$$

which, for zero pod inertia ($p_y = 0$), becomes

$$c_\Lambda\, \lambda^2 \;+\; r_y\, s_\Lambda\, \lambda \;+\; q_y \;=\; 0 \qquad (2.3'')$$

Setting $p_y = 0$ in the passive system's characteristic equation gives

$$\frac{k_{dy}^*}{r_y\, s_\Lambda}\lambda^2 \;+\; r_y\, s_\Lambda\, \lambda \;+\; q_y \;=\; 0 \qquad (4.21'')$$

From (4.32'), for the proprotor spin axes to be in the vertical plane, $k_{dy}^* = r_y\, s_\Lambda\, c_\Lambda$. Substituting this into (4.21'') yields

$$c_\Lambda\, \lambda^2 \;+\; r_y\, s_\Lambda\, \lambda \;+\; q_y \;=\; 0$$

which is exactly the OAT characteristic equation (2.3") for $p_y = 0$. Of course the OAT system will, in practice, have a time delay and not be as stable (equation (2.8)) as indicated here. However, the pod contains the proprotor, and it will be seen in Chapter 6 that a very large proprotor inertia I_R is required to stabilize the passive system.

4.4 MATLAB/Simulink Model and Disturbance Response Simulations

A Simulink model for a pitching-only aircraft, based on the equations of motion (4.2') and (4.3'), was constructed to corroborate and visualize the analytical findings of the previous sections in this chapter. Data used was that of the Nymbus aircraft in Appendix B. The full code and further details of this model are contained in Appendix C.1.

A tilt path angle of $\Lambda = 45$ degrees was chosen for all simulation runs, partly because the effects of changing Λ – at least for an OAT vehicle – have been studied before (reproduced in Fig. 2-10), and because the intention was to consider roll stability in the same manner as pitch. That is, just as gyroscopic pitching moments arise from collective tilting of the proprotors, rolling moments result from their differential tilting. These rolling and pitching moments, then, will be equal if the tilt paths are oblique with $\Lambda = 45$ degrees.

Figures (4-5b,c) plot the aircraft's automatic tilt and pitch responses to the moderate step disturbing moment of $M_{ey} = 0.10Q_0$ shown in (4-5a) for values of k_{dy}^* ranging from 0 to that for vertical steady-state proprotor axes ($k_{dyv}^* = 0.0080$, from (4.32')). Note that actual time t rather than non-dimensional time τ has been used in the abscissa of these plots (by dividing τ by ω_0 , 520 sec^{-1}).

Equation (4.24) predicts a minimum k_{dy}^* of 0.0009 (= k_{dys}^*) for stability of a free-tilt Nymbus. This is confirmed from the Simulink plots, wherein the oscillation magnitude is constant for this k_{dy}^*. The steady-state tilt and pitch angles predicted by (4.26) and (4.29) are confirmed as well. The tilt-angle curves either converge toward or

oscillate about the predicted γ_∞ of -1.64 degrees. And, as predicted, the steady-state pitch angle θ_∞ – unlike γ_∞ – is a function of k_{dy}^*; this is because tilting slows with increasing k_{dy}^*, allowing the aircraft time to pitch further before equilibrium is reached.

Figures (4-6a, b) show aircraft responses for $k_{dy}^* \geq 0.0080$. From them it is apparent there is no advantage to going to high k_{dy}^* values; the tilt responses are slowed down excessively and the corresponding steady-state pitch angles are unnecessarily large. Inspecting the automatic tilt responses of Figures (4-5b) to (4-6a), it appears that the ideal rotary damper coefficient k_{dy}^* is just slightly less than the vertical-plane value k_{dyv}^* (= 0.0080) - as a compromise between short response time and a low number of oscillations. This ideal or optimal k_{dy}^* will derived in the next section.

Figures (4-7b-g) show the aircraft pitch responses to a pulse disturbance for the same k_{dy}^* values as the step-disturbance plots. As expected, they show temporary pitch excursions when k_{dy}^* is greater than the minimum stability value of 0.0009.

Figures 4-8 and 4-9 respectively show the effects of changing proprotor inertia r_y and of reducing height h on the aircraft's response to a step pitch disturbance.

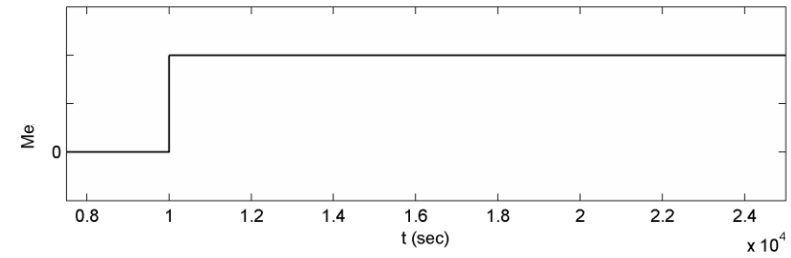

(a)

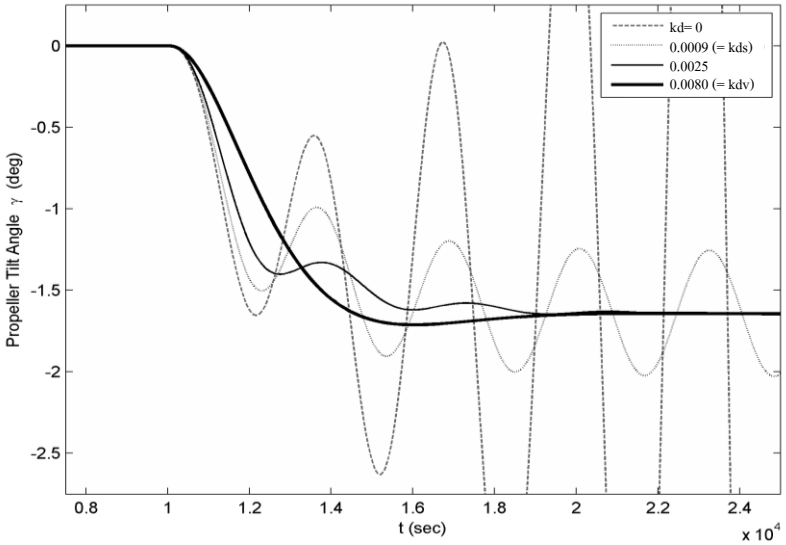

(b)

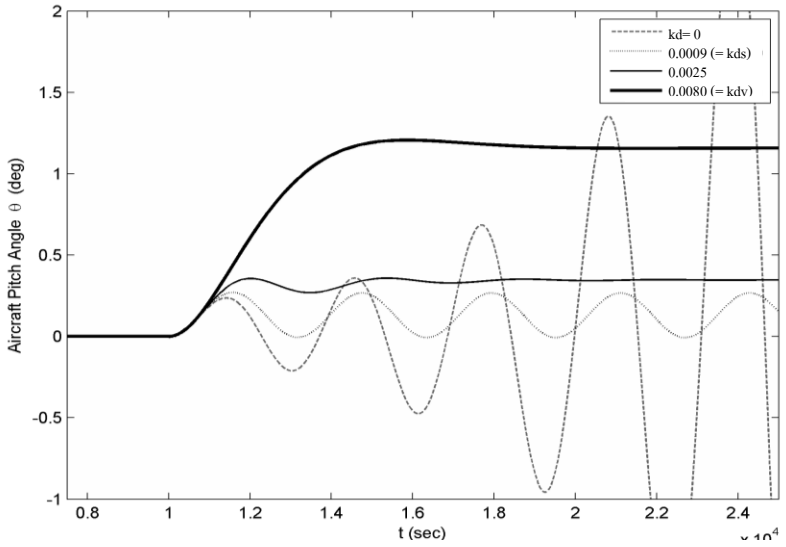

(c)

Figure 4-5. Simulation results using Simulink pitch-only model and Nymbus data. (a) Step pitch disturbance $M_{ey} = 0.10Q_0$. (b) Resulting automatic tilting of proprotors for various damping coefficients $k_{dy}^* \leq \frac{1}{2}r_y (= 0.0080)$ (kd in legend). (c) Corresponding pitching of aircraft.

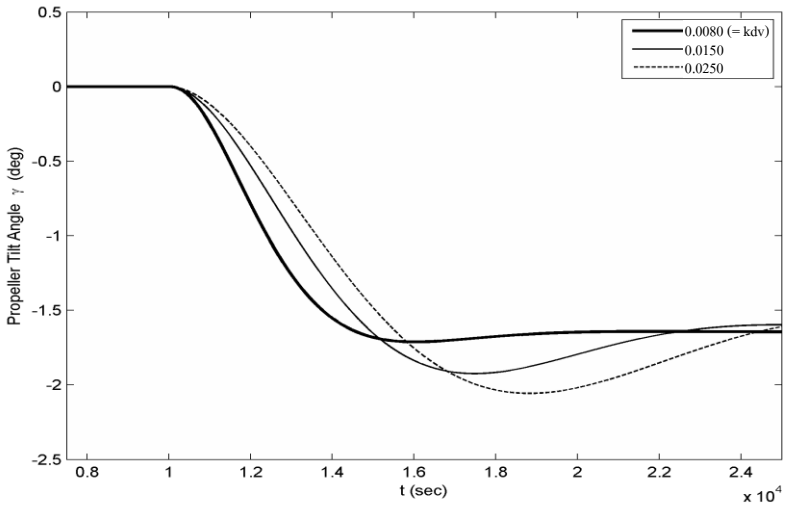

(a)

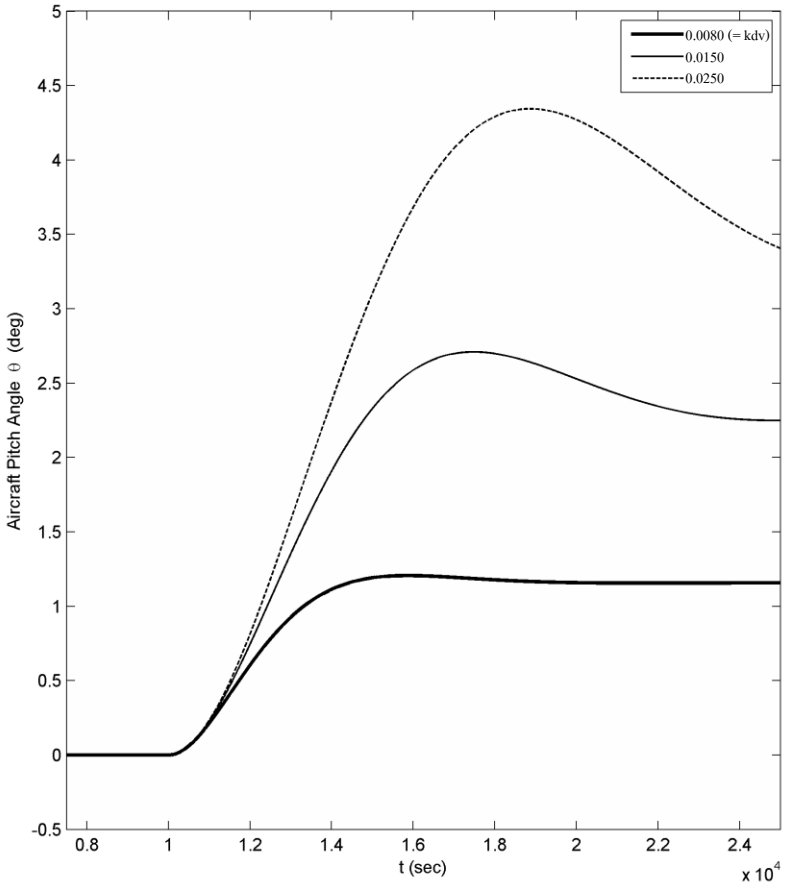

(b)

Figure 4-6. Response to step disturbance for $k^*_{dy} \geq 0.0080$

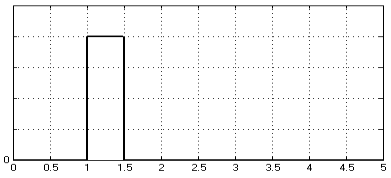

(a) Pulse disturbance $M_{ey} = 0.10Q_0$

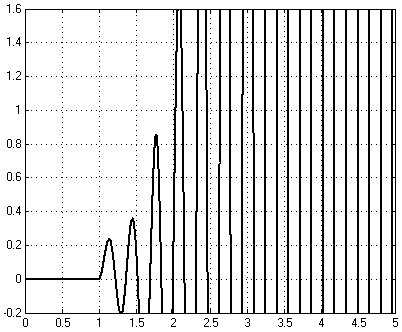

(b) $k^*_{dy} = 0$

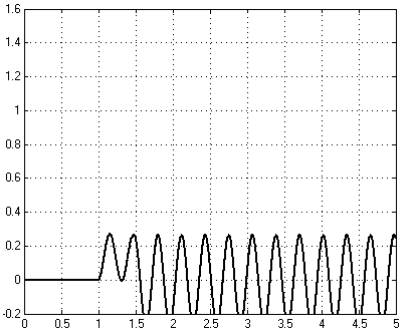

(c) $k^*_{dy} = 0.0009\ (= k^*_{ds})$

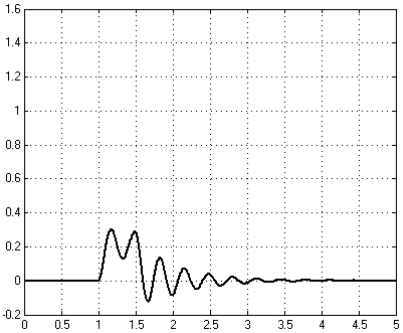

(d) $k^*_{dy} = 0.0015$

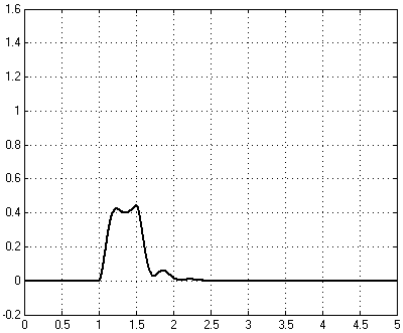

(e) $k^*_{dy} = 0.0030$

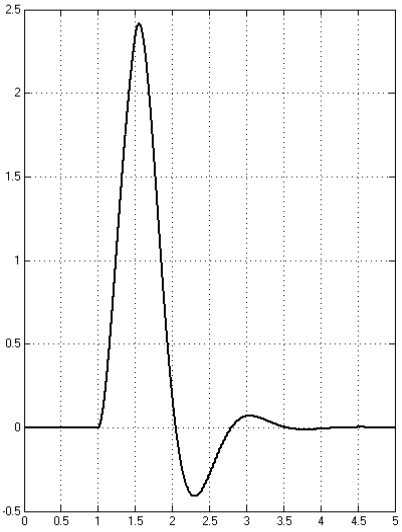

(g) $k^*_{dy} = 0.150$

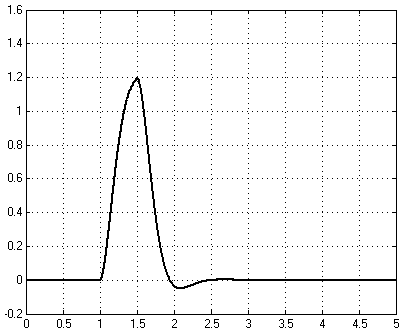

(f) $k^*_{dy} = 0.0080\ (= k^*_{dv})$

Figure 4-7. Pulse disturbance (a) and pitch responses θ (deg) for various damper coefficients k^*_{dy}.

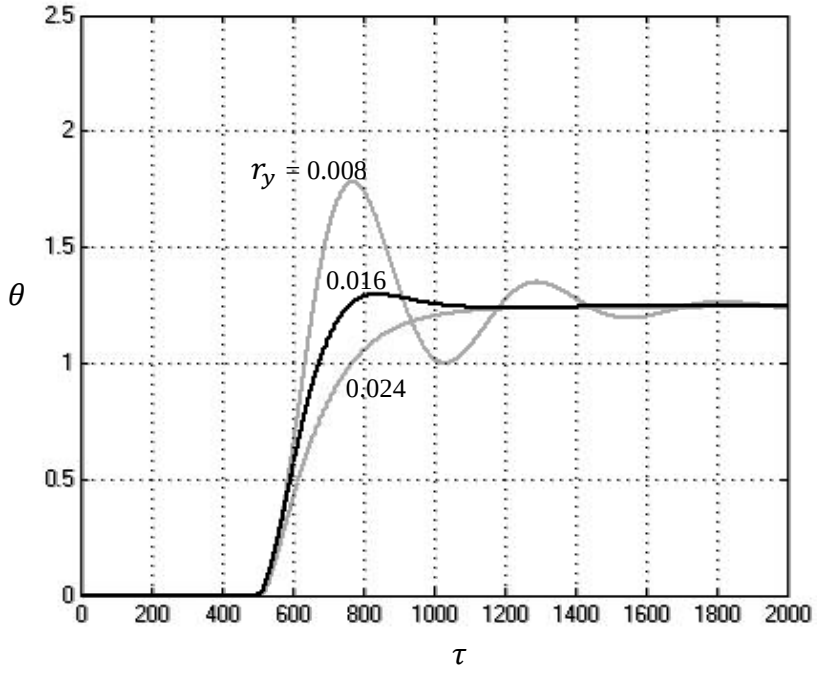

Figure 4-8. Effect of changing proprotor inertia r_y , with $k^*_{dy} = \frac{1}{2} r_y$

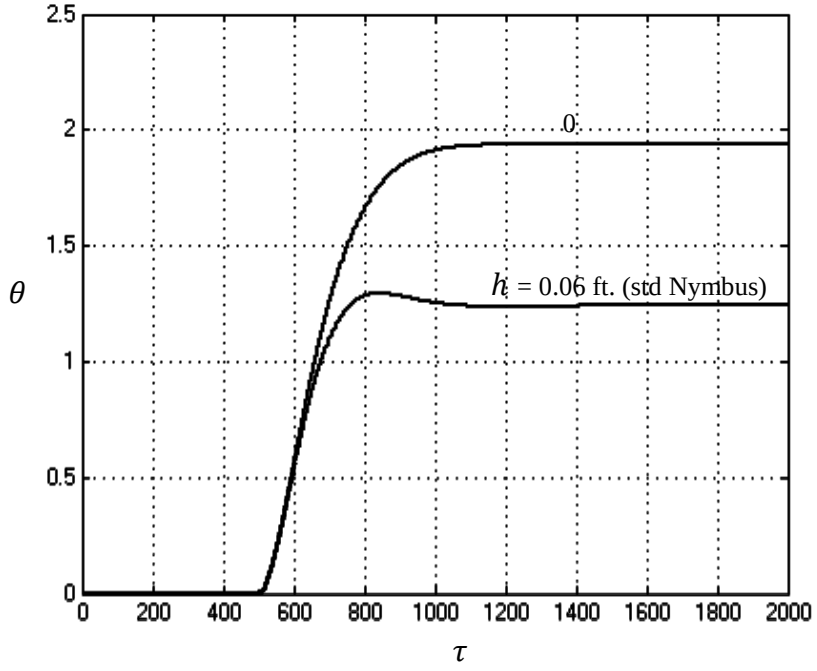

Figure 4-9. Effect of reducing height h to zero

4.5 Adding a pod centering spring: stabilization of pitch-rate only

4.5.1 The need for a centering spring

Though the damper introduced in Section 4.3 does stabilize the aircraft theoretically, in practice it is inadequate by itself because it cannot prevent drift of the pod tilt angle. A test-stand bicopter, shown in Figure 4.10, was constructed to observe the behaviour of the system developed so far. Though this bicopter resisted pitch disturbances as expected, the pods rotated for other reasons as well, listed here:

1. Construction/assembly tolerances. Proprotor spin axis must exactly intersect the pod tilt axis, otherwise a tilting moment will be generated by the offset thrust.
2. Aerodynamic imbalance. Items such as wires in the proprotor downwash will create drag forces that tend to tilt the pod.
3. Bias due to vibration. Tilting motion in one direction may be favoured over the other during operation, with the result that the pod cannot return to center.

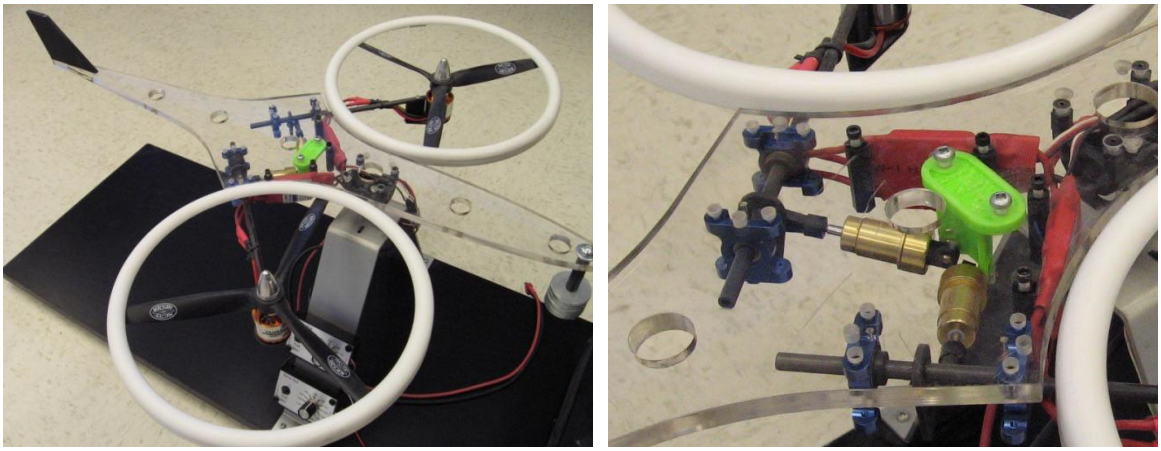

Figure 4-10. Experimental test-stand bicopter with close-up of dampers

Before the construction of this stand it was believed that drift – if any – could be corrected for by the pilot's control of the damper, but this was quickly dispelled during testing. It was concluded that a passive centering device such as a spring could be a possible remedy. In this section such a spring is incorporated into the mathematical model and its effects on the system analyzed.

Figure 4-11 shows the spring installed in parallel to a linear damper, which – because of the simplicity and ubiquity of this combination – is now the preferred type. The interface moment C between pod and airframe, previously given by (4.18), now becomes

$$C = k_d \frac{d\gamma}{dt} + k_s \gamma \qquad \left(= k_d \omega_0 \frac{d\gamma}{d\tau} + k_s \gamma \right) \tag{4.50}$$

where k_s accounts for the spring constant and length of the control arm. The spring – and consequently the spring-damper assembly – is bi-directional in that it can be compressed or extended from an equilibrium length which corresponds to zero tilt of the pod.

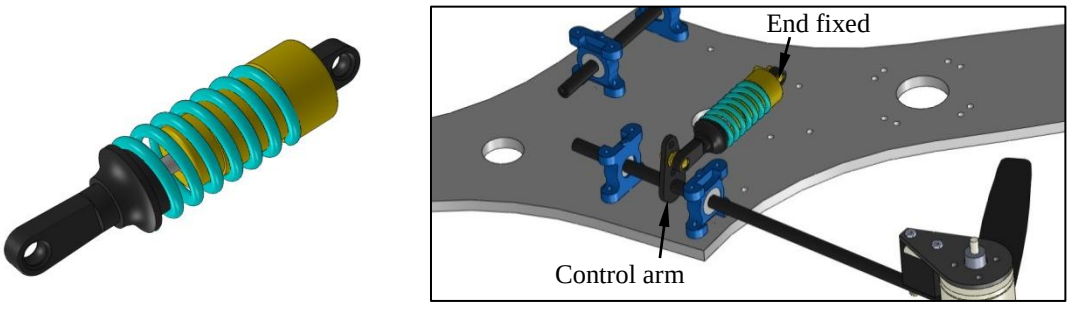

Figure 4-11. Bi-directional centering spring in parallel with linear damper

4.5.2 New characteristic equation

With this new definition for C, the state-space $\mathbf{A} - \lambda_i \mathbf{I}$ matrix of Sections 4.2 and 4.3 becomes:

$$\begin{bmatrix} -\lambda & 1 & 0 \\ -q_y c_\Lambda - k_{sy}^* \xi & -r_y s_\Lambda c_\Lambda - k_{dy}^* \xi - \lambda & -r_y s_\Lambda \xi \\ q_y + k_{sy}^* c_\Lambda & r_y s_\Lambda + k_{dy}^* c_\Lambda & r_y s_\Lambda c_\Lambda - \lambda \end{bmatrix} \tag{4.51}$$

where

$$k_{sy}^* = \frac{k_s}{\frac{1}{2} I_\theta \omega_0^2} \tag{4.52a}$$

$$\xi = c_\Lambda^2 + \frac{1}{p_y} \tag{4.52b}$$

Setting the determinant of (4.51) to zero yields the new characteristic equation for the system:

$$\lambda^3 + k_{dy}^* \xi \lambda^2 + \left[\frac{(r_y s_\Lambda)^2}{p_y} + q_y c_\Lambda + k_{sy}^* \xi \right] \lambda + \frac{q_y r_y s_\Lambda}{p_y} = 0 \tag{4.53}$$

from which it is seen that the spring is not destabilizing. However, it must be remembered that all the characteristic equations derived in this chapter, including (4.53), pertain to the pitch *rate*, and not the pitch *angle*; the state-space relations (4.10) do not contain a θ term (though the tilt angle γ is of course represented). So (4.53) can only be indicative of pitch-rate stability. That the pitch angle was also stabilized until now was somewhat fortuitous - as the next section shows.

4.5.3 Effect of spring on aircraft response to step disturbance

Figure 4-12 shows the result of adding a spring to the Simulink model studied in Figure 4-5 (for $k^*_{dy} = k^*_{dyv} = 0.0080$) and subject to a step pitch disturbance. There is

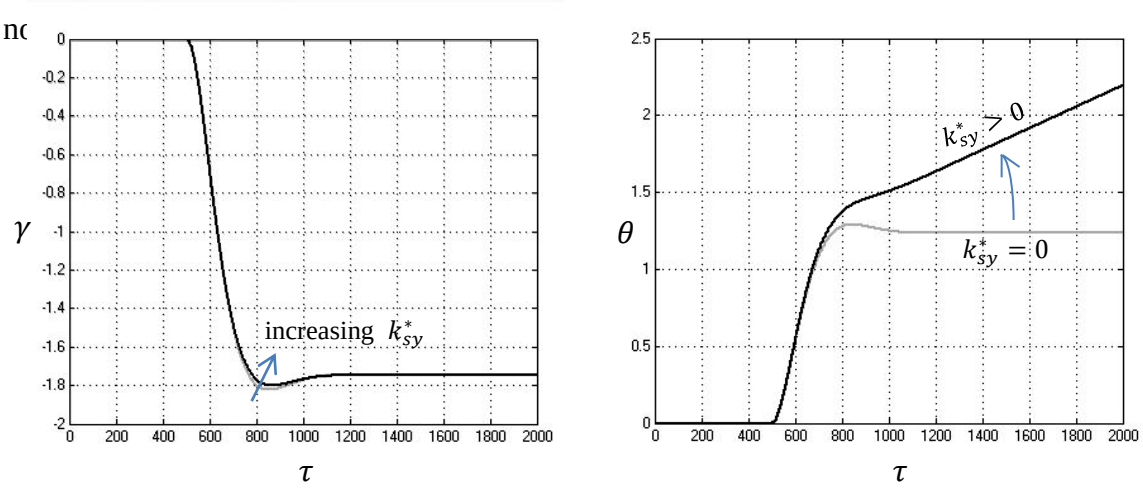

Figure 4-12. Effect of pod spring on aircraft response to step pitch disturbance. Same Simulink aircraft model as for Fig. 4-5, with $k^*_{dy} = k^*_{dyv} = 0.0080$.

no effect on the steady state value of the proprotor tilt angle, and very little effect on its transient. But it causes the aircraft to pitch continuously – at a constant rate – after the transient.

This is in effect a precession of the proprotors, the rate (of pitching) governed by gyroscopics, and the moments produced exactly balancing the external disturbing moment. They also counter the internal spring moment, allowing the tilt angle to remain constant even though the springs exert restoring moments tending to center the pods.

This tilt angle and pitch-rate can be predicted by redefining the steady-state to include rotation at constant angular velocity. Setting to zero, then, all the second-order terms (and M_{ep}) in the pitch equations of motion (4.2') and (4.3') gives:

$$-I_R\omega_0^2 s_\Lambda\left[c_\Lambda\frac{d\theta}{d\tau}+\frac{d\gamma}{d\tau}\right]_\infty-(hT_0c_\Lambda+Q_0s_\Lambda)\gamma_\infty-k_d\omega_0c_\Lambda\frac{d\gamma}{d\tau}\Big|_\infty-k_sc_\Lambda\gamma_\infty=\frac{M_{ey}}{2}\quad(4.54)$$

and

$$I_R\omega_0^2 s_\Lambda\frac{d\theta}{d\tau}\Big|_\infty+k_d\omega_0\frac{d\gamma}{d\tau}\Big|_\infty+k_s\gamma_\infty=0\qquad(4.55)$$

Note that, by definition of a step disturbance, $M_{ey}\equiv M_{ey\infty}$ in (4.54). Eliminating terms in (4.54) using (4.55) yields

$$-I_R\omega_0^2 s_\Lambda\frac{d\gamma}{d\tau}\Big|_\infty-(hT_0c_\Lambda+Q_0s_\Lambda)\gamma_\infty=\frac{M_{ey}}{2}\qquad(4.56)$$

The steady-state tilt rate must be zero, however. If it were a constant and $\neq 0$ then γ_∞would have to be infinite, which would contravene (4.56). Setting it to zero then gives the steady-state tilt angle:

$$\gamma_\infty=-\frac{M_{ey}}{2(hT_0c_\Lambda+Q_0s_\Lambda)}=-\frac{M_{ey}^*}{2q_y}\qquad(4.57)$$

which is independent of k_s and identical to the steady-state tilt angle derived previously (4.26). From (4.55) the steady-state pitch rate then is

$$\frac{d\theta}{d\tau}\Big|_\infty=\frac{k_sM_{ey}}{2(hT_0c_\Lambda+Q_0s_\Lambda)I_R\omega_0^2s_\Lambda}=\frac{k_{sy}^*M_{ey}^*}{2q_yr_ys_\Lambda}\qquad(4.58)$$

4.5.4 Effect of Spring on Aircraft Response to Pulse Disturbance

Even under a temporary or pulse disturbance, a bicopter with centering springs will become permanently disturbed. Equation (4.57) still applies in this case, with $M_{ey} = M_{ey\infty} = 0$ and therefore $\gamma_\infty = 0$. From (4.55) the steady-state pitch rate also becomes zero, and θ_∞ is now the unknown. To find it (4.2') and (4.3') need to be integrated, but first the finite pulse disturbance must be defined.

Disturbance $M_{ey}(\tau)$ is here considered to be arbitrary but finite in profile, operating over the finite interval (τ_a, τ_b), with $M_{ey} = 0$ for $\tau < \tau_a$ and $\tau > \tau_b$. Therefore the semi-infinite integral of the disturbance becomes

$$\int_0^\infty M_{ey}\, d\tau \quad = \quad \int_0^{\tau_a} 0\, dt \; + \int_{\tau_a}^{\tau_b} M_{ey}\, d\tau \; + \int_{t_b}^{\infty} 0\, d\tau \quad = \quad \int_{\tau_a}^{\tau_b} M_{ey}\, d\tau \qquad (4.59)$$

which must, by definition, be finite too. Integrating (4.2') and (4.3'), setting γ and all remaining derivatives to zero, yields

$$-I_R\omega_0^2 s_\Lambda c_\Lambda \theta_\infty - (hT_0 c_\Lambda + Q_0 s_\Lambda + k_s c_\Lambda)\int_0^\infty \gamma\, d\tau \;=\; \frac{1}{2}\int_{\tau_a}^{\tau_b} M_{ey}\, d\tau \qquad (4.60)$$

and

$$I_R\omega_0^2 s_\Lambda \theta_\infty \; + \; k_s \int_0^\infty \gamma\, d\tau \; = \; 0 \qquad (4.61)$$

Eliminating the γ-integral between (4.60) and (4.61) gives

$$\theta_\infty \;=\; \frac{k_s M_{ey}}{2(hT_0 c_\Lambda + Q_0 s_\Lambda) I_R \omega_0^2 s_\Lambda}\int_{\tau_a}^{\tau_b} M_{ey}\, d\tau$$

$$= \qquad \frac{k_{sy}^* M_{ey}^*}{2 q_y r_y s_\Lambda}\int_{\tau_a}^{\tau_b} M_{ey}\, d\tau \qquad (4.62)$$

Figure 4-13 shows these effects of the centering springs on the aircraft when it is subject to a temporary pitch disturbance.

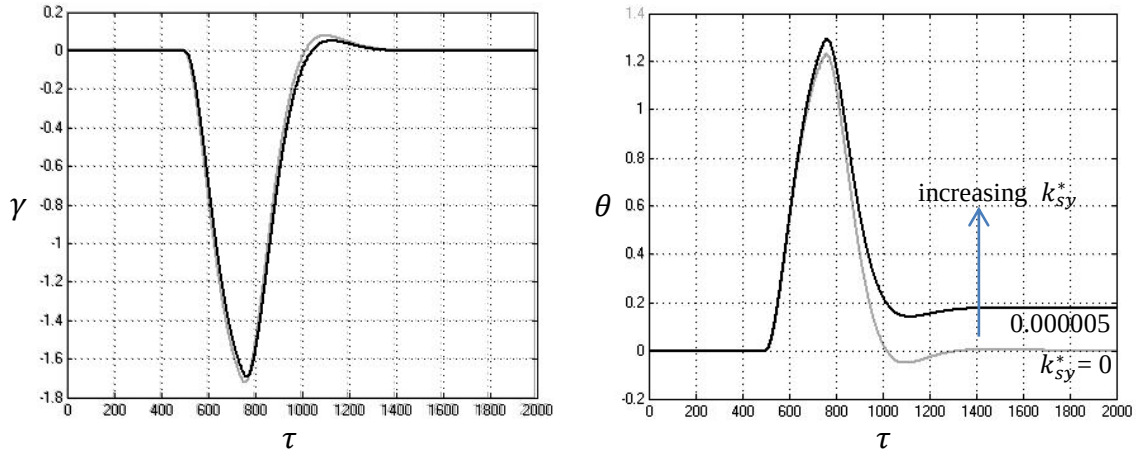

Figure 4-13. Effect of pod spring on aircraft's response to pulse disturbance. Same Simulink model as in Fig. 4-7, with $k^*_{dy} = k^*_{dyv} = 0.0080$.

The permanent pitch resulting from the disturbance implies that the aircraft will accelerate horizontally even after the disturbance has passed.

4.6 Adding a Pilot to Stabilize Aircraft Pitch

4.6.1 Modeling Aircraft Response to Pilot Input: Handling Qualities

That the aircraft under investigation is not stabilized in pitch (and roll) is very similar to the first production helicopters of the 1940's, where mechanical stabilizers such as the Bell flybar or the Hiller control rotor were really dampers, and only stabilized the pitch and roll angular velocities. These dampers effectively increased the period of helicopter oscillation to within a range that was manageable by the pilot. Therefore the pilot was an essential stabilizing element in these aircraft types. A combination of the two systems, the Bell-Hiller flybar referenced in Section 2.4, is still used today in R/C model aircraft.

In this section the response of the aircraft with spring and damper – from pilot input to the aircraft's output in pitch – is modeled and compared to the handling qualities standards established for full-size VTOL aircraft. Pilot control input δ here is the rotation angle of a servo arm which axially displaces the spring-damper's free-end as shown in Figure 4-14. The unseen servo is fixed to the airframe and the length l of its arm is the same as the pod's control arm. The input is positive when it tends to tilt the proprotor rearwards, i.e., when it tends to make γ positive as well. With these conventions the interface moment between pod and airframe is now:

$$C = k_d\left(\frac{d\gamma}{dt} - \frac{d\delta}{dt}\right) + k_s(\gamma - \delta) \tag{4.63}$$

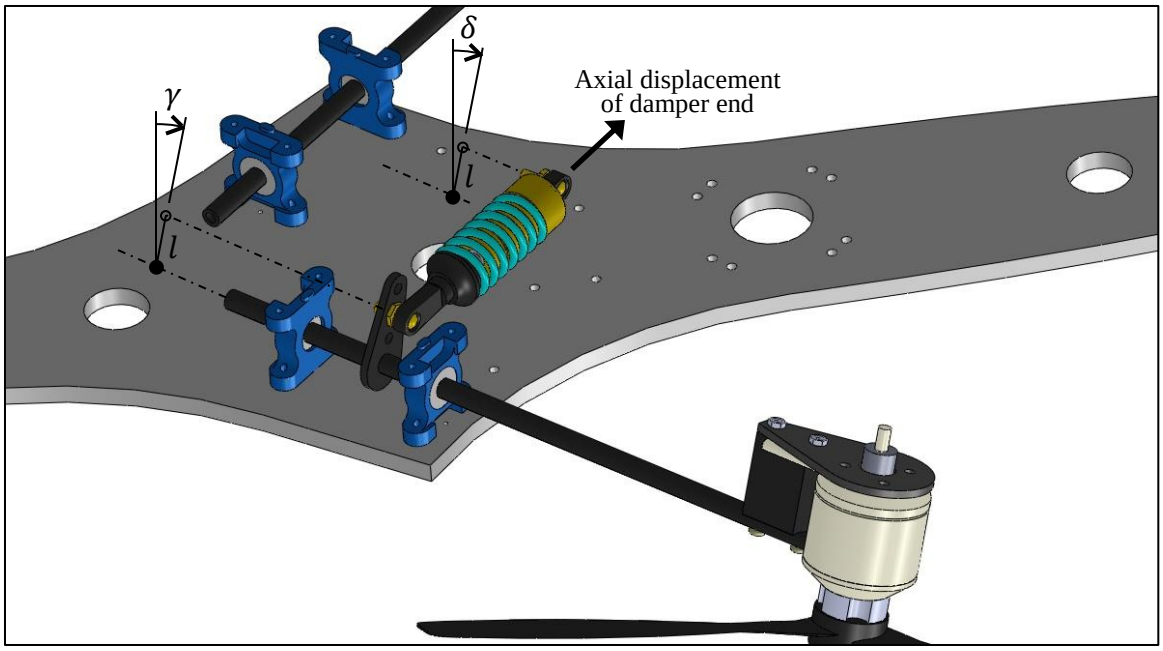

Figure 4-14. Aircraft underside showing pilot's servo control input δ and corresponding axial displacement of spring-damper end. Servo not shown.

If C is eliminated between the airframe and pod equations of motion ((4.2) and (4.3) respectively), and therefore without specifying what C is, the result is exactly the airframe equation of motion (2.1) for a general, unspecified γ, and which is repeated here:

$$(½I_\theta + I_P c_\Lambda^2)\frac{d^2\theta}{dt^2} + I_P c_\Lambda \frac{d^2\gamma}{dt^2} - I_R \omega_0 s_\Lambda \frac{d\gamma}{dt} - (hT_0 c_\Lambda + Q_0 s_\Lambda)\gamma = 0 \qquad (4.64)$$

where $½I_\theta + I_P c_\Lambda^2 = ½I_{Ay}$ (definition from (4.2) and (3.26)). In transfer function form the airframe is represented as

$$H(s) = \frac{\mathrm{L}\{\theta(t)\}}{\mathrm{L}\{-\gamma(t)\}} = \frac{\Theta(s)}{-\Gamma(s)}$$

$$= \frac{-I_P c_\Lambda \cdot s^2 + I_R \omega_0 s_\Lambda \cdot s + (hTc_\Lambda + Qs_\Lambda)}{(½I_\theta + I_P c_\Lambda^2)\cdot s^2} \qquad (4.65)$$

Substituting (4.63) into (4.3) (with $M_{ep} = 0$) yields the new pod relation, now having two inputs, θ and δ, and one output, γ:

$$I_P c_\Lambda \frac{d^2\theta}{dt^2} + I_R \omega_0 s_\Lambda \frac{d\theta}{dt} + I_P \frac{d^2\gamma}{dt^2} + k_d\left(\frac{d\gamma}{dt} - \frac{d\delta}{dt}\right) + k_s(\gamma - \delta) = 0 \qquad (4.66)$$

Representing it in transfer function form requires separation into two parallel parts, one for each of the inputs (Aziz, 2013). If the complete pod is $P(s)$, then the two parts are

$$P_\delta(s) = \frac{\mathrm{L}\{\gamma_\delta(t)\}}{\mathrm{L}\{\delta(t)\}} = \frac{\Gamma_\delta(s)}{\Delta(s)} = \frac{k_d \cdot s + k_s}{I_P \cdot s^2 + k_d \cdot s + k_s} \qquad (4.67a)$$

and

$$P_\theta(s) = \frac{-\Gamma_\theta(s)}{\Theta(s)} = \frac{I_P\, c_\Lambda \cdot s^2 + I_R\, \omega_0\, s_\Lambda \cdot s}{I_P \cdot s^2 + k_d \cdot s + k_s} \qquad (4.67b)$$

where

$$\Gamma(s) = \Gamma_\delta(s) + \Gamma_\theta(s) \qquad (4.68)$$

The corresponding transfer function diagram of the complete pitch system, including a block representing the human pilot (operating the aircraft by radio control) is shown in Figure 4-15.

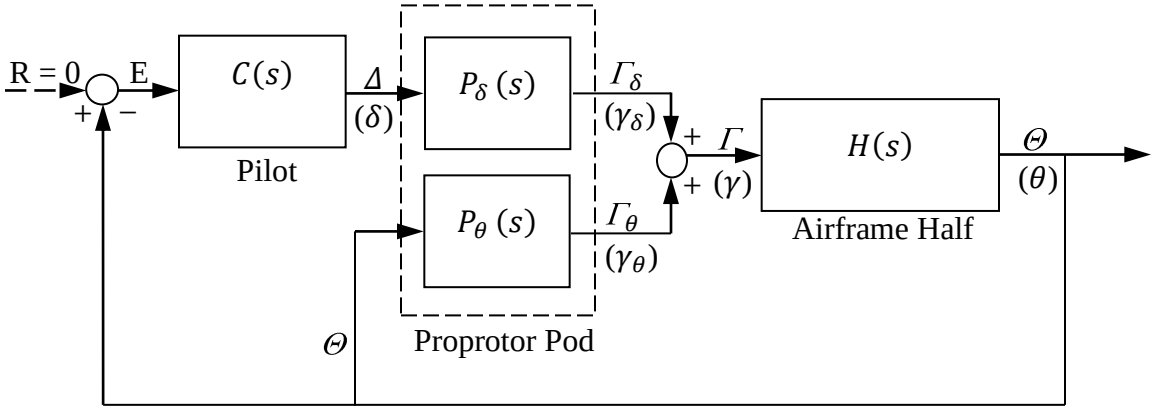

Figure 4-15. Aircraft pitch represented in transfer function form

The open loop transfer function, from pilot input δ to airframe output θ, is

$$\frac{\Theta(s)}{\Delta(s)} = \frac{P_\delta(s)H(s)}{1 + P_\theta(s)H(s)} \qquad (4.69)$$

The corresponding non-dimensional characteristic equation - using (4.65), (4.67), $s = \omega_0 \sigma$, and definitions (4.13) - is

$$\sigma \left\{ \sigma^3 \; + \; k^*_{dy}\, \xi \sigma^2 \; + \; \left[\frac{\left(r_y s_\Lambda\right)^2}{p_y} + q_y c_\Lambda \; + k^*_{sy}\, \xi \right] \sigma \; + \; \frac{q_y r_y s_\Lambda}{p_y} \right\} \; = \; 0 \qquad (4.70)$$

which of course is just the spring and damper aircraft characteristic equation (4.53) with an additional root at zero. This root signifies that the aircraft on its own cannot stabilize the pitch angle.

4.6.2 Root Locus vs. Spring Constant: Comparison to Roots recommended by military specifications and to those of OAT bicopters with electronic controllers.

The root locus of characteristic equation (4.70) is plotted in Figure 4-16 as a function of spring constant k^*_{sy} , using the Nymbus data from Appendix B. Note that the non-dimensional roots σ_i of (4.70) are multiplied by ω_0 (= 520 rad/sec) to obtain actual frequencies in the figure.

Included in the plot are the boundaries for Level 1 and 2 flying qualities defined by the US Military (MIL-F-83300, 1970, Key, 1971). The characteristic roots must fall to the left of the identified boundary to satisfy that level's requirements. It can be seen that the zero root, representing neutral stability without oscillations, does not violate any boundaries and therefore is allowable. It is also evident that the handling qualities of the self-stabilized system are acceptable for increasing values of spring constant k^*_{sy} until it becomes 0.00156. At this value the root locus passes through the Level 1 boundary, and remains within the boundary thereafter. A rigid, conventional linkage between servo and

pod – represented by a k_{sy}^* approaching infinity - therefore produces woefully unacceptable handling qualities.

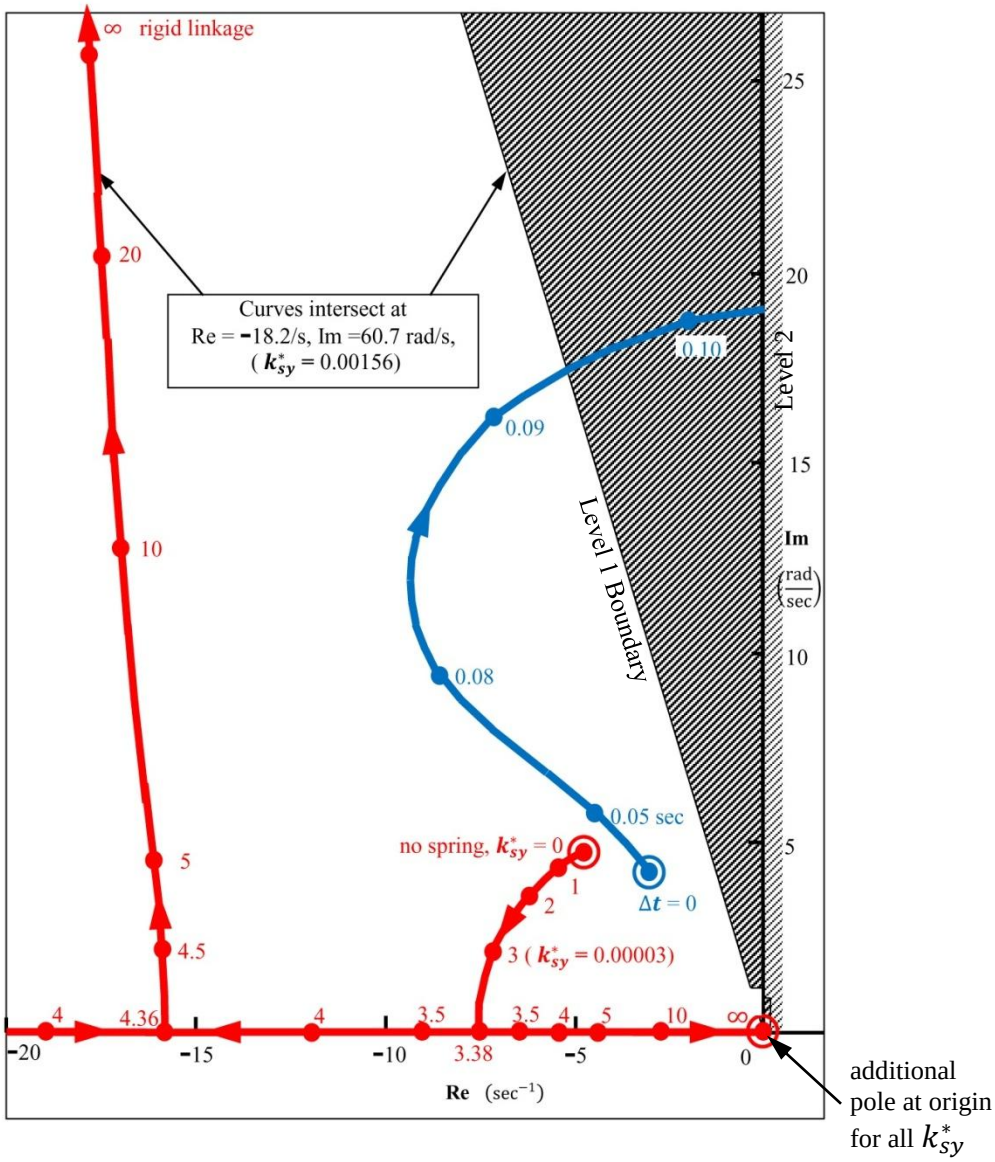

Figure 4-16. Predicted characteristic root locus (in red) of self-stabilized Nymbus aircraft for various spring constants k_{sy}^* (eqn. (4.70)), along with US Military Level 1 and 2 flying quality boundaries. Also plotted is estimated root locus (in blue) of OAT Nymbus with proportional controller having various time delays (eqn. 2.8).

It is clear from the foregoing that a flexible system (in the form of spring and damper) can be beneficial. Lowering the spring constant below 0.00156 reduces the natural frequencies of the system, to values either manageable by the pilot or to those which are damped quickly enough to be of no consequence.

For reference Figure 4-16 also includes the characteristic root locus of the proportionally-controlled OAT aircraft in Section 2.1.3.2 for various time delays. Since it has no zero roots, this system is completely stabilized in pitch at the typically high commercial frequencies of 50 to 400Hz (time delays of 0.02 to .0025 seconds respectively). Based on the plot, the pilot does not need to actively attend to pitch control during hover with so-equipped aircraft, a characteristic which has been observed in practice.

4.6.3 Scale and time delay; one benefit of the self-stabilized system

For a time delay of about 0.095 seconds – which could represent a very low quality electronic controller or no controller at all – the OAT root locus passes through the Level 1 boundary. At this point the flying qualities become unacceptable to the pilot, manifested in the workload becoming excessive. And, at just over 0.10 seconds time delay, the system becomes physically unstable and impossible to fly. At Nymbus scales and with normally good electronic controllers, this is not a real issue. But as the size of the aircraft gets smaller, time delays can become critical - but more so for the OAT rather than the self-stabilized system. Repeating the OAT characteristic equation (2.8) here:

$$\mathcal{P}\Delta t\frac{d^3\theta}{dt^3} + \left(\frac{I_{Ay}}{2k_p} - \mathcal{P} - \mathcal{R}\Delta t\right)\frac{d^2\theta}{dt^2} + [\mathcal{R} - \mathcal{Q}\Delta t]\frac{d\theta}{dt} + \mathcal{Q}\theta = 0 \qquad (2.8)$$

Non-dimensionalizing, using $k_p = 1/c_\Lambda$ (eqn. (2.5)) and $\Lambda = 45$ deg. to simplify, yields:

$$p_y(\omega_0\Delta t)\sigma^3 + \left[1 - \frac{p_y}{2} - r_y(\omega_0\Delta t)\right]\sigma^2 + \left[r_y - \sqrt{2}q_y(\omega_0\Delta t)\right]\sigma + \sqrt{2}q_y = 0 \quad (4.71)$$

Equation (4.71) is completely non-dimensional, and so one could deduce at first glance that it should be invariant for geometrically similar aircraft of different size – just as (4.70) describing the self-stabilizing system is. However, this is incorrect. Proprotor speed ω_0 will increase (with the inverse square root of the scale) as the aircraft becomes smaller, but the time delay – representative of the control electronics – will remain relatively constant. This means that the negative terms in the coefficients of (4.71) will get larger as the aircraft decreases in size, and at some scale the aircraft will become unstable. There will be a practical limit to how fast the electronics can be made to operate, and therefore there will be a limit to the size of OAT aircraft. This is not true of self-stabilized bicopters, as the invariance of (4.70) attests.

4.6.4 Sub-miniature aircraft and hybrid mechanical-electronic controllers

Based on the above observations, for very small aircraft it would be advantageous to combine the mechanical self-stabilizing and electronic systems. This hybrid system would be manifested by the control diagram of Fig. 4-15 if the pilot were replaced by the electronic proportional controller described by (2.7), its output now δ:

$$\delta(t) \;=\; -k_p\theta(t) \;+\; k_p\Delta t\cdot\theta'(t) \tag{4.72}$$

or, in transfer function form:

$$C(s) \;=\; \frac{\Delta(s)}{E} \;=\; k_p(1-\Delta t\cdot s\,) \tag{4.73}$$

The characteristic equation determining the stability of the system would now include the electronic "pilot" and be obtained from the closed loop transfer function of Fig. 4-13:

$$\frac{\Theta(s)}{R} \;=\; \frac{C(s)P_\delta\,(s)H(s)}{1+[P_\theta\,(s)+C(s)P_\delta\,(s)]H(s)} \tag{4.74}$$

4.6.5 Converting k_{sy}^* to a spring specification

The rotary spring coefficient k_{sy}^* used in the previous analyses needs to be converted to the equivalent linear spring constant so that a suitable spring can be selected. Referring to Fig. 4-17, the effects of the damper are ignored and the servo arm (and consequently the damper body) is assumed to be fixed and at zero rotation ($\delta = 0$). The moment acting upon the pod by the spring due to the former's tilting γ is, from (4.63), simply

$$C \;=\; k_s\gamma \tag{4.75}$$

The axial force on the spring-damper due to this rotation and consequent moment will be approximately

$$F_x \;=\; \frac{C}{l} \tag{4.76}$$

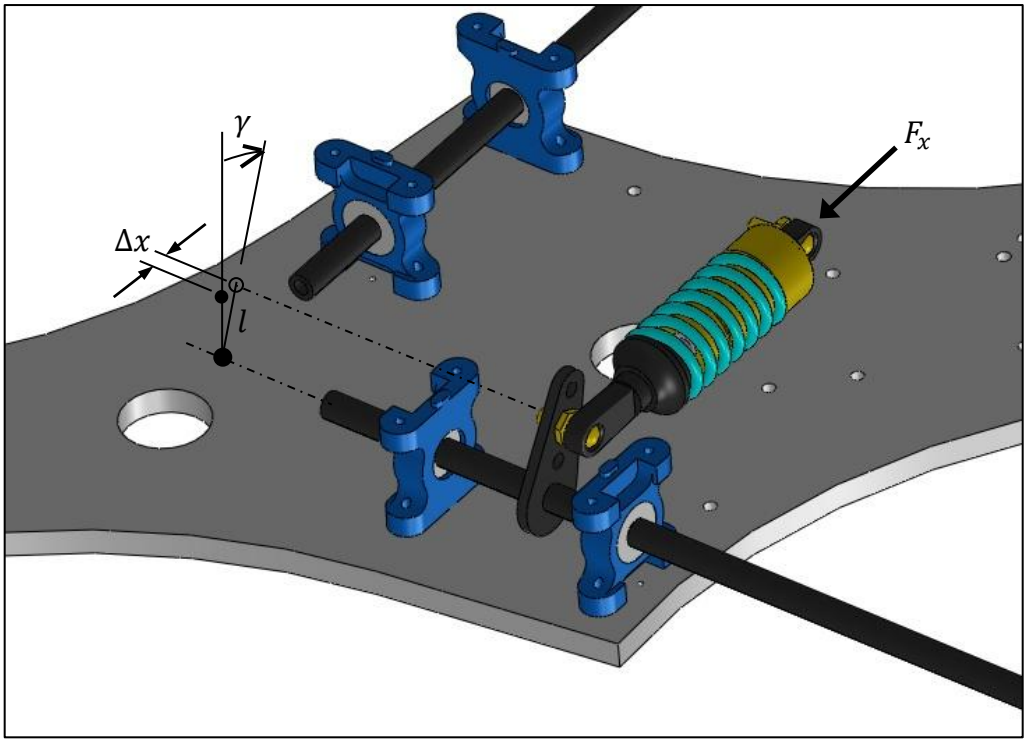

Figure 4-17. Converting rotational spring coefficient to a linear spring constant. Rotation γ of pod generates axial spring force F_x .

From geometry the approximate displacement of the spring-damper end (attached to the pod control arm) is

$$\Delta x = \gamma \cdot l \tag{4.77}$$

Combining (4.75) to (4.77) yields the force-per-unit-displacement – or spring constant – of the linear spring:

$$\frac{F_x}{\Delta x} = \frac{k_s}{l^2} \tag{4.76}$$

or, using the non-dimensional spring coefficient k_{sy}^*:

$$\frac{F_x}{\Delta x} = ½ I_\theta \omega_0^2 \frac{k_{sy}^*}{l^2} \tag{4.76′}$$

Using (4.76') with the Nymbus' l –value of 5/8-in (≅ 0.05 ft.) and Nymbus data from Appendix B, Table 4-1 lists linear spring constant values for various coefficients which appear on the root locus plot of Fig 4-16.

Table 4-1. Linear spring constant vs. rotational spring coefficient

Root locus index (Fig. 4-14)	k_{sy}^{*}	Linear spring constant $\frac{F_x}{\Delta x}$ (lb/in)
0	0	0
1	0.00001	1.25
2	0.00002	2.50
3	0.00003	3.75
4	0.00004	5.00
5	0.00005	6.25
10	0.00010	12.50

The table contains a range of values which appears reasonable in terms of stabilization of the aircraft. However, there are other requirements as well:

- the pods must resist aerodynamic tilting moments incurred in forward flight
- the aircraft must exhibit a satisfactory rate of response to the pilot's control input

4.7 Provisional Testing

Springs having a spring constant of 5 lb/in were installed along with fluid dampers in the Nymbus bicopter's pods, but their restorative forces were found to be woefully inadequate in overcoming the following resisting moments (to pod tilting) that were not mathematically modelled:

- Bushing friction (between pod and spar)
- Linkage friction
- Stiffness of electrical wires.
- Damper stickiness

Only springs with a spring constant of about 5 times the originals' were sufficient to restore the pods to center. These are shown in Figure 4-18. However, this change adversely affects handling characteristics. At speeds close to take-off values, the gyroscopic moments generated by the commercial 13-in. diameter propellers when pitching the aircraft (by hand) could not overcome the strength of the new springs; the pods remained centered in spite of aggressive pitching at high rate (higher than that observed of the OAT-equipped Nymbus).

Figure 4-18. Dampers and centering springs on Nymbus bicopter.

The most direct remedy to this problem is to increase the inertias of the proprotors. This was provisionally done in the lab by installing rings around the proprotors (Figure 4-19), which increased their moment of inertias (about the proprotor spin axis) by about tenfold.

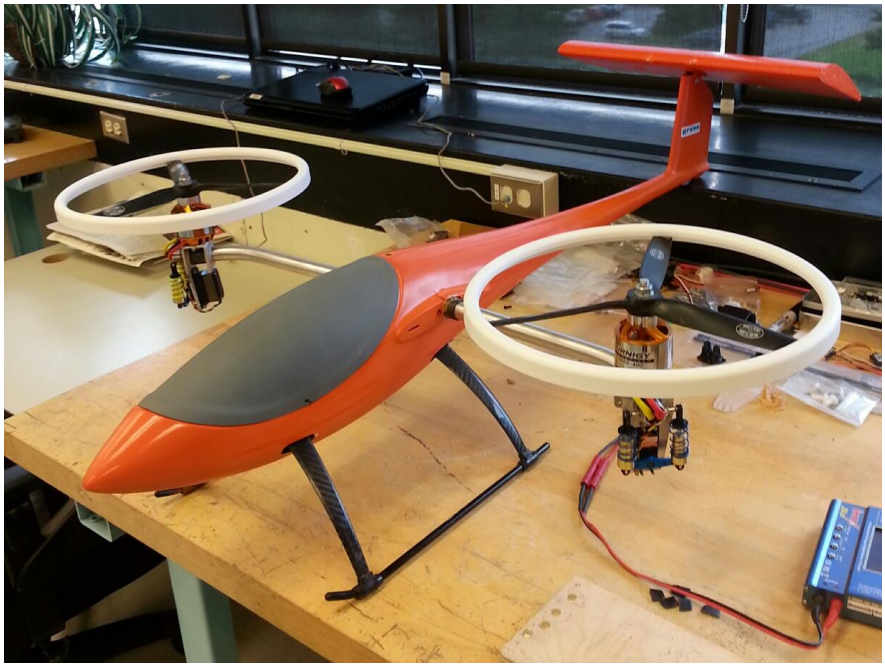

Figure 4-19. Styrene rings around Nymbus proprotors to increase their inertia.

These rings were cut from commercially available styrene dishware, and were simply stretched over the proprotor blade tips. In order to do this each blade had to be reduced in length by 0.5 in. The rings also masked another 0.5 in. of the remaining blade length, and therefore each proprotor was effectively reduced in diameterby a total of 2 inches.

This together with the fact styrene is not a high strength material did not allow the aircraft to be flown, but proprotor speeds within the 20% of the 520 rad/sec take-off

nominal were attainable. At these speeds, with the rings installed, the proprotors now visibly tilted (in the opposite direction to the pitching) when the aircraft was pitched.

In future work, account must be made of friction in the equations of motion in order to determine the proper spring specifications and proprotor inertias. It also appears that a viable self-stabilized bicopter will require a new type of proprotor, one which most probably has an integral ring.

4.8 Conclusions

The linearized pitching and related proprotor tilting behaviours of a hovering bicopter can be represented by a single, third-order characteristic equation. From it the system is found to be self-stabilizing if the pod tilting is rotationally damped relative to the airframe. Therefore, a bicopter with damped and obliquely tilting proprotors has here been mathematically proven to be self-stabilizing in pitch.

With proper choices of the design parameters, including the damping coefficient, the proprotor axes can reside in the vertical plane after the application of a step pitch disturbance. However, they will not remain in the vertical plane during oscillations or transients.

Simulations using the same mathematical pitch model corroborated the characteristic equation stability predictions.

In practice, pod centering springs are required since any imbalances will tend to tilt the pods inadvertently. Installing springs into the mathematical model causes the system to degrade from its original pitch-*angle* stability to a pitch-*rate* stability, making it equivalent to a conventional helicopter with mechanical flybar. This implies that a pilot

(human or electronic) must be present in the system, operating the tilt control and keeping the pitch angle stabilized. The lowered frequency of pitch oscillation due the rate-stabilization greatly reduces the difficulty of this task. Theoretically, the aircraft's hovering qualities in pitch will be acceptable to a human pilot according to military standards, and this characteristic is scale invariant. This is not true of OAT bicopters, which require faster electronics as their size becomes smaller.

Mechanical friction, which opposes tilting of the pods, must be included in future analyses. As well, bicopters require proprotors that have considerably higher mass-moment of inertias than those currently available commercially. This probably entails proprotors with integral rings.

Chapter Five: Roll and Yaw Stability

5.1 Parameter constraints and roll-yaw equations of motion

The roll and yaw lines in (3.44) do not contain pitching motion terms. As well, they are not affected by collective tilting ($\Delta\gamma_2 = -\Delta\gamma_1$) - the primary means by which pitch is controlled, and the type of tilting which results exclusively from aircraft pitching according to (3.44). Nor are roll and yaw affected by collective proprotor speed changes ($\Delta\omega_2 = \Delta\omega_1$). Therefore, the converse of the state outlined in Chapter 4 is also true, that rolling and yawing motion are independent of pitching motion and control in our linearized system; that roll and yaw behavior of the aircraft can be thoroughly investigated using purely differential tilt and speed changes only ($\Delta\gamma_2 = \Delta\gamma_1$ and $\Delta\omega_2 = -\Delta\omega_1$).

However, since roll and yaw are *both* direct functions of differential tilting and speeds (and vice versa), they are not independent of one another. Therefore any motion study of one must consider the other simultaneously. This condition has no effect on their non-relationship to pitch, so roll and yaw stability can still be legitimately investigated while specifying that pitch remain zero. The results can then be superimposed onto the case of general motion. Therefore, the aircraft operation can be initialized and maintained as having no pitching ($\Omega_y = 0$) with the following constraints:

$$\left.\begin{array}{rcl} \gamma_2 = \gamma_1 & \equiv & \gamma \\ \omega_1 - \omega_0 = \omega_0 - \omega_2 = \Delta\omega & \equiv & \mu\omega_0 \\ C_2 = C_1 & \equiv & C \end{array}\right\} \qquad (5.1)$$

With this specification of equal but opposite speed changes of the proprotors – now defined in terms of a single unknown speed parameter μ – their thrust and drag torques are defined as well. From their linear approximations in Section 3.5.2, they are:

$$\left.\begin{aligned} T_1 &= (1+2\mu)T_0 \quad , \quad Q_1 = (1+2\mu)Q_0 \\ T_2 &= (1-2\mu)T_0 \quad , \quad Q_2 = (1-2\mu)Q_0 \end{aligned}\right\} \tag{5.2}$$

From the definitions in Section 3.9, with $\Omega_y = 0$ the roll and yaw rates are simplified to:

$$\frac{d\phi}{dt} = \Omega_x \, , \qquad \frac{d\psi}{dt} = \Omega_z \cos\phi \;\cong\; \Omega_z \tag{5.3}$$

where the actual roll angle ϕ is assumed to be small (< 15 deg.). All the constraints above are depicted in Figure 5-1. Substituting (5.1) and (5.3) into the roll and yaw portions of the equation of motion (3.44) yields

$$\boxed{½I_\phi \frac{d^2\phi}{dt^2} + I_R\omega_0 c_\Lambda\left(s_\Lambda \frac{d\phi}{dt} + \frac{d\gamma}{dt}\right) + 2bT_0\mu - (hT_0 s_\Lambda - Q_0 c_\Lambda)\gamma - s_\Lambda C = \frac{1}{2}M_{ex}} \tag{5.4}$$

$$\boxed{½I_\psi \frac{d^2\psi}{dt^2} + I_R\omega_0 \frac{d\mu}{dt} - bT_0 c_\Lambda \gamma + 2Q_0\mu = \frac{1}{2}M_{ez}} \tag{5.5}$$

where $½I_\phi = \frac{1}{2}I_{ay} + I_P c_\Lambda^2$ and $½I_\psi = \frac{1}{2}I_{az} + I_P$ Substituting (5.1) and (5.3) into either pod equation (3.36a) or (3.36b) with $\Omega_y = 0$, and applying the small disturbance theory once more to eliminate products of the unknown variables, again results in a same single equation:

$$\boxed{I_P s_\Lambda \frac{d^2\phi}{dt^2} + I_P \frac{d^2\gamma}{dt^2} - I_R\omega_0 c_\Lambda \frac{d\phi}{dt} + C = 0} \tag{5.6}$$

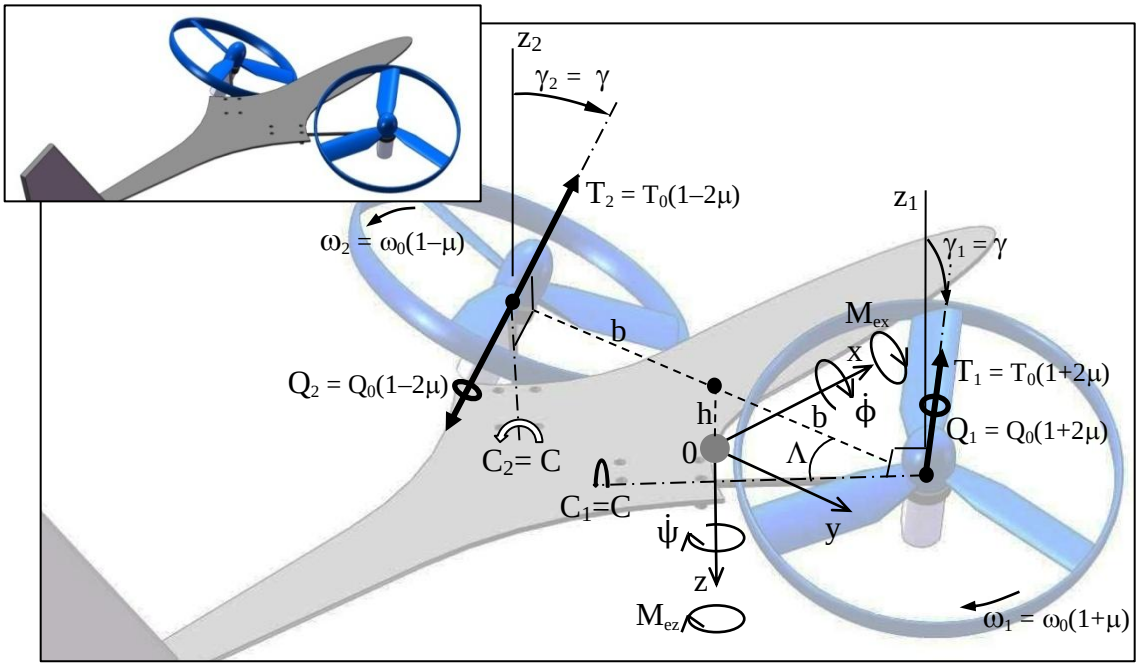

Figure 5-1. Roll and yaw model showing constraints on proprotor variables. Tilting of the two proprotors is always equal but in opposite directions. So are proprotor speed changes. Linearized thrusts and drag torques vary accordingly.

Writing the equations of motion in terms of non-dimensional time $\tau\ (= \omega_0 t)$:

$$½I_\phi\omega_0^2\frac{d^2\phi}{d\tau^2} + I_R\omega_0^2 c_\Lambda\left(s_\Lambda\frac{d\phi}{d\tau}+\frac{d\gamma}{d\tau}\right) + 2bT_0\mu - (hT_0 s_\Lambda - Q_0 c_\Lambda)\gamma - s_\Lambda C = \frac{1}{2}M_{ex} \quad (5.4')$$

$$½I_\psi\omega_0^2\frac{d^2\psi}{d\tau^2} + I_R\omega_0^2\frac{d\mu}{d\tau} - bT_0 c_\Lambda\gamma + 2Q_0\mu = \frac{1}{2}M_{ez} \quad (5.5')$$

$$I_P\omega_0^2 s_\Lambda\frac{d^2\phi}{d\tau^2} + I_P\omega_0^2\frac{d^2\gamma}{d\tau^2} - I_R\omega_0^2 c_\Lambda\frac{d\phi}{d\tau} + C = 0 \quad (5.6')$$

C in (5.4) and (5.6) has already been defined in the previous chapter. For simplicity it is assumed that – as was the result for the pitch stability analysis – the centering springs do

not adversely affect the stability of aircraft angular velocities. Therefore only the rotary damper relation (4.18) is used for C, which is repeated here:

$$C = k_d \frac{d\gamma}{dt} \qquad \left(= k_d \omega_0 \frac{d\gamma}{d\tau}\right) \tag{4.18}$$

Even with C specified, however, there are only three equations - (5.4') through (5.6') - describing the system, but there are four unknowns: γ, μ, ϕ and ψ.

5.2 Yaw gyro

5.2.1 The need for a yaw gyro

Thus far there is no control of proprotor speeds; specifically, no means of controlling μ has been prescribed. As shown in Section 3.2.2, unlike tilt angle γ, the proprotors' speeds will not change on their own due to motion of the aircraft (i.e., there are no inertial moments generated about their spin axes). As Table 5-1 shows, however, leaving the speeds constant and at their nominal values – i.e., setting $\mu = 0$ – would make ψ entirely a function of γ and ϕ (equation (5.4)). Since the latter two parameters depend only on each other in this case – and not on ψ – there could be no automatic feedback correction to ψ. This means that the aircraft could spin inadvertently once perturbed.

Table 5-1. Variables in equations of motion

Equation	Variables
(5.4)	ϕ γ (μ)
(5.5)	ψ γ (μ)
(5.6)	ϕ γ

This leads to the conclusion that some extra device must be incorporated into the system, one that senses yawing ψ (or $\dot{\psi}$) of the aircraft and corrects for it by effecting control of another parameter. Since, as we have seen, μ cannot be zero (or arbitrary), the device must effect control of μ in order to correct errors in ψ.

The necessity of an extra device for stabilizing yaw in the aircraft is not surprising when one considers that nearly all VTOL aircraft require one. Model R/C helicopters with either fully articulated main rotors or with flybars, such as the one shown in Figure 5-2, are inherently stable in pitch and roll but require electronic stabilization in yaw. In a typical model, an onboard piezo gyro senses unwanted yawing motion and sends a corrective control signal to a servo, which in turn changes the pitch of the tail rotor blades an appropriate amount through a control linkage.

Similarly, coaxial R/C helicopters (Figure 5-3), though extremely inherently stable in pitch and roll, also require electronic stabilization of yaw. In this case the piezo yaw gyro controls the speed differential of the two motors driving the co-axial rotors, slowing one down and speeding the other up to generate a net yawing moment while maintaining the model's altitude.

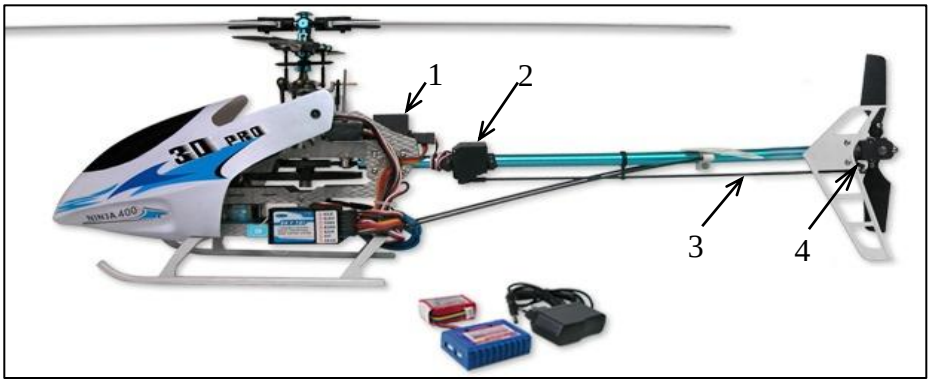

Figure 5-2. Conventional R/C helicopter, with electronic yaw stabilization consisting of: 1-yaw gyro; 2-servo; 3-control rod; 4-tail rotor pitch arm. (Source: www.skyartec.com, 2014)

Figure 5-3. Coaxial R/C helicopter, with electronic yaw stabilization consisting of yaw gyro connected to differential speed control of the two rotors. (Source: www.traxxas.com, 2014)

In terms of increasing performance and cost, typical commercial yaw gyros range from rate- or derivative-type (D) to angle or proportional (P), and on to a combination of the two (PD). Some of the higher-end ones will even contain proprietary control algorithms. For a conventional R/C helicopter, the gyro outputs a PWM (pulse width modulation) signal to the tail rotor servo, which in turn changes the angles of the tail rotor's blades – and therefore its thrust – by an amount according to the algorithm.

For a coaxial helicopter the yaw gyro output is again a PWM signal, but in this case it is sent to the rotor speed controllers, which in turn change the voltages of the drive motors and consequently their torques and speeds.

In this thesis a similar approach is used; initially, a D-type yaw gyro/speed controller system specifies speed changes of the proprotor drive-motors to keep the aircraft from yawing inadvertently (a P-type controller will be added in a subsequent section). It is actually the motor torques that are of primary importance in yaw prevention, but speed changes will of course ensue as well; in a later section it will be shown how they and automatic tilting of the proprotors work together to stabilize both yaw and roll simultaneously.

5.2.2 Drive Motor and Yaw gyro models give needed fourth equation

Assuming the proprotors are driven by brushless motors, their governing electrical equations are (Franklin, 2010):

$$\tau_m = K_m i_a \tag{5.7}$$

$$V_a = \frac{1}{K_v}\omega + R_a i_a + L_a \frac{di_a}{dt} \tag{5.8}$$

where τ_m is the electromagnetic torque of the armature, i_a and V_a are the armature current and voltage respectively, K_m and K_v are motor constants, and R_a and L_a are the resistance and inductance of the armature winding respectively. Concerning the inductance, Franklin (2010, pg. 48) states

> *"In many cases the relative effect of the inductance is negligible compared with the mechanical motion and can be neglected."*

Several papers on quadrotor dynamics (Hoffmann, 2007, Bangura, 2012) consider the inductance to be negligible as well, so this assumption is adopted here. Setting L_a to zero in (5.8) and eliminating the i_a–term using (5.7) yields:

$$V_{ai} = \frac{1}{K_v}\omega_i + \frac{R_a}{K_m}\tau_{mi} \tag{5.9}$$

where, as before, the i-subscript represents the proprotor number 1 or 2.

Ignoring friction of the motor bearings but including the proprotor drag torque Q_i, the equation of motion of the motor and its attached proprotor is:

$$I_R \frac{d\omega_i}{dt} + Q_i = \tau_{mi} \tag{5.10}$$

Eliminating τ_{mi} between (5.9) and (5.10) gives

$$I_R \frac{d\omega_i}{dt} + \frac{K_m}{K_v R_a}\omega_i + Q_i = \frac{K_m}{R_a} V_{ai} \tag{5.11}$$

We can find the nominal voltage V_{a0} (i.e., that required to hover) by setting the derivative term in (5.11) to zero:

$$\frac{K_m}{K_v R_a}\omega_0 + Q_0 = \frac{K_m}{R_a} V_{a0} \tag{5.12}$$

or

$$\frac{1}{K_v}\omega_0 + \frac{R_a}{K_m} Q_0 = V_{a0} \tag{5.12′}$$

Recalling (5.1) and (5.2):

$$\omega_1 - \omega_0 = \omega_0 - \omega_2 = \Delta\omega \equiv \mu\omega_0 \qquad \text{(from 5.1)}$$

$$Q_1 = (1 + 2\mu)Q_0 \quad , \quad Q_2 = (1 - 2\mu)Q_0 \qquad \text{(from 5.2)}$$

and writing voltages as a difference ΔV_a from the nominal voltage V_{a0}:

$$V_{a1} - V_{a0} = V_{a0} - V_{a2} = \Delta V_a \tag{5.13}$$

equation (5.11) for the two proprotors becomes the same single equation

$$I_R\omega_0\frac{d\mu}{dt} + (\vartheta_0 + 2Q_0)\mu = \frac{K_m}{R_a}\Delta V_a \tag{5.14}$$

where ϑ_0 represents the nominal back-EMF effective torque coefficient, given by

$$\vartheta_0 = \frac{K_m}{K_v R_a}\omega_0 \tag{5.15}$$

From inspection of Figure 5-1, if the aircraft was yawing inadvertently in the positive direction, the yaw gyro should increase the speed of proprotor 1 and decrease the speed of proprotor 2 in order to counter the yawing. Therefore the D-type yaw model, which changes motor voltages according to the aircraft's yaw rate, would normally take the form (assuming no time delay)

$$\Delta V_a = k_q\frac{d\psi}{dt}$$

where k_q is the gyro gain. However, in order to simplify the equations, $k_q$can be arbitrarily redefined to include the motor parameters:

$$\frac{K_m}{R_a}\Delta V_a = k_q\frac{d\psi}{dt} \tag{5.16}$$

Equating (5.16) to (5.14) produces then the fourth equation of motion for the system:

$$\boxed{I_R\omega_0\frac{d\mu}{dt} + (\vartheta_0 + 2Q_0)\mu = k_q\frac{d\psi}{dt}} \tag{5.17}$$

Using non-dimensional time, this is

$$I_R\omega_0^2\frac{d\mu}{d\tau} \quad + \quad (\vartheta_0 + 2Q_0)\mu \quad = \quad k_q\omega_0\frac{d\psi}{d\tau} \qquad (5.17')$$

Table 5-2 once more shows the list of variables, now with those of (5.17) included.

Table 5-2. Variables in equations of motion, including (5.17)

Equation	Variables
(5.4)	ϕ γ μ
(5.5)	ψ γ μ
(5.6)	ϕ γ
(5.17)	ψ μ

5.3 State Space and the Eigenvalue Matrix

Using the same method taken in the Chapter 4 for determining pitch stability, the system variables in state space form are:

$$\left.\begin{aligned} x_1 &= \gamma \\ x_2 &= \dot{\gamma} = \dot{x}_1 \\ \dot{x}_2 &= \ddot{\gamma} \\ x_3 &= \mu \\ \dot{x}_3 &= \dot{\mu} \\ x_4 &= \dot{\phi} \\ \dot{x}_4 &= \ddot{\phi} \\ x_5 &= \dot{\psi} \\ \dot{x}_5 &= \ddot{\psi} \end{aligned}\right\} \qquad (5.18)$$

Substituting these into equations of motion (5.4) to (5.6), with C obtained from (4.18) and $M_{ey} = 0$, yields

$$\dot{x}_4 + r_x c_\Lambda s_\Lambda x_4 + (r_x c_\Lambda - k^*_{dx} s_\Lambda) x_2 + 2\rho x_3 - q_x x_1 = 0 \tag{5.19}$$

$$\zeta \dot{x}_5 + r_x \dot{x}_3 - \rho c_\Lambda x_1 + 2\varphi x_3 = 0 \tag{5.20}$$

$$s_\Lambda \dot{x}_4 + \dot{x}_2 - \frac{r_x}{p_x} c_\Lambda x_4 + \frac{k^*_{dx}}{p_x} x_2 = 0 \tag{5.21}$$

$$r_x \dot{x}_3 + (\vartheta^*_{0x} + 2\varphi) x_3 = k^*_{qx} x_5 \tag{5.22}$$

where the coefficient definitions are

$$p_x = \frac{I_P}{½ I_\phi} \tag{5.23a}$$

$$q_x = \frac{h T_0 s_\Lambda - Q_0 c_\Lambda}{½ I_\phi \omega_0^2} \tag{5.23b}$$

$$r_x = \frac{I_R}{½ I_\phi} \tag{5.23c}$$

$$\rho = \frac{b T_0}{½ I_\phi \omega_0^2} \tag{5.23d}$$

$$\varphi = \frac{Q_0}{½ I_\phi \omega_0^2} \tag{5.23e}$$

$$\vartheta^*_{0x} = \frac{\vartheta_0}{½ I_\phi \omega_0^2} \tag{5.23f}$$

$$k_{dx}^{*}\,, k_{qx}^{*} \;=\; \frac{k_d\,, k_q}{½ I_\phi \omega_0} \tag{5.23g}$$

$$\zeta \;=\; \frac{I_\psi}{I_\phi} \tag{5.23h}$$

Eliminating $\dot{x}_4$ between (5.19) and (5.21) produces a state equation with $\dot{x}_2$ as the sole derivative:

$$\dot{x}_2 \;=\; r_x c_\Lambda \left(s_\Lambda^2 + \frac{1}{p_x}\right) x_4 \;+\; \left[r_x s_\Lambda c_\Lambda - k_{dx}^{*}\left(s_\Lambda^2 + \frac{1}{p_x}\right)\right] x_2 \;+\; 2\rho s_\Lambda x_3 \;-\; q_x s_\Lambda x_1 \tag{5.24}$$

And eliminating between (5.20) and (5.22) yields another, with $\dot{x}_5$ as the lone derivative:

$$\zeta \dot{x}_5 \;=\; \rho c_\Lambda x_1 \;+\; \vartheta_{0x}^{*} x_3 \;-\; k_{qx}^{*} x_5 \tag{5.25}$$

As was done in Section 4.2, the eigenvalue matrix $(\mathbf{A} - \lambda_i \mathbf{I})$ can be obtained from the system state equations, in this case (5.18), (5.19), (5.22), (5.24) and (5.25):

$$\begin{bmatrix} -\lambda & 1 & 0 & 0 & 0 \\ -q_x s_\Lambda & r_x s_\Lambda c_\Lambda - k_{dx}^{*}\left(s_\Lambda^2 + \frac{1}{p_x}\right) - \lambda & 2\rho s_\Lambda & r_x c_\Lambda \left(s_\Lambda^2 + \frac{1}{p_x}\right) & 0 \\ 0 & 0 & -\frac{1}{r_x}(\vartheta_{0x}^{*} + 2\varphi) - \lambda & 0 & \frac{k_{qx}^{*}}{r_x} \\ q_x & -r_x c_\Lambda + k_{dx}^{*} s_\Lambda & -2\rho & -r_x s_\Lambda c_\Lambda - \lambda & 0 \\ \frac{\rho c_\Lambda}{\zeta} & 0 & \frac{\vartheta_{0x}^{*}}{\zeta} & 0 & -\frac{k_{qx}^{*}}{\zeta} - \lambda \end{bmatrix} \tag{5.26}$$

5.4 Characteristic Equation for Λ = 45 degrees

Setting the determinant of (5.26) to zero yields the characteristic equation for the system, which was performed using MATLAB for tilt-path angle Λ = 45 degrees. The program code and its output are contained in Appendix D.1. From them it is observed that the yaw-inertial term ζ (e in the program) and the yaw-gyro gain k_{qx}^* only appear together, in the ratio $\frac{k_{qx}^*}{\zeta}$, which is now defined as k_{qz}^*. With this change the coefficients of the various powers of the eigenvalues in the characteristic equation are

$$\lambda^5: \qquad 1 \tag{5.27a0}$$

$$\lambda^4: \qquad \left[\frac{1}{r_x}(\vartheta_{0x}^* + 2\varphi) + k_{qz}^*\right] \; + \; k_{dx}^*\left(\frac{1}{2} + \frac{1}{p_x}\right) \tag{5.27a1}$$

$$\lambda^3: \; k_{dx}^*\left[\frac{1}{r_x}(\vartheta_{0x}^* + 2\varphi) + k_{qz}^*\right]\left(\frac{1}{2} + \frac{1}{p_x}\right) \; + \; \frac{1}{2}\left(\sqrt{2}q_x + \frac{r_x^2}{p_x}\right) \; + \; k_{qz}^*\frac{2\varphi}{r_x} \tag{5.27a2}$$

$$\lambda^2: \quad \frac{1}{2}\left[\frac{1}{r_x}(\vartheta_{0x}^* + 2\varphi) + k_{qz}^*\right]\left(\sqrt{2}q_x + \frac{r_x^2}{p_x}\right) + k_{qz}^*k_{dx}^*\frac{2\varphi}{r_x}\left(\frac{1}{2} + \frac{1}{p_x}\right) - \frac{\sqrt{2}q_x r_x}{2p_x} \tag{5.27a3}$$

$$\lambda^1: \; -\frac{\sqrt{2}q_x}{2p_x}(\vartheta_{0x}^* + 2\varphi) \; + \; k_{qz}^*\frac{\varphi}{r_x}\left(\sqrt{2}q_x + \frac{r_x^2}{p_x}\right) \; - \; k_{qz}^*\left(\frac{\rho^2}{r_x} + \frac{\sqrt{2}q_x r_x}{2p_x}\right) \tag{5.27a4}$$

$$\lambda^0: \qquad \frac{k_{qz}^*}{p_x}\left(\rho^2 - \sqrt{2}q_x\varphi\right) \tag{5.27a5}$$

5.5 Conditions for Stability

One condition for stability, of course, is that all the coefficients a_i in the fifth-order characteristic equation, written here as

$$\lambda^5 + a_1\lambda^4 + a_2\lambda^3 + a_3 x\lambda^2 + a_4\lambda + a_5 = 0 \tag{5.28}$$

are positive. For a fifth-order equation there are three further Routh-Hurwitz conditions (Franklin 2010, pg133), where the S_j are here termed *Routh sums*:

$$\underbrace{a_1 a_2 - a_3}_{S_1} > 0 \tag{5.29}$$

$$\underbrace{a_3 S_1 - a_1(a_1 a_4 - a_5)}_{S_2} > 0 \tag{5.30}$$

$$\underbrace{(a_1 a_4 - a_5)S_2 - a_5 {S_1}^2}_{S_3} > 0 \tag{5.31}$$

5.5.1 Special Case of $q_x = 0$ (and also $b = 0$)

Upon inspection of (5.27), it is evident that all coefficients except the λ^1 one (5.27a4) are guaranteed to be positive when $q_x = 0$ ($hT_0 = Q_0$). The λ^1-coefficient is positive under this constraint only when

$$k_{qz}^* \left(\frac{\varphi r_x}{p_x} - \frac{\rho^2}{r_x} \right) > 0 \tag{5.32}$$

or, assuming yaw-gyro gain k_{qz}^* is positive and using definitions (5.23), when

$$b < \frac{I_R \omega_0}{T_0} \sqrt{\frac{Q_0}{I_P}} \tag{5.33}$$

This would specify a maximum span b of 0.90 ft. for the Nymbus (compared to an actual 1.25 ft.) if the height h was reduced from 0.25 to 0.13 ft. such that q_x was zero.

A MATLAB symbolic program was written to express the Routh sums in terms of the aircraft design parameters. It and its output for $q_x = 0$ are contained in Appendix sections D.2.2 and D.2.3 respectively. From the latter it is apparent that, of the three Routh sums, only S_1 and S_1 are guaranteed to be positive when $q_x = 0$. The convoluted S_3 sum, on the other hand, contains many negative terms; without further simplification it appears impossible to discern under what conditions S_3 might be positive. One such simplification can be obtained by going to design extremes. Appendix section D.2.3 shows that the S_3 expression is always positive for the unrealistic case of $q_x = 0$ and $b = 0$, the latter condition of course inferring that the two proprotors occupy the same location at the centre of the aircraft.

5.5.2 General Case of $q_x \in \mathcal{R}$ and $b > 0$: Pseudo-proof Plot

Though unrealistic, the case of $b = 0$ aids the understanding of the general system. Since coefficients a_i and the Routh sums S_j are continuous functions of the aircraft design parameters, stability cannot be confined to just special cases, and therefore ranges of the parameter values for which the aircraft is stable must exist. However, as we have seen, it is difficult to discern those ranges in a wholly algebraic or analytic manner for the more general cases. Though it may be possible to find some simple, non-

exhaustive parameter ranges that guarantee positivity of the a_i coefficients (the same can be done for S_1 and S_2), the last Routh sum S_3 cannot be reduced so easily.

Instead, a pseudo-proof of stability is developed here, in which the Routh sums are simplified by assigning typical (or nominal) values to some of the aircraft design parameters. Using definitions (5.23) and Appendix B.1 data, one hypothetical set of assignments corresponding to massive pods and low propeller drag-torques is chosen as:

$$
\begin{aligned}
p_x &= 0.10 && \text{(Nymbus actual value} = 0.042) \\
\frac{\varphi}{r_x^2} &= 0.25 && \text{(Nymbus actual value} = 0.96) \\
k_{dx}^* &= k_{dxv}^* = r_x && \text{per (4.32)} \\
k_{qz}^* &= (0.5 \text{ and } 5) \cdot k_{dx}^* && \text{(arbitrarily chosen)} \\
\frac{\vartheta_{0x}^*}{r_x^2} &= 0 \text{ \& } 2.5 && \text{(Nymbus value} = 25)
\end{aligned}
\qquad (5.34a)
$$

Another set, with values closer to those of the actual Nymbus, is:

$$
\begin{aligned}
p_x &= 0.05 && \text{(Nymbus actual value} = 0.042) \\
\frac{\varphi}{r_x^2} &= 1.0 && \text{(Nymbus actual value} = 0.96) \\
k_{dx}^* &= k_{dxv}^* = \frac{1}{2} r_x && \text{from (4.32)} \\
k_{qz}^* &= (0.05\ ) \cdot k_{dx}^* && \text{(reduced to improve stability boundary)} \\
\frac{\vartheta_{0x}^*}{r_x^2} &= 25 && \text{(Nymbus value} = 25)
\end{aligned}
\qquad (5.34b)
$$

The powers of the divisor r_x were chosen such that r_x could be factored out of the Routh stability boundary equations of Appendix D.3.2.

For commercial proprotors, drive-motors and tilt-servos there will be little actual variability in the values of the first two parameters in (5.34b). Of far more flexibility and at the discretion of the designer are $\frac{q_x}{r_x^2}$ and $\frac{\rho}{r_x^2}$. These parameters represent the aircraft geometry through their contained height h and span b variables respectively.

MATLAB programs in Appendix D.3 find the stability boundaries – as functions of this geometry and for values of the other parameters given by (5.34). From these it is apparent that – with some minor and impractical exceptions (the extreme geometries indicated by the a_5 and S_2 boundary locations) – satisfying the $S_3 > 0$ condition is sufficient to ensure stability of the system. This simplified stability boundary, adapted from Appendix D.3.4 – and corresponding to the (5.34a) data set – is depicted in Figure 5-4a.

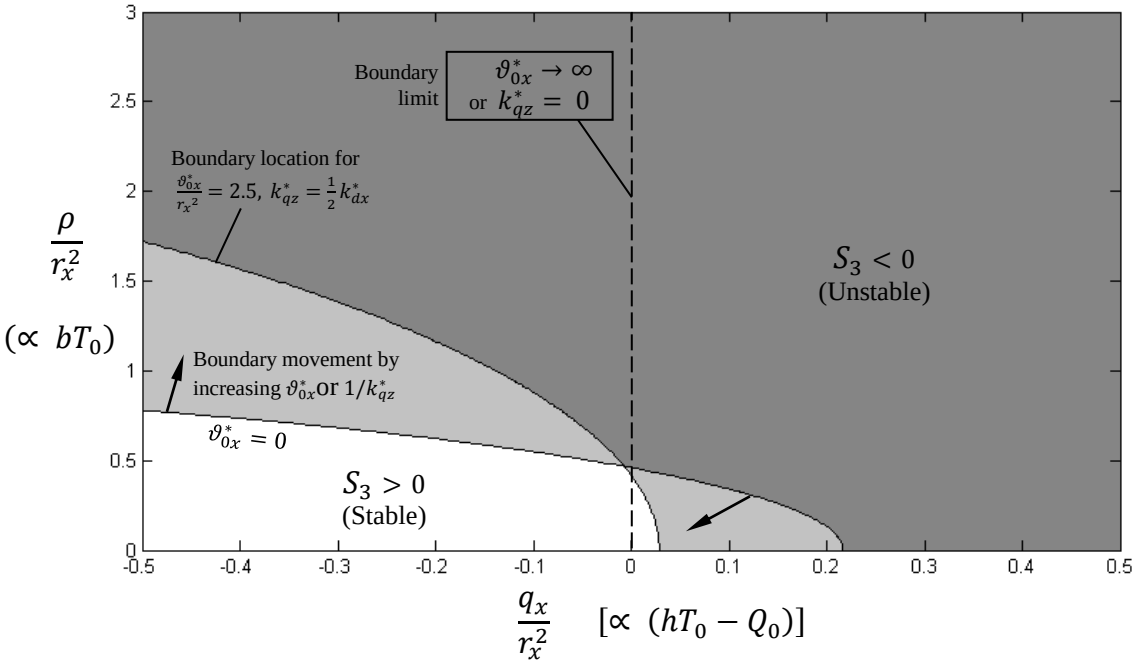

Figure 5-4a. Roll-yaw stability boundary for data of (5.34a).

Figure 5-4b shows the stability boundary plot for the (5.34b) or Nymbus data set.

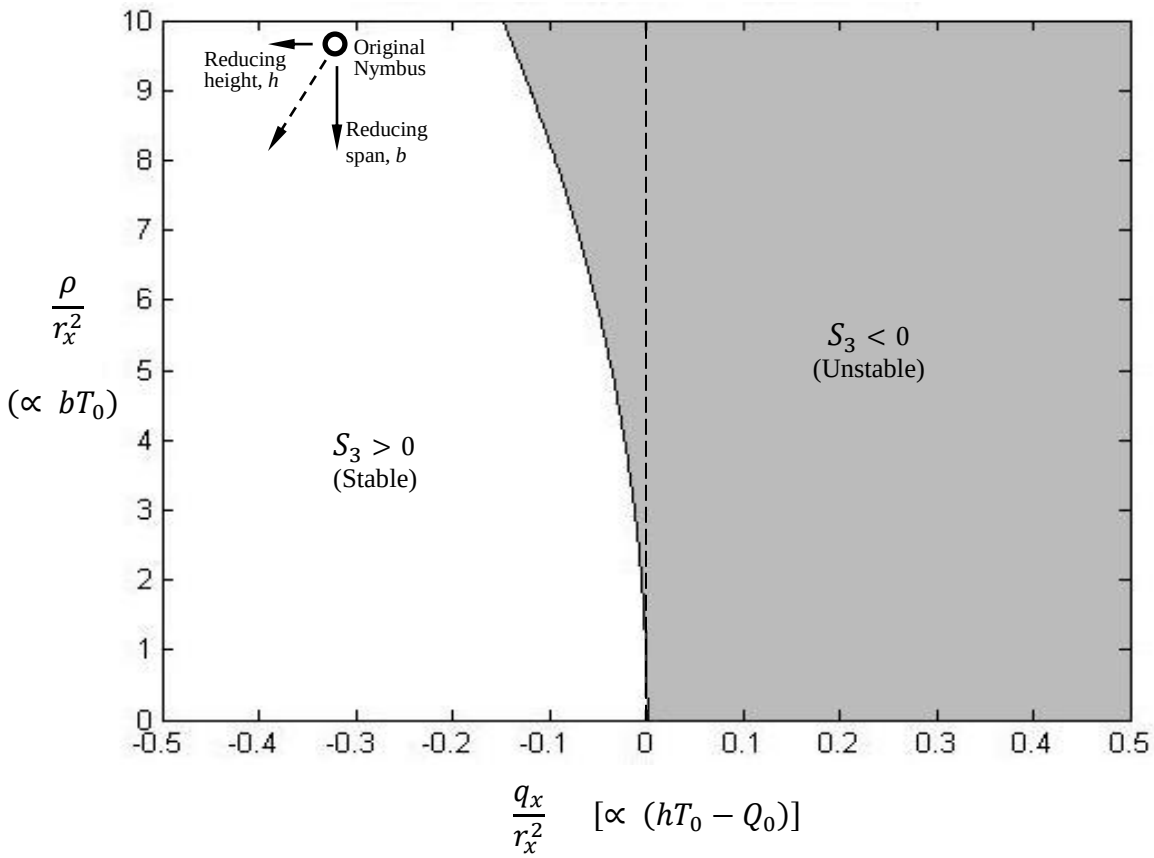

Figure 5-4b. Roll-yaw stability boundary for data of (5.34b).

The figure shows that a stable aircraft requires that $q_x \leq 0$, which primarily means that the aircraft centre of mass cannot be far below the pod tilt axes. Considering that oblique-tilting bicopters use the Q_0 torque vector to complement the hT_0 thrust-vector for static pitch stability, low center of masses are not necessary in the first place. Indeed, Figure 4.9 showed the effect on pitch stability of reducing h to zero, which was just to increase the steady-state pitch angle somewhat.

It also appears that reducing the span b will improve the stability margin of the self-stabilized aircraft, which is quite the opposite of conventional OAT aircraft. In the

latter, where roll is primarily controlled by differential throttle changes, advantage is had by increasing the span b (and hence the roll control moments).

Finally, it is noted that ϑ_{0x}^* and k_{qz}^* have roughly the same but opposite effect on the location of the stability boundary. Increasing ϑ_{0x}^* will essentially be the same as decreasing k_{qz}^* (and vice versa), both in the limit driving the boundary to become the vertical line $q_x = 0$. (the $a_5 > 0$ condition does not allow $k_{qz}^* = 0$, however). Why this should be is readily apparent when one considers the yaw-gyro equation in either of its forms (5.17) or (5.22).

5.6 Effect of Increasing Proprotor Inertia I_R (or r_x)

Though both axes of Figures 5.4 are divided by r_x^2 a change in r_x will nonetheless shift the stability boundary because $\frac{\varphi}{r_x^2}$ and $\frac{\vartheta_{0x}^*}{r_x^2}$ also change. Increasing proprotor inertia I_r (and therefore r_x) by a factor of 10 – but just doubling the pod inertia I_p (which is feasible per Appendix B) – changes the (5.34b) parameter values to

$$\left.\begin{array}{lcll} p_x & = & 0.10 & \text{(previously 0.05)} \\ \frac{\varphi}{r_x^2} & = & 0.01 & \text{(previously 1.0)} \\ k_{dx}^* & = & k_{dvx}^* = \frac{1}{2} r_x & \text{(same definition)} \\ k_{qz}^* & = & 0.05 \cdot k_{dx}^* & \text{(same definition)} \\ \frac{\vartheta_{0x}^*}{r_x^2} & = & 0.25 & \text{(previously 25.)} \end{array}\right\} \quad (5.34c)$$

The resulting stability boundary plot is shown in Figure 5-5, with the Nymbus geometry point now being $\frac{q_x}{r_x^2} = -0.003$ and $\frac{\rho}{r_x^2} = 0.096$.

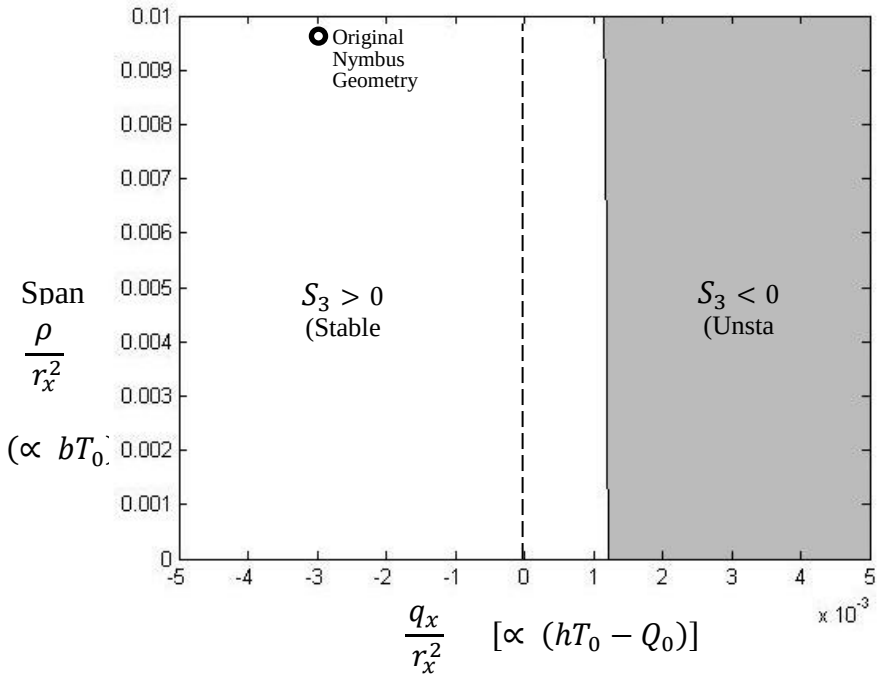

Figure 5-5. Effect of increasing proprotor inertia by 10x. Compare to Fig. 5-4b.

5.7 Simulink Modeling and Simulation

5.7.1 Model

A Simulink roll-yaw model based on the equations of motion at the beginning of this chapter was constructed to corroborate the stability analysis and is shown Appendix C.2. It consists of the three main components of airframe, tilting proprotor pods, and yaw gyro/prop motors. As in the pitch-only Simulink model of the previous chapter, the airframe and proprotor pods are connected by a viscous damper block representing Eqn.4-18).

5.7.2 Basic Simulation: Corroborating the effects of gyro gain

To coordinate the output of this model with the stability boundary plot of Figure 5-4a, data used is per (5.34a) in slightly different form:

$$
\begin{aligned}
p_x &= 0.10 && \text{(Nymbus value } = 0.042\text{)} \\
r_x &= 0.011 && \text{(Nymbus value } = 0.0056\text{)} \\
k^*_{dx} &= k^*_{dxv} = \frac{1}{2} r_x && \text{(per (4.32))} \\
k^*_{qz} &= \text{varies} \\
\varphi &= 0.00003 && \text{(corresponds to } \frac{\varphi}{r_x^2} = 0.25\text{)} \\
\vartheta^*_{0x} &= 0.00030 && \text{(corresponds to } \frac{\vartheta^*_{0x}}{r_x^2} = 2.50\text{)} \\
\rho &= \text{varies} && \text{(Nymbus nom. } = 0.00030\text{ , for } \frac{\rho}{r_x^2} = 2.50\text{)} \\
q_x &= \text{varies} && \text{(Nymbus nom.} = -0.00001\text{ , for } \frac{q_x}{r_x^2} = -0.083\text{)}
\end{aligned}
\qquad (5.35)
$$

External moment magnitudes, in either pulse or step form, are:

$$|M^*_{ex}, M^*_{ez}| = \frac{|M_{ex}, M_{ez}|}{½ I_\phi \omega_0^2} = 0.1 \frac{Q_0}{½ I_\phi \omega_0^2} = 0.1\varphi = 0.000003$$

As shown in Figure 5-9, a small pulse disturbance in roll is used in the model to corroborate the stability results of Section 5.5. Using the Nymbus' proprotor speed of 520 rad/sec the non-dimensional time of 2500 corresponds to approximately 5 seconds of real time.

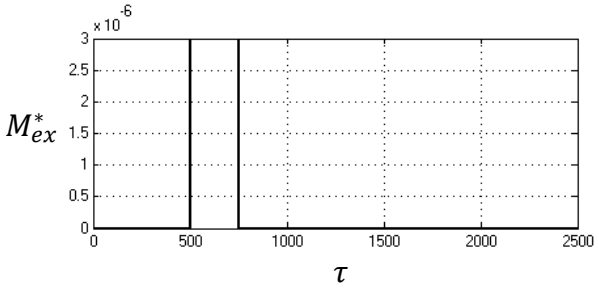

Figure 5-7. Applied external roll disturbance in Simulink

As noted in Section 5.5, reducing the value for k^*_{qz} raises the stability boundary, and is an alternative to reducing the span b to gain stability as Figure 5-8 shows.

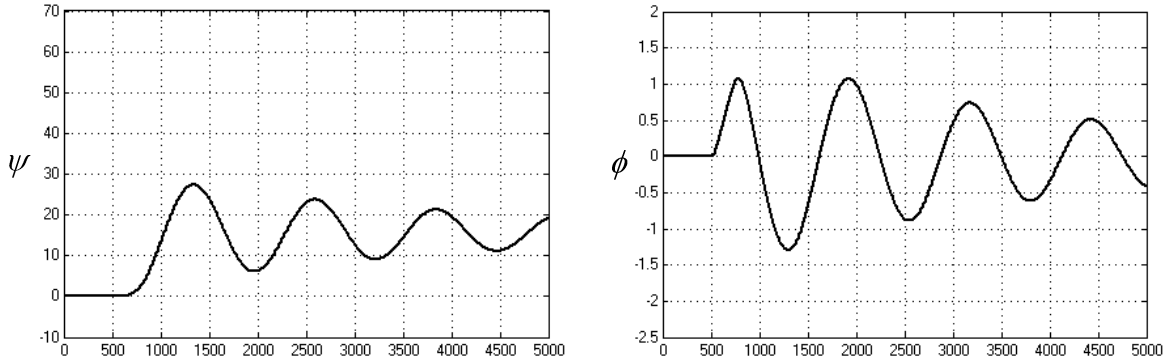

Figure 5-8a. Disturbance response with gyro gain of $k_{qz}^{*} = 0.15k_{dvx}^{*}$.

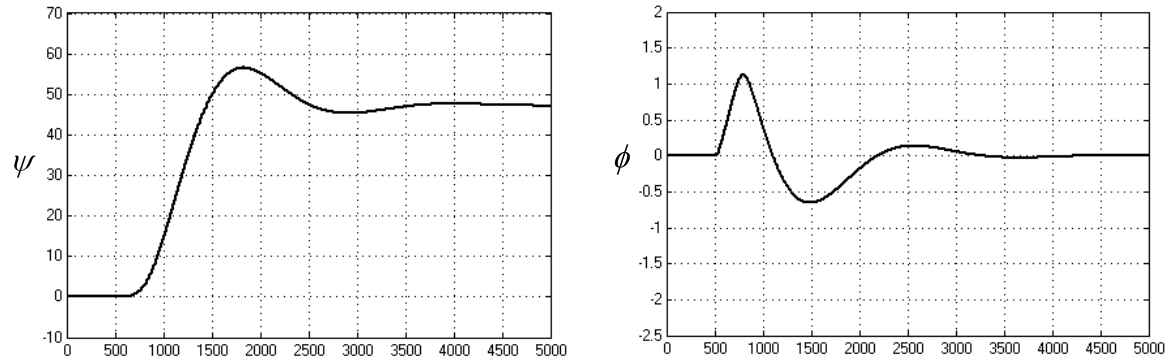

Figure 5-8b. Less oscillation with $k_{qz}^{*} = 0.05k_{dvx}^{*}$, but greater heading change

However, this entails an increasingly large heading change in response to roll disturbances, which is in keeping with the characteristic equation signifying stability of angular velocities, not angles. Defying it by using $k_{qz}^{*} = 0$ ($\therefore a_5 = 0$ in (5.27)) gives the lowest roll angle response but also a continuously yawing aircraft, as Figure 5-9 attests.

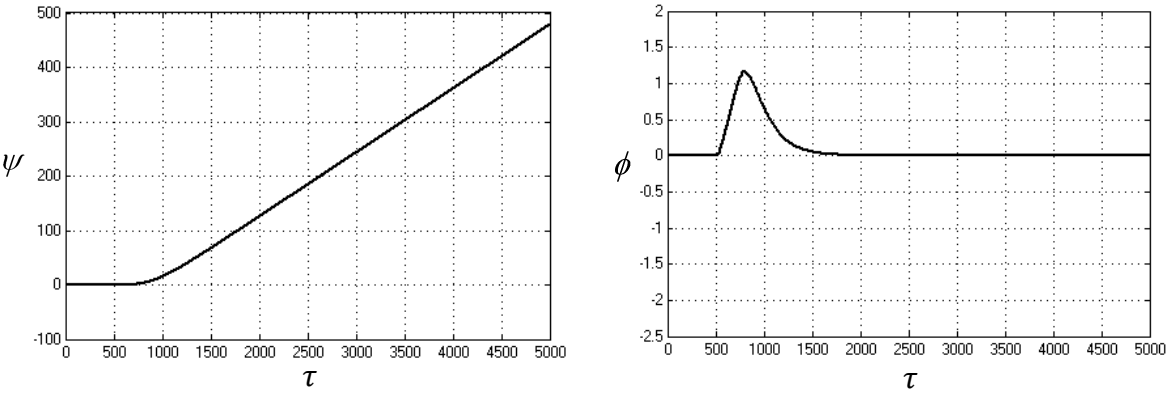

Figure 5-9. Continuous spinning of aircraft in response to pulse roll disturbance when rate gyro gain $k_{qz}^{*} = 0$.

In contrast, when $k_{qz}^{*} > 0$, the proprotors' torque differences will eventually abate the yawing of the aircraft, and it will come to rest at a new heading. Any yawing energy the vehicle possessed will have been absorbed by the commanded aerodynamic torque differences of the proprotors. Such damping, represented by (5.17), is equivalent to that of the rotational viscous dampers of Chapter 4 and defined by (4.18).

5.7.3 Heading change after a finite roll or yaw disturbance

Using the same steady-state analysis method used Chapter 4, it is possible to analytically predict the heading the aircraft will converge to after a finite disturbance such as a pulse. Assuming the system to be stable, then the steady-state condition is that in which the derivatives in the equations of motion (5.4) to (5.6) become zero. This occurs at an infinite time after such a disturbance has subsided. Applying this condition to (5.4) and (5.5) gives:

$$\begin{aligned} \gamma_{\infty} &= 0 \\ u_{\infty} &= 0 \end{aligned}$$

Integrating (5.6'), and substituting the above end-values and steady-state conditions into it results in $\phi_{\infty} = 0$. And, from (5.17'), one obtains $\dot{\psi}_{\infty} = 0$. Integrating equations of motion (5.4) and (5.5), setting their remaining derivatives to zero and applying the above end-conditions yields:

$$2bT_0 \int_0^{\infty} \mu \cdot dt \quad - \quad (hT_0 s_{\Lambda} - Q_0 c_{\Lambda}) \int_0^{\infty} \gamma \cdot dt \quad = \quad \frac{1}{2} \int_0^{\infty} M_{ex} \cdot dt \qquad (5.36)$$

and

$$-bT_0 c_{\Lambda} \int_0^{\infty} \gamma \cdot dt \quad + \quad 2Q_0 \int_0^{\infty} \mu \cdot dt \quad = \quad \frac{1}{2} \int_0^{\infty} M_{ez} \cdot dt \tag{5.37}$$

Doing the same with yaw gyro/drive-motor torque relation (5.17) gives

$$(\vartheta_0 + 2Q_0) \int_0^{\infty} \mu \cdot dt \quad = \quad k_q \psi_{\infty} \tag{5.38}$$

Substituting this relation for $\int_0^{\infty} \mu$ into (5.36) and (5.37), and eliminating $\int_0^{\infty} \gamma$ between them produces the relation for heading change ψ_{∞} in terms of the design parameters and external moments which, for $\Lambda = 45$ degrees, is:

$$\psi_{\infty} \quad = \quad \frac{(\vartheta_0 + 2Q_0)}{4k_q} \left[\frac{bT_0 \int_0^{\infty} M_{ex} dt \; - \; (hT_0 - Q_0) \int_0^{\infty} M_{ez} dt}{(bT_0)^2 \; - \; (hT_0 - Q_0) Q_0} \right] \tag{5.39a}$$

Equation (5.39a) confirms that there can be no steady-state yaw angle when the yaw gyro gain k_q is zero. However, obtaining a real value for ψ_{∞} from (5.39a) is not an indicator of stability; it may well be the yaw angle about which the aircraft oscillates. For a disturbance M in the form of a rectangular pulse starting at time t_0, ending at time $t_0 + \Delta t$, and having amplitude $|M|$, its integral expression can be written as

$$\int_0^{\infty} M dt \quad = \quad |M| \int_{t_0}^{t_0 + \Delta t} dt \quad = \quad |M| \Delta t \tag{5.40}$$

Using this for the roll disturbance while setting the yaw disturbance to zero, (4.39) becomes:

$$\psi_\infty\big|_{M_{ex}} \;=\; \frac{(\vartheta_0 + 2Q_0)}{4k_q}\left[\frac{bT_0|M_{ex}|\Delta t}{(bT_0)^2 \;-\; (hT_0 - Q_0)Q_0}\right] \tag{5.39b}$$

In non-dimensional form this is:

$$\psi_\infty\big|_{M^*_{ex}} \;=\; \frac{(\vartheta^*_{0x} + 2\varphi)}{4\zeta k^*_{qz}}\left[\frac{\rho|M^*_{ex}|\Delta\tau}{\rho^2 \;-\; q_x\;\varphi}\right] \tag{5.39b′}$$

which correctly predicts a steady-state yaw of 0.8223 rad (47.12 degrees) for the aircraft condition of Figure 5-13c. See (5-35) and Appendix B.2 for data used.

The span b that minimizes heading change ψ_∞ can be found by taking the partial derivative of (5.39b), setting it to zero:

$$\frac{\partial\,\psi_\infty}{\partial b} \;=\; 0 \;=\; \frac{\partial}{\partial b}\left[\frac{b}{(bT_0)^2 \;-\; (hT_0 - Q_0)Q_0}\right] \tag{5.41}$$

and solving the result for b, giving

$$b \;=\; \sqrt{\left(\frac{Q_0}{T_0}\right)^2 \;-\; h\frac{Q_0}{T_0}} \tag{5.42}$$

which shows that larger spans b favor negative values for height h.

5.7.4 Step disturbances and the need for a yaw gyro with proportional component

Up until now the disturbances used have been the temporary pulse-type, which have allowed stable aircraft to return to a steady state for $k^*_{qz} > 0$. Without further remedy, however, infinite duration step disturbances (Figure 5-10) will cause continuous

spinning (yawing) of the aircraft when $k_{qz}^{*} > 0$, just as pulse disturbances do when $k_{qz}^{*} = 0$. Figures 5-11 shows the response to a step roll disturbance of an aircraft having exactly the same parameter values as that in Figure 5-8b

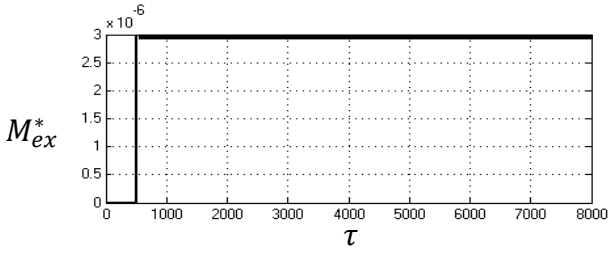

Figure 5-10. External step disturbance

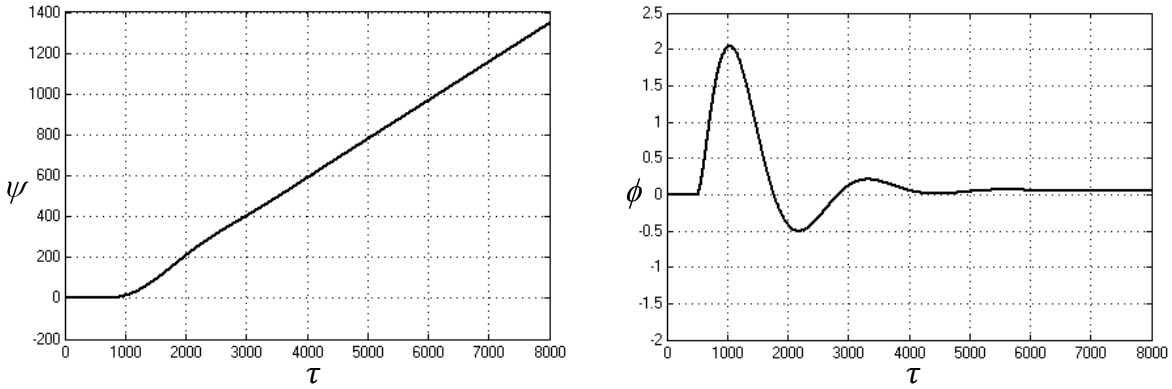

Figure 5-11. Continuous spinning using a rate-type yaw gyro ($k_{qz}^{*} = 0.05k_{dvx}^{*}$).

In an attempt to remedy this, a proportional component is introduced directly into the yaw gyro relation, without redeveloping the system characteristic equation to check for stability. With the original derivative gain k_q now written as k_{qd} and the new, proportional gain as k_{qp} , (5.17) becomes:

$$I_R\omega_0\frac{d\mu}{dt} + (\vartheta_0 + 2Q_0)\mu = k_{qp}\psi + k_{qd}\frac{d\psi}{dt} \qquad (5.43)$$

or, in non-dimensional form

$$r_x \frac{d\mu}{d\tau} \quad + \quad (\vartheta_0^* + 2\varphi)\mu \quad = \quad \zeta k_{qzp}^* \psi \quad + \quad \zeta k_{qzd}^* \frac{d\psi}{d\tau} \qquad (5.43')$$

where $k_{qzp}^* = \frac{k_{qp}}{½ I_\psi \omega_0^2}$ and, as before, $k_{qzd}^* = \frac{k_{qd}}{½ I_\psi \omega_0}$.

With this change there can be a permanent speed difference between the proprotors without movement of the aircraft. Using the same value of $k_{qzd}^* = 0.05 k_{dvx}^*$ as in Figure 5-16, Figure 5-12 shows spinning of the aircraft being abated with a positive proportional gain k_{qzp}^* (in this case $= 0.00005 k_{dvx}^*$).

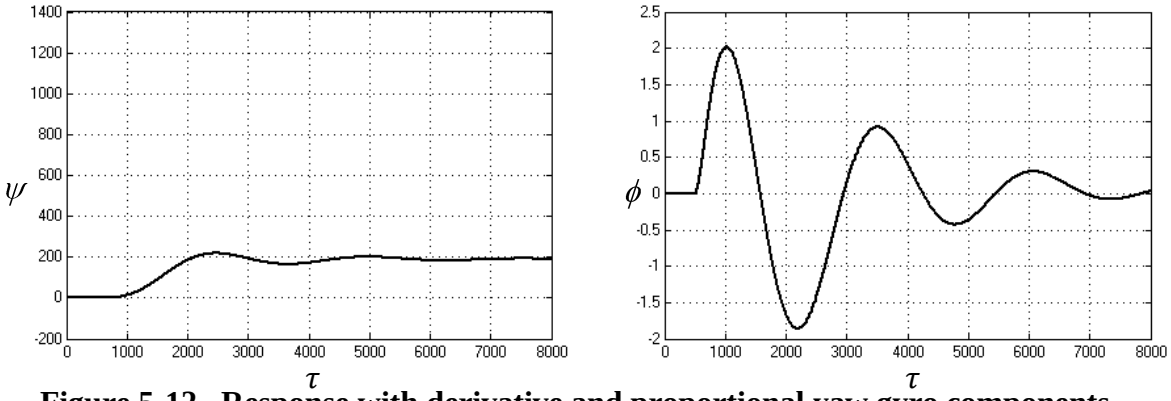

Figure 5-12. Response with derivative and proportional yaw gyro components.

It is evident that this abatement comes at the expense of the proportional gyro reducing the stability of the aircraft in roll. Lowering the proportional gain will improve the roll stability, but this will increase the steady-state yaw angle ψ_∞. When selecting the proportional gain, therefore, there will be a trade-off between roll stability and the steady-state yaw angle, a situation exactly analogous to that of the derivative gain with respect to pulse disturbances.

However, a secondary benefit of the proportional gyro is in fact its ability to return a pulse-disturbed aircraft to its original heading, so this previous limitation no longer exists. Figure 5-13 shows how the proportional control above completely nullifies the aircraft's heading change of Figure 5-8b when it is subjected to a pulse disturbance.

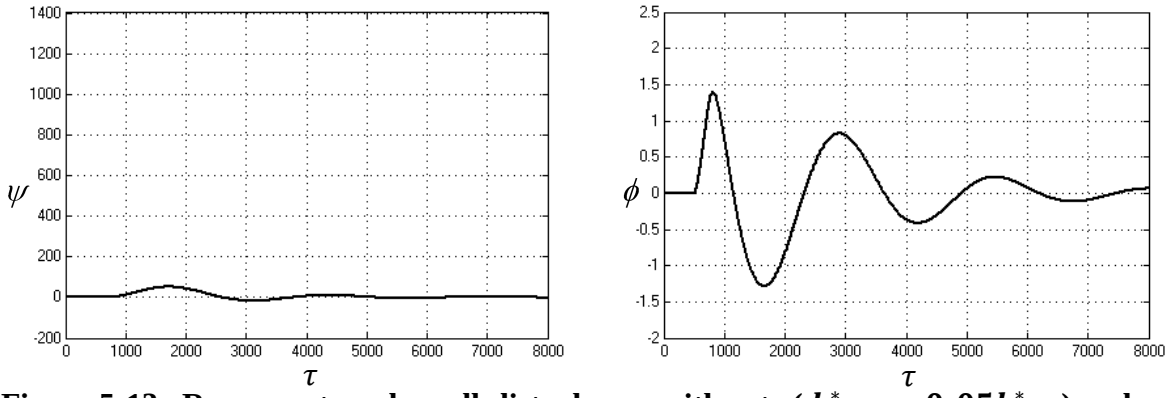

Figure 5-13. Response to pulse roll-disturbance with rate ($k^*_{qzd} = 0.05k^*_{dxv}$) and proportional ($k^*_{qzp} = 0.00005k^*_{dxv}$) yaw gyro components. Compare to Fig. 5-8b.

5.7.5 Heading change after a step disturbance

Just as was done for pulse disturbances and derivative yaw gyros in Section 5.7.4, it is possible to analytically predict the heading the aircraft will converge to during an infinitely long-duration disturbance of constant amplitude (i.e., a step disturbance). During such a disturbance the derivatives of all the parameters should converge to zero:

$$\begin{aligned} \dot{\psi}_\infty &= 0 \\ \dot{\phi}_\infty &= 0 \\ \dot{\gamma}_\infty &= 0 \\ \dot{u}_\infty &= 0 \end{aligned}$$

Generally, the parameters themselves will converge to non-zero values. Setting all the derivatives in (5.4) and (5.5) to zero and replacing the parameters with end-values yields:

$$2bT_0\mu_\infty - (hT_0 s_\Lambda - Q_0 c_\Lambda)\gamma_\infty = \frac{1}{2}M_{ex\infty} \qquad (5.44)$$

and

$$-bT_0 c_\Lambda \gamma_\infty \quad + \quad 2Q_0 \mu_\infty \quad = \quad \frac{1}{2} M_{ez\infty} \tag{5.45}$$

Doing the same with yaw gyro/prop-motor torque relation (5.43) gives

$$(\vartheta_0 + 2Q_0)\mu_\infty \quad = \quad k_{qp}\, \psi_\infty \tag{5.46}$$

Substituting this relation for μ_∞ into (5.44) and (5.45), and eliminating γ_∞ between them produces the relation for heading change ψ_∞ in terms of the design parameters and external moments which, for $\Lambda = 45$ degrees, is:

$$\psi_\infty \quad = \quad \frac{(\vartheta_0 + 2Q_0)}{4k_{qp}} \left[\frac{bT_0 M_{ex\infty} \; - \; (hT_0 - Q_0) M_{ez\infty}}{(bT_0)^2 \; - \; (hT_0 - Q_0) Q_0} \right] \tag{5.47}$$

Note that (5.47) is identical in form to (5.39a), and as such the results of the optimization performed on the latter will apply to it as well.

5.8 Conclusions

The bicopter requires a yaw gyro just as conventional and coaxial helicopters do. This gyro must control the differential proprotor torques (and subsequent speeds) as is done in small electric coaxial helicopters.

With this addition the linearized rolling, yawing and related proprotor tilting behaviours of the hovering bicopter can be represented by a single fifth-order characteristic equation. However, the complexity of this equation's coefficients prevents stability from being determined analytically as it was for pitch in Chapter 4. In this case, some of the parameter values, such as (non-dimensional) pod inertia and proprotor drag

torque, must be first specified. Then stability can be ascertained for ranges of the remaining parameters in the form of stability boundary plots.

Using this method, the system is found to be stable for parameter values typical of aircraft such as the Nymbus model bicopter, whose center of mass is relatively high and span between proprotors relatively short.

Simulations using the same mathematical roll and yaw models corroborated the characteristic equation stability predictions.

With just a rate-type yaw gyro, it was found that a step roll disturbance caused continuous spinning (yawing) of the aircraft. The addition of a proportional yaw gyro abates this spinning and causes the aircraft heading (yaw angle, relative to initial) to converge to a finite value. The proportional yaw gyro will also cause a pulse-disturbed aircraft to return to its original heading. However, this gyro will reduce the roll stability of the aircraft, so a trade-off must be accepted.

Chapter Six: Non-Linear 3D SimMechanics Model

6.1 Introduction

The construction of a more realistic SimMechanics model of the hovering bicopters is briefly described and some of the simulation results that bear upon accuracy of the linear analysis of Chapters Four and Five are discussed. The model does not use the linearized equations of motion formulated in Chapter Three, but is based instead upon the non-linear, three-dimensional dynamics internal to the SimMechanics simulation environment. Each simulation represents the behaviour of a specific physical aircraft; a single numerical value must be entered for each of the design variables in order to run the program. As such the program cannot be used to categorically prove or disprove stability of a concept or configuration, but rather only that of particular aircraft on a case by case basis. Nevertheless, it can be used to indicate the degree of correctness of the linear stability predictions for a particular design point, and this is its purpose here.

6.2 Brief Description of Model

A diagram of the SimMechanics self-stabilized bicopter model constructed by the author is shown in Figure 7-1. The airframe has six degrees of freedom and can move horizontally and vertically depending on the magnitudes and directions of the proprotor thrust vectors. At the beginning of a simulation, the aircraft is suspended motionless by the balance of forces in its nominal condition. It is subsequently subjected to a disturbing moment in the form of a rectangular pulse about the roll axis. Disturbances about the other axes could be applied, either separately or simultaneously. However, these are not

attempted in this brief linear versus non-linear results comparison, for a roll disturbance will incur coupling and the associated non-linearities on its own.

For the sake of further simplicity in this comparison, there are just rotational dampers and no springs between the pods and airframe. Similarly, the yaw gyro – which directs the (differential) torques of the proprotor drive motors – is a rate type, not a proportional one.

6.3 Simulation Results

The aircraft parameter values used for the simulations are from the Nymbus dimensional data in Appendix B,. The damping coefficient and gyro gain calculated from the non-dimensional values (5.34b) are

$$k_d = \ 0.063 \ \text{ft-lb/(rad/sec)} \ \text{or ft-lb-sec}$$

$$k_q = \ 0.00315 \ \ \text{ft-lb-sec}$$

and are included in the SimMechanics model.

Figure 6-2 shows the aircraft attitude results of running the simulation with a pulse roll disturbance of 0.0035 ft-lb and 1 second duration. Figure 6-3 shows the linear Simulink reults for the exact same data. There is fairly good agreement between the linear and non-linear responses, except that the latter shows a permanent roll offset of about -0.4 degrees. The non-linear response indicates as well a slight but stable pitching motion, which of course is non-existent by definition in the two-dimensional Simulink response.

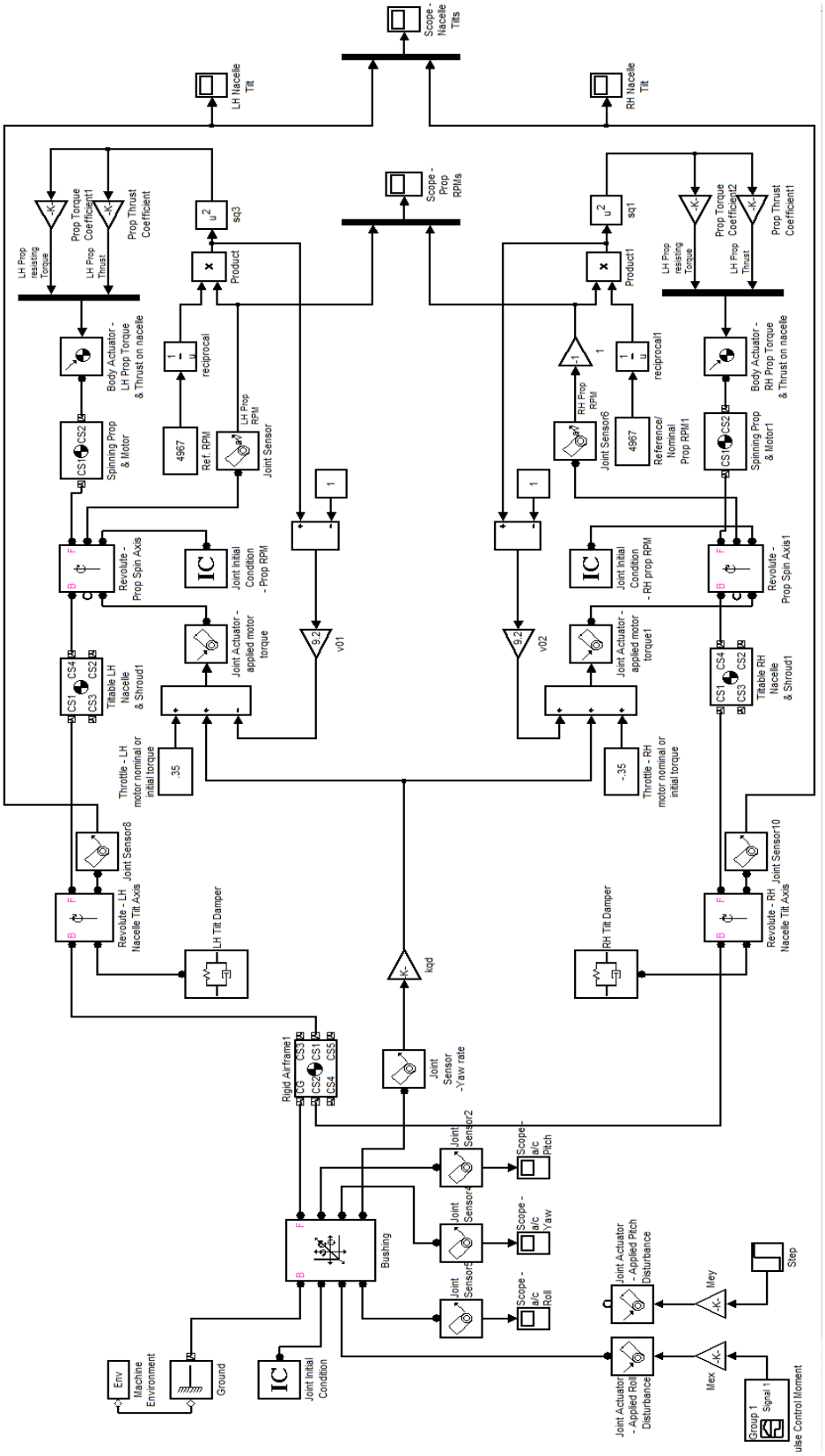

Figure 6-1. SimMechanics model of hovering bicopter.

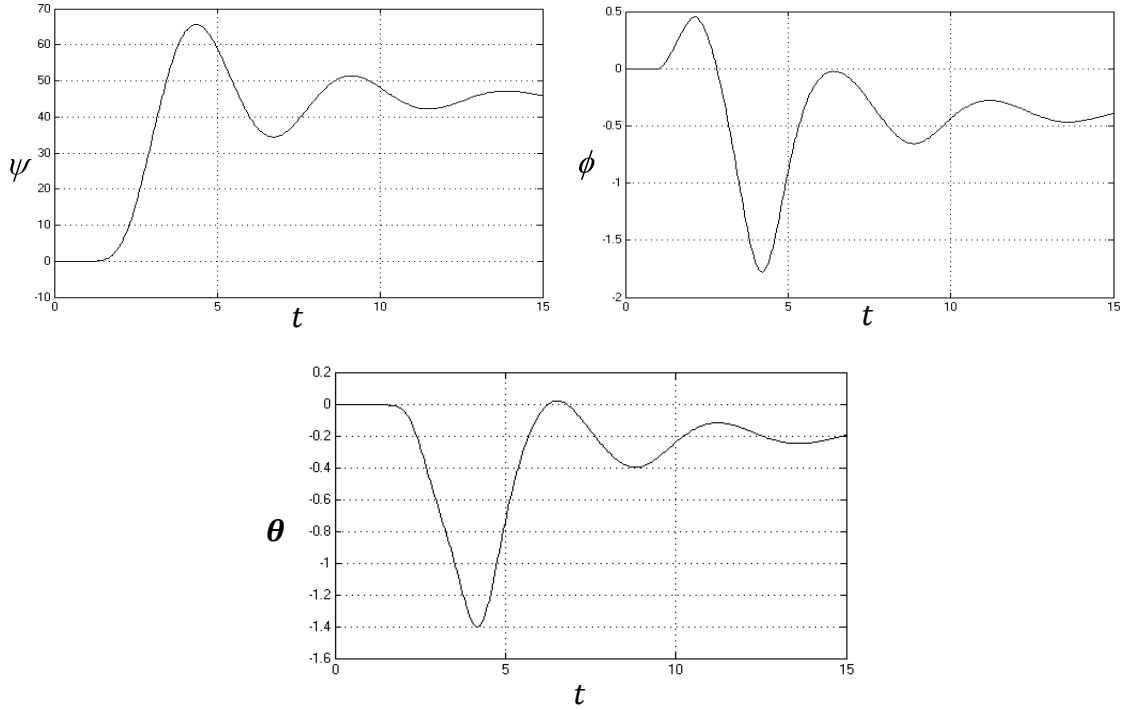

Figure 6-2. SimMechanics bicopter response to pulse roll disturbance of 0.0035 ft-lb. (angles in degrees and time t in seconds ($\tau = 520t$)). Compare to linear Simulink response of Fig. 6-3.

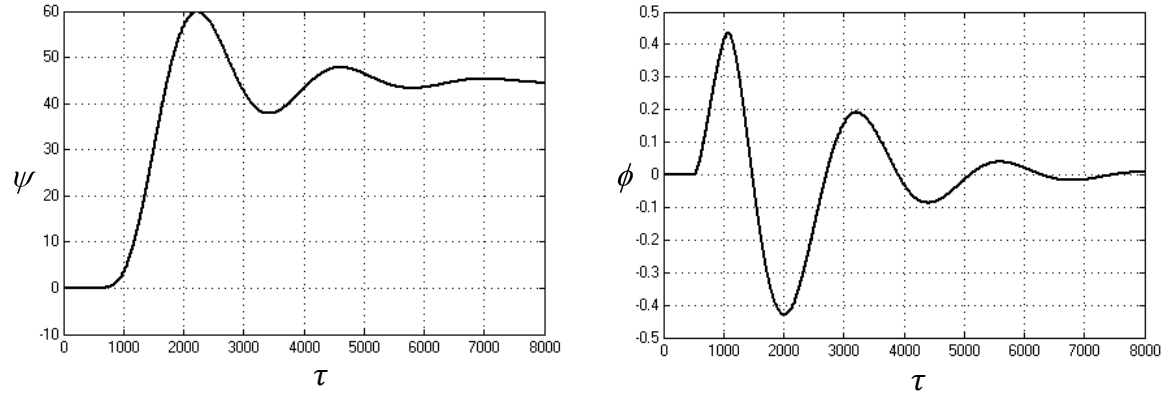

Figure 6-3. Simulink linear response to same pulse roll disturbance of 0.0035 ft-lb

When the magnitude of the pulse roll disturbance is increased ten-fold (to 0.035 ft-lb) the similarities disappear, as a comparison of Figures 6-4 and 6-5 shows. This roll disturbance, equal in magnitude to just $0.1Q_0$, is not large. However, it is sufficient in magnitude for non-linear characteristics to become predominant and overwhelm the

system, and, as a result, completely destabilize it. The prevalent effect appears to be extreme pitching of the vehicle, which the proprotors are unable to correct as they also deal with its rolling and yawing.

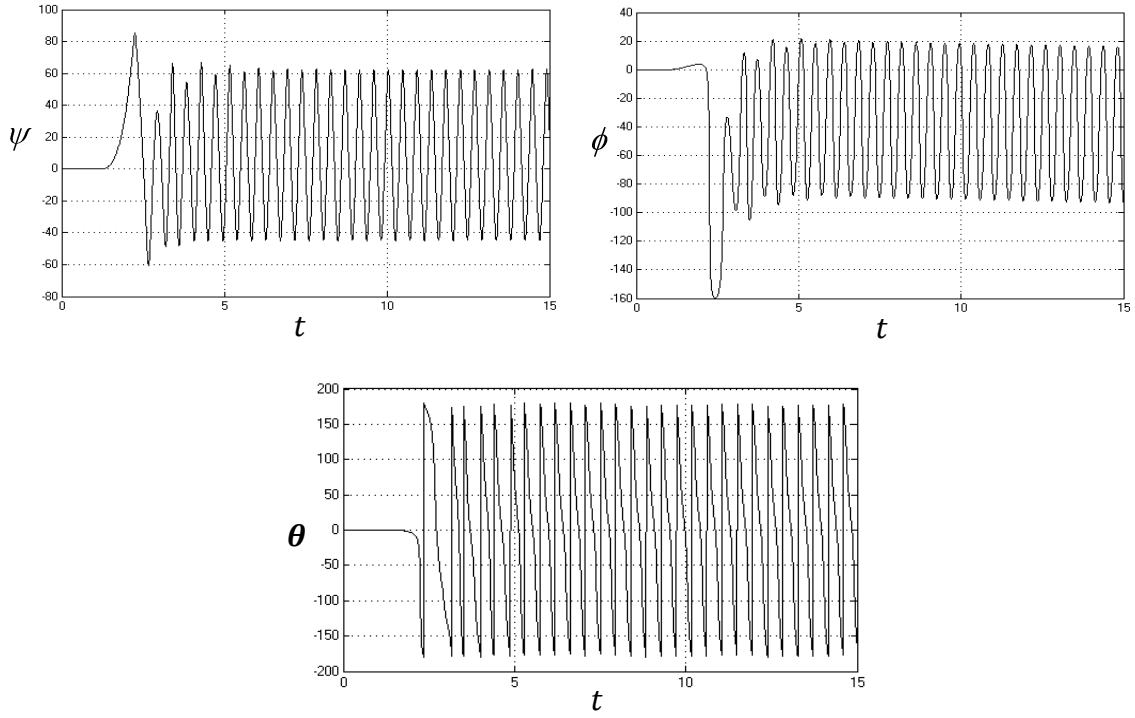

Figure 6-4. SimMechanics bicopter response to pulse roll disturbance of 0.035 ft-lb. Compare to linear Simulink response of Fig. 6-5.

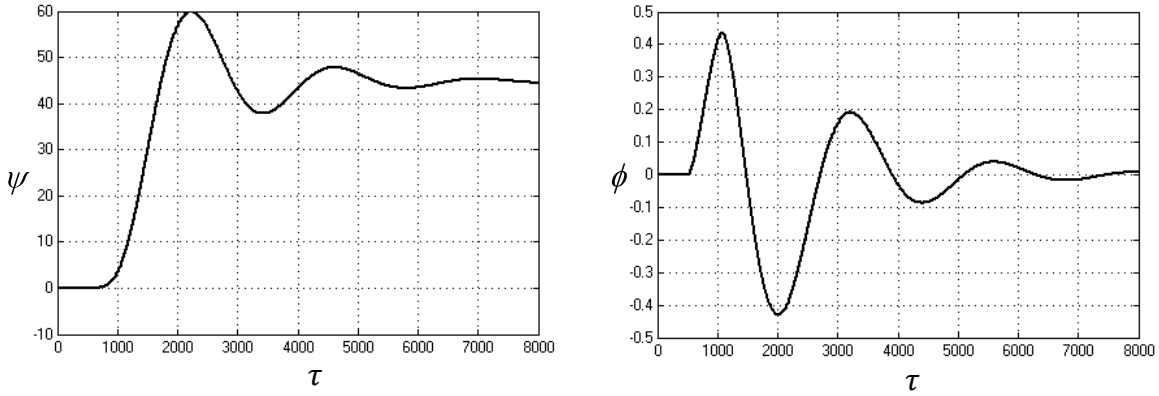

Figure 6-5. Simulink linear response to same pulse roll disturbance of 0.035 ft-lb.

Figures 6-6 and 6-7 show the substantial increase (50x and 100x) in proprotor inertia required to stabilize the non-linear system for the $0.1Q_0$ disturbance. It appears that the only way to achieve this to incorporate integral rings about the proprotors.

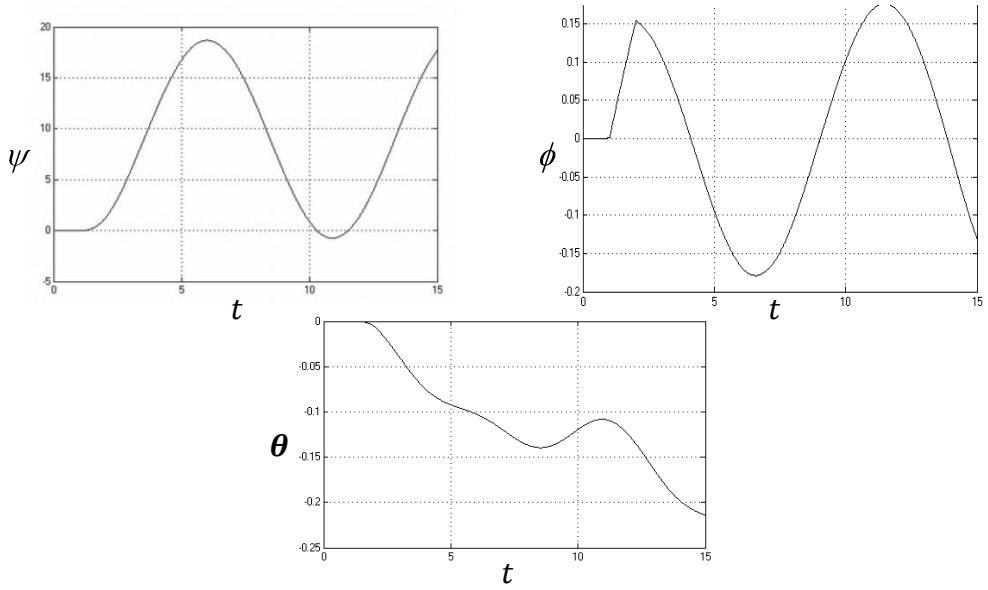

Figure 6-6. SimMechanics bicopter response to same disturbance as in Figure 6-4, but with proprotor inertia I_R , damper coefficient k_d, and yaw gyro gain k_q all increased by a factor of 50.

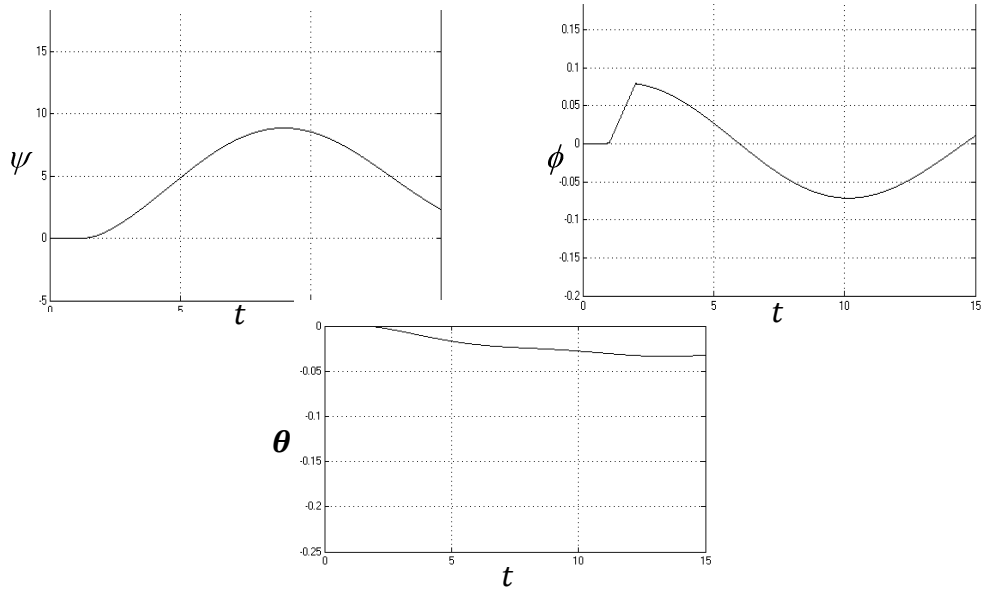

Figure 6-7. SimMechanics bicopter response to same disturbance as in Figure 6-4, but with proprotor inertia I_R , damper coefficient k_d, and yaw gyro gain k_q all increased by a factor of 100.

Chapter Seven: Conclusions

7.1 Pitch Stability

The linearized bicopter pitching and related proprotor tilting behaviours can be represented by a single, third-order characteristic equation. From it stability of the pitch angle can be mathematically proven and conditions on the parameters specified. Stabilization requires the use of dampers between the pods and airframe. Centering springs are also required to overcome imbalances. Their use degrades the system from that of angular stability to angular velocity stability, which is similar to that of a conventional helicopter with flybar. A pilot (human or electronic) is therefore required to stabilize the pitch angle. However, the lowered frequency of pitch oscillation due the rate-stabilization greatly reduces the difficulty of this task.

Mechanical friction, not included in the mathematical analysis, requires the use of much stiffer springs than those theoretically determined, which in turn necessitates the incorporation of proprotors having mass moment of inertias much higher than those of commercially available propellers.

7.2 Roll Stability

The bicopter requires a yaw gyro just as conventional and coaxial helicopters do. With it the linearized rolling and yawing behaviours – and associated proprotor tilting – can be represented by a single, fifth-order characteristic equation. From this equation stability can only be established when some parameter values are specified explicitly and the remainder fall within specified ranges. With this method it is found that the angular

roll and yaw velocities of bicopters such as the Nymbus, whose center of mass is relatively high and whose span between proprotors is relatively short, can be self-stabilized. Again, this roll characteristic is similar to that of conventional helicopters with flybars.

The yaw gyro should be at least a proportional-derivative (PD) type in order to abate the continuous spinning caused by step roll disturbances.

7.3 Limitations to Linear Analysis

Three-dimensional, non-linear simulations (using SimMechanics) reveal that the linear predictions may be overly optimistic, and that a bicopter with commercially available airplane propellers (such as the Nymbus aircraft of Appendix B) may be passively stable only when subjected to unusually small disturbances. Only by greatly increasing the proprotor inertia I_R (by 50 to 100 times, based on Nymbus data), can the non-linear system represented by the SimMechanics model be stable through the $0.1Q_0$ roll disturbance moments used in the linear analysis.

While linear analysis can identify geometries which are potentially stable, actual aircraft design must include more accurate non-linear simulation or methods.

7.4 Contributions

This thesis has made the following contributions in the field of aviation:

1. It formulates a non-cyclic VTOL aircraft configuration which has passively stable pitch and roll angular velocities. This configuration is a bicopter with laterally spaced proprotors having high inertias about their

spin axes, and whose oblique tilting is moderated with springs and dampers. As with conventional and coaxial helicopters, this bicopter does require stability augmentation about the yaw axis, usually in the form of an electronic yaw gyro commanding differential torques – and consequently speeds – of the proprotor drive motors.

2. It achieves simultaneous control of proprotor tilting by the pilot.

7.5 Items for Future Investigation

1. Component friction (include in mathematical models).
2. Aerodynamic effects (including forward motion and transient effects) on system behaviour.
3. Effect of payload weight and distribution on roll-yaw stability
4. (Further investigation into) effects of large proprotor inertias. Is there an optimum value?
5. (Further investigation into) effects of damper coefficient, spring stiffness, and yaw gyro gains.
6. Quantify potential benefits, such as time delay reduction, self-adaptiveness, and stress and energy reduction.

References

Adams, J. D. and McKenney, S. W. (2005). Gyroscopic Roll Stabilizer for Boats. US Patent No. 6.973,847

Al-Rihani, Y. (2012). Development of a Dual-axis Tilt Rotorcraft UAV: Design, Prototyping and Control. MSc. Thesis, Cranfield University, UK

Anderson, S. B. (1981). Historical Overview of V/STOL Aircraft Technology. NASA-TM-280. Ames Research Center. NASA

Aziz, M. M. (2013). Transfer Functions and Block Diagrams: Multiple inputs. *ECM2105 Control Engineering Lecture note no. 4.* University of Exeter, College of Engineering, Mathematics and Physical Sciences. pg. 11

Bangura, M. and Mahony R. (2012). Nonlinear Dynamic Modelling for High Performance Control of a Quadrotor. *Proceedings of Australian Conference on Robotics and Automation*, December 3-5. Victoria University of Wellington, New Zealand

Barczyk, M., and Lynch, A. F. (2013). Control-oriented Modeling of a Helicopter UAV with a Bell-Hiller Stabilizer mechanism. 2013 American Control Conference (ACC), Washington, DC. 978-1-4799-0178-4

Borst, H. (1990). The Curtiss-Wright X-19 Experimental Aircraft – Lessons Learned. AIAA 90-3206. *AIAA/AHS/ASEE Aircraft Design, Systems and Operations Conference*. September 17-19, 1990. Dayton, OH.

Benson, L. A. (1909). Edison's Picture of the Future of the Aeroplane. *The New York Times*. August 1, 1909. Section Part 5, Magazine Section. pg. SM5

Brennan, L. (1905). Means for Imparting Stability to Unstable Bodies." US Patent No. 796,893

Campbell, J. P. (1963). Status of V/STOL Research and Development in the United States. AIAA/CASI/RAeS 9th Anglo-American Conference. Oct 16-18, M.I.T., Cambridge, MA and Oct 21-24, Queen Elizabeth Hotel, Montreal, Canada

Chalk, C. R., Key, D. L., Kroll, J., Jr., Wasserman, R., and Radford, R. C. (1971). Background Information and User Guide for MIL-F-83300, Military Specification-flying Qualities of Piloted V/STOL Aircraft. US Air Force Flight Dynamics Lab., AFFDL-TR-70-88, Wright-Patterson AFB, OH.

Cunha, R. and Silvestre, C. (2003). Dynamic Modeling and Stability Analysis of Model-scale Helicopters with Bell-Hiller Stabilizing Bar. AIAA Guidance, Navigation and Control Conference. Austin, TX. 978-1-62410-090-1

Daley, D. (2001). A Big Future for Micro Air Vehicles. *Vertiflite, Fall/Winter 2001, Vol. 47, No. 4*. American Helicopter Institute. pg. 32

DARPA-BAA-13-19. (2013). Vertical Take-Off and Landing Experimental Aircraft (VTOL X-Plane). DARPA Broad Agency Announcement. Tactical Technology Office (TTO).

Daughady, H. and DuWaldt. F.A. (1955). Helicopter Handling Qualities Investigation, Phase II: Analysis of Helicopter Stabilization and Control Problems. Part C: Characteristics and Comparison of Existing Helicopter Stabilizing Devices. Cornell Aeronautical Laboratory, Inc., Buffalo, NY. Report no. TB-707-S-2.

Etkin, B. and Reid, L. D. (1996). *Dynamics of flight: Stability and control*. 3rd ed. John Wiley & Sons Inc.

Farley, J. (2006). A V/STOL Flight Control Journey Enabled by RAE Scientists. *The RAF Harrier Story*. The Royal Air Force Historical Society. Advance Book. UK. pp. 121-122

Ferry, E. S. (1933). *Applied Gyrodynamics: For students, Engineers and Users of Gyroscopic Apparatus*. 1st revised ed. John Wiley & Sons, Inc. NY. pp. 131-161

Franklin, G. F., Powell, J. D. and Emami-Naeini, A. (2010). *Feedback Control of Dynamic Systems*. 6th ed. Prentice-Hall/Pearson Higher Education. pp. 438-439

Franklin, J. A. (2002). *Dynamics, Control and Flying Qualities of V/STOL Aircraft*. AIAA Education Series. Reston, VA

Gabriel, D. L., Meyer, J. and du Plessis, F. (2011). Brushless DC Motor Characterization and Selection for a Fixed Wing UAV. *IEEE Africon Conference*. 978-1-61284-993-5/11

Gasco, P. S., Al-Rihani, Y., Shin, H., and Savvaris, A. (2013). A Novel Actuation Concept for a Multi Rotor UAV. *J. of Intelligent Robotic Systems*. DOI 10.1007/s10846-013-9987-3

Gress, G. R. (2002). Using Dual Propellers as Gyroscopes for Tilt-Prop Hover Control. *AIAA 2002 Biennial Powered Lift Conference*, Nov. 5-7, 2002. Williamsburg, VA

Gress, G. R. (2003). A Dual-Fan VTOL Aircraft using Opposed Lateral Tilting for Pitch Control. *American Helicopter Society 59th Annual Forum*, May 6-8, 2003. Phoenix, AZ

Gress, G. R. (2007). Lift Fans as Gyroscopes for Controlling Compact VTOL Air Vehicles: Overview and Development Status of Oblique Active Tilting. *American Helicopter Society 63rd Annual Forum*, May 1-3, 2007. Virginia Beach, VA

Gress, G. R. (2008). VTOL Air Vehicles with High Flight Speeds and 3D Mobility within Helicopter-Impenetrable Environments. *American Helicopter Society, Next Generation Vertical Lift Technologies, Southwest Region Specialists Meeting*, October 15-17, 2008. Dallas, TX

Gress, G. R. (2012). Bicopter Roll-Yaw Decoupling and Dynamic Control Augmentation. *Unpublished notes.*

Gurrisi, C. et al (2010). Space Station Control Moment Gyroscope Lessons Learned. *Proceedings of the 40th Aerospace Mechanisms Symposium*, NASA Kennedy Space Center, May 12-14, 2010. NASA/CP-2010-216272

Hirschberg, M. J. (1997). V/STOL: The First Half-Century. *Vertiflite, Vol. 43, No. 2*. The American Helicopter Society. pp. 34-54

Hirschberg, M. J. (2000). An Overview of the History of Vertical and/or Short Take-Off and Landing (V/STOL) Aircraft. CENTRA Technology, Inc. (www.vstol.org)

Hirschberg, M. J. (2013). Project Zero. *Vertiflite, Vol. 59, No. 3* The American Helicopter Society. pp. 10-14

Hoffmann, G. M., Huang, H., Waslander, S. L. and Tomlin, C. J. (2007). Quadrotor Helicopter Flight Dynamics and Control: Theory and Experiment. *AIAA Guidance, Navigation and Control Conference and Exhibit*. August 20-23. Hilton Head, South Carolina. AIAA 2007-6461 company

Hoh, R. H., and Ashkenas, I. L. (1979). Development of VTOL Flying Qualities Criteria for Low Speed and Hover. Systems Technology, Inc., Hawthorne, CA and Naval Air Development Center, Warminster, PA. NADC-77052-30.

Jacot, A. D., and Liska, D. J. (1966), Control Moment Gyros in Attitude Control. Journal of Spacecraft and Rockets, Vol. 3, No. 9. pp. 1313-1320. DOI: 10.2514/3.28653

Karnopp, D. (2202). Tilt Control for Gyro-stabilized Two-Wheeled Vehicles. Vehicle System Dynamics, Vol. 37, No. 2. pp. 145-156

Kelley, B. (1945). Helicopter Stability with Young's Lifting Rotor. *SAE Journal (Transactions)* Vol. 53, No. 12. Presented at meeting of Peoria Section of SAE and Central Illinois Section of ASME, Peoria, IL. March 19, 1945.

Kendoul, F., Fantoni, I., and Lozano, R. (2005). Modelling and Control of a Small Autonomous Aircraft having Two Tilting Rotors. 44th IEEE Conference on Decision and Control, and 2005 European Control Conference, CDC-ECC'05, pp. 8144-8149

Key, D. L. (1971). The Generation of a Military Specification for Flying Qualities of Piloted V/STOL Aircraft – MIL-F-83300. Flight Research Dept. of Cornell Aeronautical Laboratory, Inc. Buffalo, NY, and US Air Force Flight Dynamics Lab., Wright-Patterson AFB, OH. AFFDL-TR-70-88

Kim, S. K., and Tilbury, D. M. (2004). Mathematical Modeling and Experimental Identification of an Unmanned Helicopter Robot with Flybar Dynamics. *J. of Robotic Systems*. 21(3). Wiley Periodicals, Inc. pp. 95-116

Kuo, B. C. (1995). *Automatic Control Systems*. Prentice Hall, 7th ed. pp. 330-332

Kurokawa, H. (2007). "Survey of Theory and Steering Laws of Single-Gimbal Control Moment Gyros" *Journal of Guidance, Control, and Dynamics,* Vol. 30, No. 5. pp. 1331-1340. DOI: 10.2514/1.27316

Leishman, J. (2007). Is there a Case for the Tiltrotor? *RUSI Defence Systems, Oct 2007.* Royal United Services Institute. pp. 52-55

Lim, K. B., Shin, J. Y., Moerder, D. D. (2004). Variable Speed CMG Control of a Dual-spin Stabilized Unconventional VTOL Air Vehicle. AIAA 3rd Unmanned Unlimited Technical Conference, Workshop and Exhibit, September 20-23. Citeseer, Chicago, IL AIAA Paper 2004-6537.

Lim, K. B., Shin, J. Y., Moerder, D. D. (2006). "A feasibility study on the control of a generic air vehicle using control moment gyros," AIAA Guidance, Navigation, & Control Conference, August 21-24, Keystone, CO, AIAA Paper 2006-6313.

Lim, K. B., Shin, J. Y., Moerder, D. D. (2007). "CMG-augmented control of a hovering VTOL platform." AIAA Navigation, Guidance and Control Conference and Exhibit. Hilton Head, SC

Marquardi, H. C. (1970). *X-22A Progress Report No. 73*. Bell Aerospace Company Report No. 2127-933073 under contract to U.S. Navy.

Martin, D. M., Giulianetti, D. J., and Dugan, D. C. (2000). *The History of the XV-15 Tilt Rotor Research Aircraft*. NASA History Division. NASA SP-2000-4517. Washington, D. C.

McCormick, B. W. (1967). *Aerodynamics of V/STOL flight*. Academic Press. NY.

Model Motors (2103). *Axi Products Catalogue*. CZ. , www.modelmotors.cz

MIL-F-83300 (1970). US Military Specification: Flying Qualities of Piloted V/STOL Aircraft

NAVAIR (2011). *V-22 Osprey Guidebook 2011/2012*. Naval Air Systems Command. NAVAIR PMA-275. Control Number 11-607

Shilovskii, P. P. (1924). *The Gyroscope: its Practical Construction and Application*. Spon and Chamberlain. NY

Spry, S. C. and Girard, A. R. (2008). Gyroscopic Stabilization of Unstable Vehicles: Configurations, Dynamics and Control. *Vehicle System Dynamics*, Volume 46, Issue S1, pp.247-260, DOI: 10.1080/00423110801935863

Thorne, C. E. and Yim, M. (2012), Design and Analysis of a Gyroscopically Controlled Micro Air Vehicle. *J. of Robotic Systems*. 65:417-435

Wang, J. (2013). *Convertiplane*. European Patent Specification EP 2 551 190 B1. Assignee: Augusta-Westland

Wham, J. L., et al. (1987). *Propeller System with Electronically Controlled Cyclic and Collective Blade Pitch*. US Patent 4,648,345

Whittle, J. R. (2010). *The Dream Machine: The Untold History of the Notorious V-22 Osprey*. Simon & Schuster, NY

Yoon, H. and Tsiotras, P. (2004). "Singularity Analysis of Variable Speed Control Moment Gyros", *Journal of Guidance, Control, and Dynamics*, Vol. 27, No. 3, pp. 374-386.

APPENDIX A: SCALE INVARIANCE AND NON-DIMENSIONAL TIME

The following shows that the aircraft's proprotor speed ω can be considered the representative time element in the aircraft's operation, and with it the actual time can be non-dimensionalized.

A.1. Proprotor speeds and drag-torques of geometrically similar aircraft

Assume there are two aircraft of different size. Aircraft #2 is S times the size of aircraft #1 (based on some representative length), but otherwise the two are geometrically similar. The relationship between their weights, W, would then be:

$$W_2 = S^3 W_1 \tag{A.1}$$

If these aircraft are hovering then the relationship between their proprotors' thrusts T, diameters D and rotational speeds ω – from dimensional analysis – is

$$\frac{T_2}{\omega_2^2 D_2^4} = \frac{T_1}{\omega_1^2 D_1^4} \tag{A.2}$$

The proprotor diameters will be related by the scale factor S. Also, since the aircraft are hovering, the proprotor thrusts are equal to (half) the aircraft weight and (A.1) applies, giving the relationship between proprotor rotational speed and scale:

$$\frac{S^3}{\omega_2^2 S^4} = \frac{1}{\omega_1^2}$$

$$\rightarrow \quad \frac{\omega_2}{\omega_1} = \frac{1}{\sqrt{S}} \tag{A.3}$$

This allows the relationship between the proprotor drag-torques Q to be determined. Again, using dimensional analysis

$$\frac{Q_2}{\omega_2^2 D_2^5} = \frac{Q_1}{\omega_1^2 D_1^5}$$

$$\rightarrow \quad \frac{Q_2}{Q_1} = S^4 \tag{A.4}$$

A.2. Natural frequency of OAT aircraft pitch as a function of scale

The equation of pitching motion of an OAT aircraft with proportional controller (without time delay) is given by (2.3). Using $k_p = 1/c_\Lambda$ for the controller gain, the definition (3.26) for I_{Ay} and Λ =45 degrees, the equation simplifies to:

$$\frac{I_{ay}}{2}\frac{d^2\theta}{dt^2} + I_R\omega\frac{d\theta}{dt} + \mathcal{Q}\theta = 0 \tag{A.5}$$

where here $\mathcal{Q} = hT + Q$. From it the natural frequency of aircraft #2's pitch oscillation is:

$$f_2 = \sqrt{\left(\frac{I_{R2}}{I_{ay2}}\omega_2\right)^2 - \frac{2\mathcal{Q}_2}{I_{ay2}}} \tag{A.6}$$

Writing this in terms of aircraft #1 parameters and the scale factor S gives:

$$f_2 = \sqrt{\left(\frac{I_{R1}S^5}{I_{ay1}S^5}\frac{\omega_1}{\sqrt{S}}\right)^2 - \frac{2\mathcal{Q}_1 S^4}{I_{ay1}S^5}}$$

$$= \frac{1}{\sqrt{S}}\sqrt{\left(\frac{I_{R1}}{I_{ay1}}\omega_1\right)^2 - \frac{2\mathcal{Q}_1}{I_{ay1}}} \qquad = \frac{1}{\sqrt{S}} f_1$$

$$\therefore \quad \frac{f_2}{f_1} = \frac{1}{\sqrt{S}} \tag{A.7}$$

which is the same relationship as between the propproprotor speeds given by (A.3). This means that all geometrically similar aircraft can be considered to behave identically if their time scales are multiplied by ω. Replacing t in (A.5) with τ/ω, where τ is the non-dimensional time, gives

$$½I_{ay}\omega^2\frac{d^2\theta}{d\tau^2} + I_R\omega^2\frac{d\theta}{d\tau} + \mathcal{Q}\theta = 0$$

$$\rightarrow \quad \frac{d^2\theta}{d\tau^2} + \left(\frac{I_R}{½I_{ay}}\right)\frac{d\theta}{d\tau} + \left(\frac{\mathcal{Q}}{½I_{ay}\omega^2}\right)\theta = 0 \tag{A.8}$$

which remains the same regardless of aircraft size, i.e., it is scale-invariant.

A.3. Non-scalable Phenomenon

Care must be taken not to attempt extension of this invariance to phenomenon which truly do not scale. One example is wind gusts, whose velocities do not decrease as the aircraft decreases in size, and whose effects could have been included on the RHS of aircraft pitch equation (A.5) or (A.8) as an external disturbance.

The only aircraft element that a gust directly interacts with is surface area, which, together with the associated arm length, produces the pitching moment. Their product varies only as S^3, but the divisor $\frac{1}{2}I_{ay}\omega^2$ in (A.8) varies with S^4, which means that the effect of the gust becomes more prominent as the aircraft gets smaller.

Therefore, the scale-invariant equation of motion may not remain so when real life effects such as gusts are included – it is a well-known fact that smaller aircraft are more susceptible to them – but it can be a useful tool when investigating inherent dynamic behavior such as stability.

It is interesting to note, however, how the gust velocity would have to vary (with aircraft size) if the system was to remain scale-invariant. Aerodynamic drag and lift both vary with velocity squared, but the gust-moment is only deficient by a single S-term. Therefore, one can only deduce that the velocity should vary as $\sqrt{S}$. With this change it should be impossible to tell the two different-sized systems apart.

To check this, for simplicity assume that the gust travels the length of the aircraft in one unit of time, which here is taken to be the aircraft's period of oscillation (2π times the inverse of frequency given by (B.6)). Now consider a second aircraft, S times larger than the first. The corresponding time period for the gust traverse would now be larger, by $\sqrt{S}$ (according to (B.7)). But the second aircraft is S times longer. Therefore, for the second system to appear as the first, the gust velocity would have to increase by

$$\frac{S}{\sqrt{S}} = \sqrt{S}$$

APPENDIX B: NYMBUS AIRCRAFT DATA

B.1. Nymbus physical data

I_{ay}	=	0.0284	ft-lb-sec^2	(4.09 slug-in^2)
½I_θ	=	0.0150	ft-lb-sec^2	$(\frac{1}{2}I_{ay} + I_P s_\Lambda^2)$
I_{ax}	=	0.0850	ft-lb-sec^2	
½I_ϕ	=	0.0434	ft-lb-sec^2	$(\frac{1}{2}I_{ax} + I_P c_\Lambda^2)$
ζ	=	$\frac{I_\psi}{I_\phi}$	$\cong$ 1	
I_P	=	0.00180	ft-lb-sec^2	
I_R	=	0.00024	ft-lb-sec^2	
ω_0	=	520	rad/sec	(4967 RPM)
R_t	=	6.5	in.	(propeller tip radius)
T_0	=	3.25	lb.	
Q_0	=	0.35	ft-lb	(from $Q = 0.2R_tT$, 3-bl MA props)
h	=	0.06	ft.	(3/4")
b	=	1.08	ft.	(13")
Λ	=	45	deg.	

B.2. Reduced Nymbus Data

B.2.1. Pitch parameters

$$p_y = \frac{I_P}{½ I_\theta} = 0.120$$

$$q_y = \frac{hT_0 c_\Lambda + Q_0 s_\Lambda}{½ I_\theta \omega_0^2} = 0.000095$$

$$r_y = \frac{I_R}{½ I_\theta} = 0.016$$

$$k^*_{dyv} = r_y s_\Lambda c_\Lambda = 0.0080$$

B.2.2. Roll-yaw parameters

$$p_x = \frac{I_P}{½ I_\phi} = 0.042$$

$$q_x = \frac{hT_0 s_\Lambda - Q_0 c_\Lambda}{½ I_\phi \omega_0^2} = -0.0000093$$

$$r_x = \frac{I_R}{½ I_\phi} = 0.0056$$

$$\varphi = \frac{Q_0}{½ I_\phi \omega_0^2} = 0.000030$$

$$\rho = \frac{bT_0}{½ I_\phi \omega_0^2} = 0.00030$$

$$\frac{q_x}{r_x^2} = -0.297$$

$$\frac{\varphi}{r_x^2} = 0.96$$

$$\frac{\rho}{r_x^2} = 9.6$$

B.3. eVader Motor Data – used in place of unknown Nymbus motor data

The only known parameter value for the Nymbus Turnigy 50-55 drive-motor is its K_v of 400 RPM/Volt. Data and motor constants for a somewhat larger motor, the AXI 5320/34 were found in (Gabriel, 2011) and are used here instead. In that paper the electrical resistance R_a of 0.14 (ohms) is the combined resistance of the motor windings and the electronic speed controller (ESC). For reference, the motor winding resistance is 0.084 ohms (Model Motors, 2013). All of the relevant motor data then is:

$$\begin{aligned} K_v &= 220 \ \text{RPM/Volt} \\ &= 23.0 \ (\text{rad} \cdot \text{sec}^{-1})/\text{Volt} \\ K_m &= \frac{0.46 \ \text{N} \cdot \text{m}}{6\text{A}} \\ &= 0.057 \ \text{ft} \cdot \text{lb/A} \\ R_a &= 0.14 \ \text{ohms} \ (= \text{Volts/A}) \end{aligned}$$

The values for the ϑ_0-term in its various forms then are

$$\vartheta_0 = \frac{K_m}{K_v R_a}\omega_0 = 9.2 \ \text{ft} \cdot \text{lb} \qquad \text{from (5.15)}$$

$$\vartheta_{0x}^* = \frac{\vartheta_0}{\frac{1}{2} I_\phi \omega_0^2} = 0.000784 \qquad \text{from (5.23f)}$$

$$\frac{\vartheta_{0x}^*}{r_x{}^2} = 25.0$$

APPENDIX C: SIMULINK MODELS

C.1. Simulink Pitch Stability Model

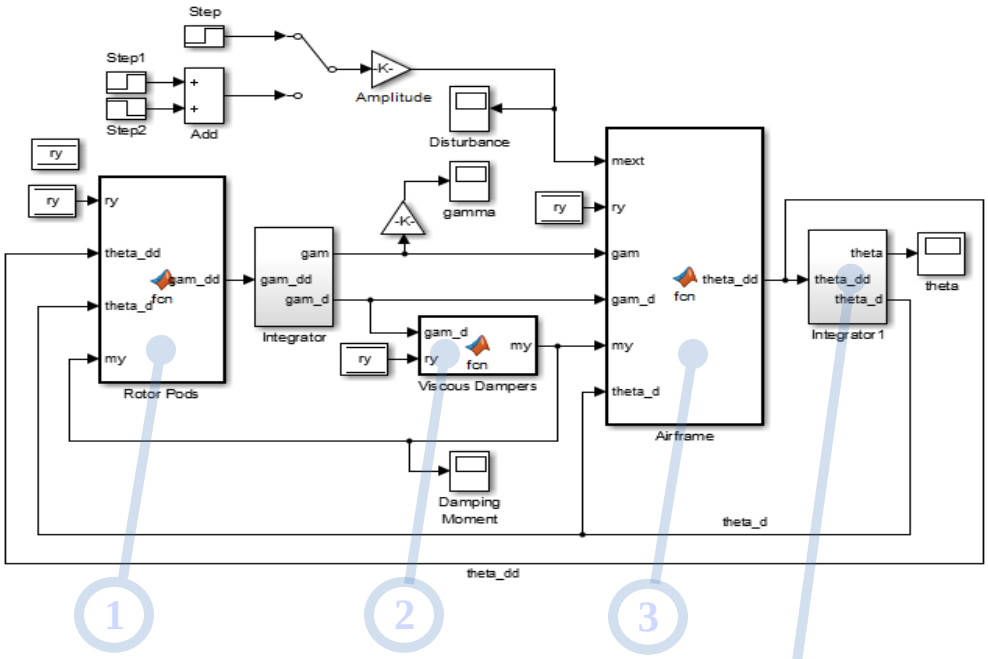

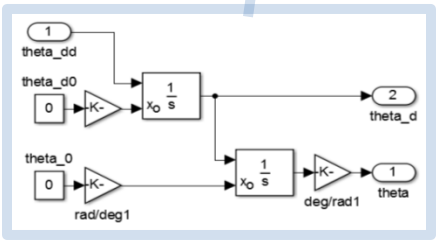

1 Rotor Pods

```
function gam_dd   = fcn(ry,theta_dd,theta_d,my)

 del=45;s=sind(del);c=cosd(del);
%ry            = Ir/(I_theta/2) = 0.0161 eVader
 py   = 0.12;% = Ip/(I_theta/2) = 0.121  eVader

%pod equation of motion:
 gam_dd = -c*theta_dd -(ry/py)*s*theta_d -my/py;
```

2 Viscous Dampers

```
function my = fcn(gam_d,ry)

kdy = ry/2;      %= kd/(I_theta*wo)
                 %= ry/2 usually
my  = kdy*gam_d;%= (damper moment)
                 %/(0.5*I_theta*wo^2)
%gam_d is in non-dim time tau =wo*t
```

3 Airframe

```
function theta_dd   = fcn(mext,ry,gam,gam_d,my,theta_d)

del   = 45;c=cosd(del);s=sind(del);
qy    = 0.00010;%(h*T*c+Q*s)/(0.5*I_theta*wo^2)=0.0000954 eVader
%mext  = Mext/(0.5*I_theta*wo^2)

%airframe eqn of motion:
theta_dd  =  ry*s*(gam_d+c*theta_d) + qy*gam + c*my + 0.5*mext;
```

The Simulink solver used was ode4 (Runge Kutta). The step size when using real time is typically 0.0001. Here, non-dimensional time is approximately 500 ($\sim\omega_0$) times larger numerically than real time, so the step size was correspondingly increased to 0.05. Pulse disturbance lengths were increased accordingly as well.

C.2. Simulink Roll-Yaw Stability Model

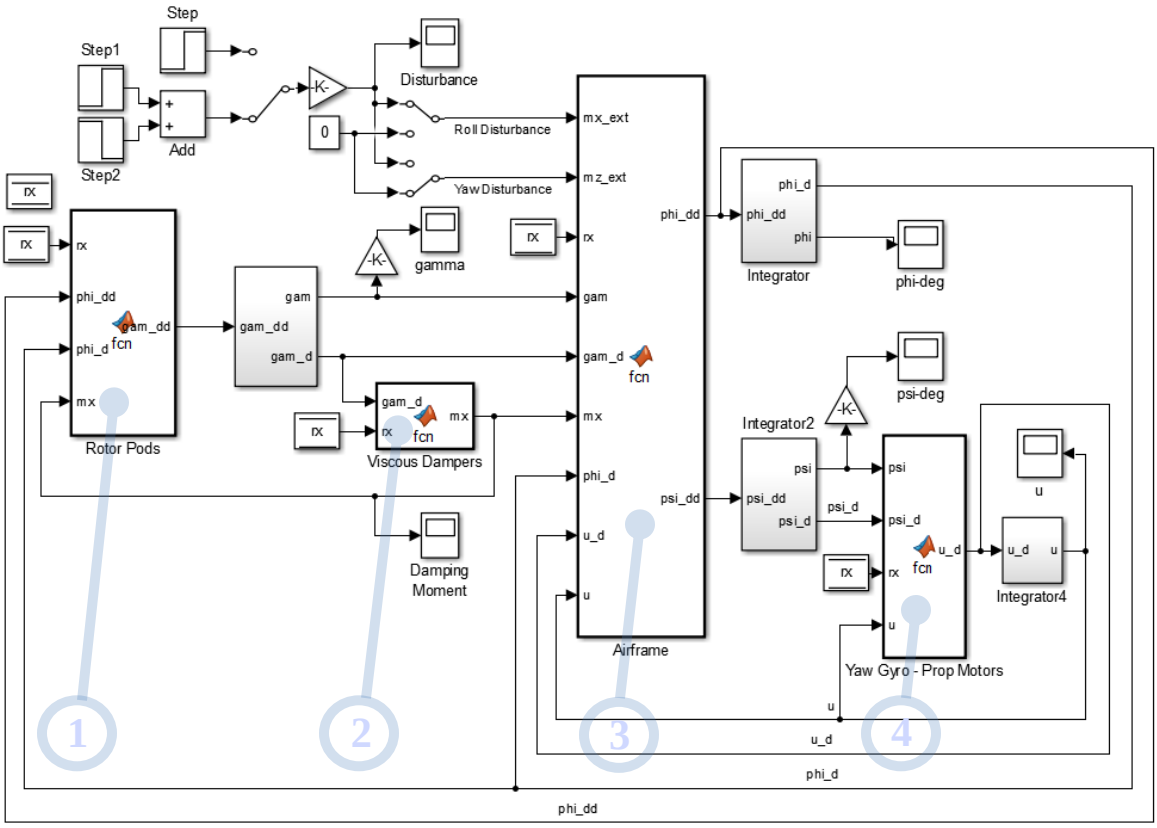

1 Rotor Pods

```
function gam_dd    = fcn(rx,phi_dd,phi_d,mx)

del=45;s=sind(del);c=cosd(del);
%rx                  = Ir/(I_phi/2)      =  0.0110  eVader;
px      =  0.10; %   = Ip/(I_phi/2)      =  0.0822  eVader

%pod equation of motion:
gam_dd  = -s*phi_dd + c*(rx/px)*phi_d - mx/px;
```

2 Viscous Dampers

```
function mx    = fcn(gam_d,rx)

kdx     =  rx/2;            %= kd/(I_phi*wo)
                            %= rx/2 usually
mx      =  kdx*gam_d;       %(damper moment)
                            %/(0.5*I_phi*wo^2)
%gam_d is in non-dimensional time tau =wo*t
```

3 Airframe

```
function [phi_dd,psi_dd]  = fcn(mx_ext,mz_ext,rx,gam,gam_d,mx,phi_d,u_d,u)
del           =  45; s=sind(del);c=cosd(del);

%                              I2    =  0.5*I_phi*wo^2
qx            = -0.0000214;    %    = (h*To*s-Qo*c)/I2  = + 0.00002 eVader
b             =  0.000221;     %    =  b*To/I2          =   0.00030 eVader
Qx            =  0.00003025;   %    =  Qo/I2            =   0.000032eVader
axz           =  0.75   ;      %    =  I_phi/I_psi      =   0.75    eVader

%Common values (Fig. 5-4):
%qx/rx^2      =  0.00002/0.011^2    =  0.16                 original eVader
%b /rx^2      =  0.00030/0.011^2    =  2.47                  original & pt1
%Qx/rx^2      =  0.00003025/0.011^2 =  0.25
%qx(h=0)      = -0.7071*0.00003025  = -0.0000214
%qx(h=0)/rx^2 = -0.0000214/0.011^2  = -0.177                      pts 1 to 4
%b(pt.2)      =  0.000221 ->b/rx^2  =  1.826              (pt. 2 mid-point)
%b(pt.3)      =  0.0001337->b/rx^2  =  1.105         neutr stab @ h=0 (pt3)
%b(pt.4)      =  0.000100 ->b/rx^2  =  0.8264

%mx_ext       =  Mex/I2   (ext roll disturb)
%mz_ext       =  Mez/I2   (ext yaw  disturb)

%airframe eqns of motion:
phi_dd        = -rx*c*(s*phi_d+gam_d) - 2*b*u + qx*gam + s*mx + mx_ext/2;
psi_dd        =(-rx*u_d + b*c*gam - 2*Qx*u + mz_ext/2)*axz;
```

4 Yaw Gyro – Prop Motors

```
function u_d   = fcn(psi,psi_d,rx,u)

del   =  45; s=sind(del); c=cosd(del);
kqpz  =  0.000025*rx;%= kqp/(0.5*I_psi*wo^2)  gyro gain, P
kqdz  =  0.025*rx;   %= kqd/(0.5*I_psi*wo)    gyro gain, D (0.25*rx, Fig 5-4)
vox   =  0.0003025;  %= vo /(0.5*I_phi*wo^2)= 0.000277   actual eVader
Qx    =  0.00003025; %= Qo /(0.5*I_phi*wo^2)= 0.00003    actual eVader

%vox/rx^2 = 0.0003025/0.011^2  = 2.5
%Qx /rx^2 = 0.00003025/0.011^2 = 0.25

axz   =  0.75;       %=  I_phi/I_psi        = 0.75       eVader
kqpx  =  kqpz/axz;
kqdx  =  kqdz/axz;

%prop-motor accel equation:
u_d   =  (-(vox+2*Qx)*u + kqdx*psi_d + kqpx*psi)/rx;
```

APPENDIX D: DETERMINING ROLL-YAW STABILITY USING MATLAB SYMBOLIC VARIABLES

D.1. Roll-Yaw Characteristic Equation

D.1.1. Program code:

```
%CHARACTERISTIC EQUATION FROM ROLL-YAW EIGENVALUE MATRIX
clear all;close all

%Symbolic Varaiable Assignment:
%tilt path angle (del) = 45 deg here.
%'non-dim0' means division by            [0.5*I_phi]
%'non-dim1' means division by            [0.5*I_phi*wo]
%'non-dim2' means division by            [0.5*I_phi*wo^2]
syms p      % non-dim0 pod inertia        Ip
syms q      % non-dim2 aerodynamic        [.7071*(h*T0-Q0)] for del=45
syms r      % non-dim0 gyroscopic         Ir
syms kd     % non-dim1 damping coeff      kd
syms kq     % non-dim1 yaw gyro gain      kq
syms v      % non-dim2 motor param        v0
syms b      % non-dim2 thrust moment      b*T0
syms c      % non-dim2 torque             Q0
syms e      % non-dim0 z-inertia ratio    0.5*I_psi
% Matrix Coefficients:
s2      =  1/sqrt(2); % = 0.7071
A       =  sym(zeros(5,5)); %
A(1,2)  =  1;
A(2,1)  = -q*s2;
A(2,2)  =  0.5*r-kd*(0.5+1/p);
A(2,3)  =  2*b*s2;
A(2,4)  =  r*s2*(0.5+1/p);
A(3,3)  = -(v+2*c)/r;
A(3,5)  =  kq/r;
A(4,1)  =  q;
A(4,2)  = -r*s2+kd*s2;
A(4,3)  = -2*b;
A(4,4)  = -0.5*r;
A(5,1)  =  b*s2/e;
A(5,3)  =  v/e;
A(5,5)  = -kq/e;
P = charpoly(A);        %Coeffs of characteristic polynomial,
det(lambda*I-A)
P = expand(P);
P = simplify(P);
simplify(P, 'Steps', 10)
simplify(P, 'Steps', 30)
simplify(P, 'Steps', 50)
syms x
P = collect(P,x)
```

D.1.2. Program Output: Symbolic coefficients of characteristic equation

z^5 : 1

z^4 : kd/2 + kq/e + (2*c)/r + v/r + (kd)/p

z^3 : (e*r^3 + 4*c*e*kd + 4*c*kq*p + 2*e*kd*v + 2*kd*kq*r + 2*c*e*kd*p +
e*kd*p*v + kd*kq*p*r + 2^(1/2)*e*p*q*r)/(2*e*p*r),

z^2 : (kq*r^3 + e*r^2*v + 4*c*kd*kq + 2*c*e*r^2 + 2*c*kd*kq*p - 2^(1/2)*e*q*r^2 +
2*2^(1/2)*c*e*p*q + 2^(1/2)*e*p*q*v + 2^(1/2)*kq*p*q*r)/(2*e*p*r),

z^1 : -(2*b^2*kq*p - 2*c*kq*r^2 + 2^(1/2)*kq*q*r^2 + 2*2^(1/2)*c*e*q*r –
2*2^(1/2)*c*kq*p*q + 2^(1/2)*e*q*r*v)/(2*e*p*r)

z^0 : (kq*(b^2 - 2^(1/2)*c*q))/(e*p)

D.2. Symbolic expression of roll-yaw Routh sums S_j

D.2.1. Program

```
s1 = sqrt(2); % = 1.4142

%Symbolic Varaiable Assignment:
%tilt path angle (del) = 45 deg here.
%'non-dim0' means division by            [0.5*I_phi]
%'non-dim1' means division by            [0.5*I_phi*wo]
%'non-dim2' means division by            [0.5*I_phi*wo^2]
syms p      % non-dim0 pod inertia       Ip
syms q      % non-dim2 aerodynamic       (h*T0-Q0)/s1 for del=45
syms r      % non-dim0 gyroscopic        Ir
syms kd     % non-dim1 damping coeff     kd
syms kq     % non-dim1 yaw gyro gain     kq
syms v      % non-dim2 motor param       v0
syms b      % non-dim2 thrust moment     b*T0
syms c      % non-dim2 torque            Q0

q  =  0;

syms b1;syms b2;syms b3;syms b4;syms b5;syms b6
b1 = (v+2*c)/r;
b2 = b1+kz;
b3 = kd*(0.5+1/p);
b4 = 0.5*(s1*q+r^2/p);
b5 = 2*c*kz/r;
b6 = 0.5*s1*q*r/p;

syms a1; syms a2; syms a3; syms a4; syms a5
a1 = b2 + b3;
a2 = b2*b3 + b4+ b5;
a3 = b2*b4 + b5*b3 - b6;
a4 =-b1*b6 + b5*b4 - kz*(b^2/r+b6);
a5 = kz*(b^2-s1*q*c)/p;

%S = a1*a2 - a3;                                %1st condition, S1 > 0
%S = a1*a2*a3 - a3^2 - a1^2*a4 + a1*a5;         %2nd condition, P2 > 0
S = a3*(a1*a4-a5)*(a1*a2-a3)-a1*(a1*a4-a5)^2-a5*(a1*a2-a3)^2;  %P3 > 0

S = expand(S);
S = simplify(S);
%S = factor(S)
simplify(S, 'Steps', 100)
```

D.2.2. Output: Routh sums S_j for special case of $q_x = 0$ ($hT_0 = Q_0$)

S_1 :

((2*c + v + kz*r)*(4*c*kd + 8*c*kz + 2*kd*v + kd^2*r + 2*kd*kz*r))/(4*r^2) + (kd*(r^3 + 2*kd*kz*r + 4*c*kd + 2*kd*v))/(2*p^2*r) + (kd*(16*c^2 + 16*c*kz*r + 8*kd*c*r + 16*c*v + 4*kz^2*r^2 + 4*kd*kz*r^2 + 8*kz*r*v + r^4 + 4*kd*r*v + 4*v^2))/(4*p*r^2)

S_2 :

(32*b^2*c^2*kz*p^3 + 16*b^2*c*kd*kz*p^3*r + 32*b^2*c*kd*kz*p^2*r + 32*b^2*c*kz^2*p^3*r + 32*b^2*c*kz*p^3*v + 16*b^2*c*kz*p^2*r^2 + 2*b^2*kd^2*kz*p^3*r^2 + 8*b^2*kd^2*kz*p^2*r^2 + 8*b^2*kd^2*kz*p*r^2 + 8*b^2*kd*kz^2*p^3*r^2 + 16*b^2*kd*kz^2*p^2*r^2 + 8*b^2*kd*kz*p^3*r*v + 4*b^2*kd*kz*p^2*r^3 + 16*b^2*kd*kz*p^2*r*v + 8*b^2*kd*kz*p*r^3 + 8*b^2*kz^3*p^3*r^2 + 16*b^2*kz^2*p^3*r*v + 8*b^2*kz^2*p^2*r^3 + 8*b^2*kz*p^3*v^2 + 8*b^2*kz*p^2*r^2*v + 16*c^3*kd^2*kz*p^3 + 64*c^3*kd^2*kz*p^2 + 64*c^3*kd^2*kz*p + 32*c^3*kd*kz^2*p^3 + 64*c^3*kd*kz^2*p^2 + 16*c^3*kd*p^2*r^2 + 32*c^3*kd*p*r^2 + 4*c^2*kd^3*kz*p^3*r + 24*c^2*kd^3*kz*p^2*r + 48*c^2*kd^3*kz*p*r + 32*c^2*kd^3*kz*r + 16*c^2*kd^2*kz^2*p^3*r + 64*c^2*kd^2*kz^2*p^2*r + 64*c^2*kd^2*kz^2*p*r + 16*c^2*kd^2*kz*p^3*v + 64*c^2*kd^2*kz*p^2*v + 64*c^2*kd^2*kz*p*v + 4*c^2*kd^2*p^2*r^3 + 16*c^2*kd^2*p*r^3 + 16*c^2*kd^2*r^3 + 16*c^2*kd*kz^3*p^3*r + 32*c^2*kd*kz^3*p^2*r + 16*c^2*kd*kz^2*p^3*v + 32*c^2*kd*kz^2*p^2*v + 8*c^2*kd*kz*p^2*r^3 + 16*c^2*kd*kz*p*r^3 + 24*c^2*kd*p^2*r^2*v + 48*c^2*kd*p*r^2*v + 2*c*kd^3*kz^2*p^3*r^2 + 12*c*kd^3*kz^2*p^2*r^2 + 24*c*kd^3*kz^2*p*r^2 + 16*c*kd^3*kz^2*r^2 + 2*c*kd^3*kz*p^3*r*v + 12*c*kd^3*kz*p^2*r*v + 24*c*kd^3*kz*p*r*v + 16*c*kd^3*kz*r*v + 4*c*kd^2*kz^3*p^3*r^2 + 16*c*kd^2*kz^3*p^2*r^2 + 16*c*kd^2*kz^3*p*r^2 + 8*c*kd^2*kz^2*p^3*r*v + 32*c*kd^2*kz^2*p^2*r*v + 32*c*kd^2*kz^2*p*r*v + 4*c*kd^2*kz*p^3*v^2 + 4*c*kd^2*kz*p^2*r^4 + 16*c*kd^2*kz*p^2*v^2 + 16*c*kd^2*kz*p*r^4 + 16*c*kd^2*kz*p*v^2 + 16*c*kd^2*kz*r^4 + 4*c*kd^2*p^2*r^3*v + 16*c*kd^2*p*r^3*v + 16*c*kd^2*r^3*v + 4*c*kd*kz^2*p^2*r^4 + 8*c*kd*kz^2*p*r^4 + 16*c*kd*kz*p^2*r^3*v + 32*c*kd*kz*p*r^3*v + 12*c*kd*p^2*r^2*v^2 + 2*c*kd*p*r^6 + 24*c*kd*p*r^2*v^2 + 4*c*kd*r^6 + kd^2*kz^2*p^2*r^5 + 4*kd^2*kz^2*p*r^5 + 4*kd^2*kz^2*r^5 + 2*kd^2*kz*p^2*r^4*v + 8*kd^2*kz*p*r^4*v + 8*kd^2*kz*r^4*v + kd^2*p^2*r^3*v^2 + 4*kd^2*p*r^3*v^2 + 4*kd^2*r^3*v^2 + 2*kd*kz^3*p^2*r^5 + 4*kd*kz^3*p*r^5 + 6*kd*kz^2*p^2*r^4*v + 12*kd*kz^2*p*r^4*v + 6*kd*kz*p^2*r^3*v^2 + kd*kz*p*r^7 + 12*kd*kz*p*r^3*v^2 +

2*kd*kz*r^7 + 2*kd*p^2*r^2*v^3 + kd*p*r^6*v + 4*kd*p*r^2*v^3 +
2*kd*r^6*v)/(8*p^3*r^3)

S_3:

-(kz*(4*c*p + 2*kd*r + 2*p*v + kd*p*r + 2*kz*p*r)*(32*b^4*c^2*kz*p^4 +
16*b^4*c*kd*kz*p^4*r + 32*b^4*c*kd*kz*p^3*r + 32*b^4*c*kz^2*p^4*r +
32*b^4*c*kz*p^4*v + 32*b^4*c*kz*p^3*r^2 + 2*b^4*kd^2*kz*p^4*r^2 +
8*b^4*kd^2*kz*p^3*r^2 + 8*b^4*kd^2*kz*p^2*r^2 + 8*b^4*kd*kz^2*p^4*r^2 +
16*b^4*kd*kz^2*p^3*r^2 + 8*b^4*kd*kz*p^4*r*v + 8*b^4*kd*kz*p^3*r^3 +
16*b^4*kd*kz*p^3*r*v + 16*b^4*kd*kz*p^2*r^3 + 8*b^4*kz^3*p^4*r^2 +
16*b^4*kz^2*p^4*r*v + 16*b^4*kz^2*p^3*r^3 + 8*b^4*kz*p^4*v^2 +
16*b^4*kz*p^3*r^2*v + 8*b^4*kz*p^2*r^4 + 16*b^2*c^3*kd^2*kz*p^4 +
64*b^2*c^3*kd^2*kz*p^3 + 64*b^2*c^3*kd^2*kz*p^2 + 16*b^2*c^3*kd^2*p^3*r +
64*b^2*c^3*kd^2*p^2*r + 64*b^2*c^3*kd^2*p*r + 32*b^2*c^3*kd*kz^2*p^4 +
64*b^2*c^3*kd*kz^2*p^3 + 64*b^2*c^3*kd*kz*p^3*r + 128*b^2*c^3*kd*kz*p^2*r +
16*b^2*c^3*kd*p^3*r^2 + 32*b^2*c^3*kd*p^2*r^2 + 64*b^2*c^3*kz^2*p^3*r -
32*b^2*c^3*kz*p^3*r^2 + 4*b^2*c^2*kd^3*kz*p^4*r + 24*b^2*c^2*kd^3*kz*p^3*r +
48*b^2*c^2*kd^3*kz*p^2*r + 32*b^2*c^2*kd^3*kz*p*r + 4*b^2*c^2*kd^3*p^3*r^2 +
24*b^2*c^2*kd^3*p^2*r^2 + 48*b^2*c^2*kd^3*p*r^2 + 32*b^2*c^2*kd^3*r^2 +
16*b^2*c^2*kd^2*kz^2*p^4*r + 64*b^2*c^2*kd^2*kz^2*p^3*r +
64*b^2*c^2*kd^2*kz^2*p^2*r + 16*b^2*c^2*kd^2*kz*p^4*v +
32*b^2*c^2*kd^2*kz*p^3*r^2 + 64*b^2*c^2*kd^2*kz*p^3*v +
128*b^2*c^2*kd^2*kz*p^2*r^2 + 64*b^2*c^2*kd^2*kz*p^2*v +
128*b^2*c^2*kd^2*kz*p*r^2 + 4*b^2*c^2*kd^2*p^3*r^3 +
24*b^2*c^2*kd^2*p^3*r*v + 16*b^2*c^2*kd^2*p^2*r^3 + 96*b^2*c^2*kd^2*p^2*r*v
+ 16*b^2*c^2*kd^2*p*r^3 + 96*b^2*c^2*kd^2*p*r*v + 16*b^2*c^2*kd*kz^3*p^4*r +
32*b^2*c^2*kd*kz^3*p^3*r + 16*b^2*c^2*kd*kz^2*p^4*v +
64*b^2*c^2*kd*kz^2*p^3*r^2 + 32*b^2*c^2*kd*kz^2*p^3*v +
128*b^2*c^2*kd*kz^2*p^2*r^2 - 8*b^2*c^2*kd*kz*p^3*r^3 +
64*b^2*c^2*kd*kz*p^3*r*v - 16*b^2*c^2*kd*kz*p^2*r^3 +
128*b^2*c^2*kd*kz*p^2*r*v + 24*b^2*c^2*kd*p^3*r^2*v + 8*b^2*c^2*kd*p^2*r^4 +
48*b^2*c^2*kd*p^2*r^2*v + 16*b^2*c^2*kd*p*r^4 + 32*b^2*c^2*kz^3*p^3*r^2 -
32*b^2*c^2*kz^2*p^3*r^3 + 32*b^2*c^2*kz^2*p^3*r*v - 32*b^2*c^2*kz*p^3*r^2*v -
16*b^2*c^2*kz*p^2*r^4 + 2*b^2*c*kd^3*kz^2*p^4*r^2 +
12*b^2*c*kd^3*kz^2*p^3*r^2 + 24*b^2*c*kd^3*kz^2*p^2*r^2 +
16*b^2*c*kd^3*kz^2*p*r^2 + 2*b^2*c*kd^3*kz*p^4*r*v + 4*b^2*c*kd^3*kz*p^3*r^3
+ 12*b^2*c*kd^3*kz*p^3*r*v + 24*b^2*c*kd^3*kz*p^2*r^3 +
24*b^2*c*kd^3*kz*p^2*r*v + 48*b^2*c*kd^3*kz*p*r^3 + 16*b^2*c*kd^3*kz*p*r*v +
32*b^2*c*kd^3*kz*r^3 + 4*b^2*c*kd^3*p^3*r^2*v + 24*b^2*c*kd^3*p^2*r^2*v +

48*b^2*c*kd^3*p*r^2*v + 32*b^2*c*kd^3*r^2*v + 4*b^2*c*kd^2*kz^3*p^4*r^2 +
16*b^2*c*kd^2*kz^3*p^3*r^2 + 16*b^2*c*kd^2*kz^3*p^2*r^2 +
8*b^2*c*kd^2*kz^2*p^4*r*v + 16*b^2*c*kd^2*kz^2*p^3*r^3 +
32*b^2*c*kd^2*kz^2*p^3*r*v + 64*b^2*c*kd^2*kz^2*p^2*r^3 +
32*b^2*c*kd^2*kz^2*p^2*r*v + 64*b^2*c*kd^2*kz^2*p*r^3 +
4*b^2*c*kd^2*kz*p^4*v^2 + 2*b^2*c*kd^2*kz*p^3*r^4 +
28*b^2*c*kd^2*kz*p^3*r^2*v + 16*b^2*c*kd^2*kz*p^3*v^2 +
8*b^2*c*kd^2*kz*p^2*r^4 + 112*b^2*c*kd^2*kz*p^2*r^2*v +
16*b^2*c*kd^2*kz*p^2*v^2 + 8*b^2*c*kd^2*kz*p*r^4 +
112*b^2*c*kd^2*kz*p*r^2*v + 4*b^2*c*kd^2*p^3*r^3*v +
12*b^2*c*kd^2*p^3*r*v^2 + 4*b^2*c*kd^2*p^2*r^5 + 16*b^2*c*kd^2*p^2*r^3*v +
48*b^2*c*kd^2*p^2*r*v^2 + 16*b^2*c*kd^2*p*r^5 + 16*b^2*c*kd^2*p*r^3*v +
48*b^2*c*kd^2*p*r*v^2 + 16*b^2*c*kd^2*r^5 + 16*b^2*c*kd*kz^3*p^3*r^3 +
32*b^2*c*kd*kz^3*p^2*r^3 - 4*b^2*c*kd*kz^2*p^3*r^4 +
32*b^2*c*kd*kz^2*p^3*r^2*v - 8*b^2*c*kd*kz^2*p^2*r^4 +
64*b^2*c*kd*kz^2*p^2*r^2*v + 8*b^2*c*kd*kz*p^3*r^3*v +
16*b^2*c*kd*kz*p^3*r*v^2 + 4*b^2*c*kd*kz*p^2*r^5 + 16*b^2*c*kd*kz*p^2*r^3*v
+ 32*b^2*c*kd*kz*p^2*r*v^2 + 8*b^2*c*kd*kz*p*r^5 + 12*b^2*c*kd*p^3*r^2*v^2 +
2*b^2*c*kd*p^2*r^6 + 8*b^2*c*kd*p^2*r^4*v + 24*b^2*c*kd*p^2*r^2*v^2 +
4*b^2*c*kd*p*r^6 + 16*b^2*c*kd*p*r^4*v - 8*b^2*c*kz^3*p^3*r^4 -
16*b^2*c*kz^2*p^3*r^3*v - 8*b^2*c*kz^2*p^2*r^5 - 8*b^2*c*kz*p^3*r^2*v^2 -
8*b^2*c*kz*p^2*r^4*v + b^2*kd^3*kz^2*p^3*r^4 + 6*b^2*kd^3*kz^2*p^2*r^4 +
12*b^2*kd^3*kz^2*p*r^4 + 8*b^2*kd^3*kz^2*r^4 + 2*b^2*kd^3*kz*p^3*r^3*v +
12*b^2*kd^3*kz*p^2*r^3*v + 24*b^2*kd^3*kz*p*r^3*v + 16*b^2*kd^3*kz*r^3*v +
b^2*kd^3*p^3*r^2*v^2 + 6*b^2*kd^3*p^2*r^2*v^2 + 12*b^2*kd^3*p*r^2*v^2 +
8*b^2*kd^3*r^2*v^2 + 2*b^2*kd^2*kz^3*p^3*r^4 + 8*b^2*kd^2*kz^3*p^2*r^4 +
8*b^2*kd^2*kz^3*p*r^4 + b^2*kd^2*kz^2*p^3*r^5 + 6*b^2*kd^2*kz^2*p^3*r^3*v +
4*b^2*kd^2*kz^2*p^2*r^5 + 24*b^2*kd^2*kz^2*p^2*r^3*v +
4*b^2*kd^2*kz^2*p*r^5 + 24*b^2*kd^2*kz^2*p*r^3*v + 2*b^2*kd^2*kz*p^3*r^4*v +
6*b^2*kd^2*kz*p^3*r^2*v^2 + 2*b^2*kd^2*kz*p^2*r^6 + 8*b^2*kd^2*kz*p^2*r^4*v
+ 24*b^2*kd^2*kz*p^2*r^2*v^2 + 8*b^2*kd^2*kz*p*r^6 + 8*b^2*kd^2*kz*p*r^4*v +
24*b^2*kd^2*kz*p*r^2*v^2 + 8*b^2*kd^2*kz*r^6 + b^2*kd^2*p^3*r^3*v^2 +
2*b^2*kd^2*p^3*r*v^3 + 2*b^2*kd^2*p^2*r^5*v + 4*b^2*kd^2*p^2*r^3*v^2 +
8*b^2*kd^2*p^2*r*v^3 + 8*b^2*kd^2*p*r^5*v + 4*b^2*kd^2*p*r^3*v^2 +
8*b^2*kd^2*p*r*v^3 + 8*b^2*kd^2*r^5*v + 2*b^2*kd*kz^3*p^3*r^5 +
4*b^2*kd*kz^3*p^2*r^5 + 6*b^2*kd*kz^2*p^3*r^4*v + 2*b^2*kd*kz^2*p^2*r^6 +
12*b^2*kd*kz^2*p^2*r^4*v + 4*b^2*kd*kz^2*p*r^6 + 6*b^2*kd*kz*p^3*r^3*v^2 +
b^2*kd*kz*p^2*r^7 + 4*b^2*kd*kz*p^2*r^5*v + 12*b^2*kd*kz*p^2*r^3*v^2 +
2*b^2*kd*kz*p*r^7 + 8*b^2*kd*kz*p*r^5*v + 2*b^2*kd*p^3*r^2*v^3 +

b^2*kd*p^2*r^6*v + 2*b^2*kd*p^2*r^4*v^2 + 4*b^2*kd*p^2*r^2*v^3 + b^2*kd*p*r^8 + 2*b^2*kd*p*r^6*v + 4*b^2*kd*p*r^4*v^2 + 2*b^2*kd*r^8 - 16*c^4*kd^2*kz*p^3*r^2 - 64*c^4*kd^2*kz*p^2*r^2 - 64*c^4*kd^2*kz*p*r^2 - 32*c^4*kd*kz^2*p^3*r^2 - 64*c^4*kd*kz^2*p^2*r^2 - 16*c^4*kd*p^2*r^4 - 32*c^4*kd*p*r^4 - 4*c^3*kd^3*kz*p^3*r^3 - 24*c^3*kd^3*kz*p^2*r^3 - 48*c^3*kd^3*kz*p*r^3 - 32*c^3*kd^3*kz*r^3 - 16*c^3*kd^2*kz^2*p^3*r^3 - 64*c^3*kd^2*kz^2*p^2*r^3 - 64*c^3*kd^2*kz^2*p*r^3 - 16*c^3*kd^2*kz*p^3*r^2*v - 64*c^3*kd^2*kz*p^2*r^2*v - 64*c^3*kd^2*kz*p*r^2*v - 4*c^3*kd^2*p^2*r^5 - 16*c^3*kd^2*p*r^5 - 16*c^3*kd^2*r^5 - 16*c^3*kd*kz^3*p^3*r^3 - 32*c^3*kd*kz^3*p^2*r^3 - 16*c^3*kd*kz^2*p^3*r^2*v - 32*c^3*kd*kz^2*p^2*r^2*v - 8*c^3*kd*kz*p^2*r^5 - 16*c^3*kd*kz*p*r^5 - 24*c^3*kd*p^2*r^4*v - 48*c^3*kd*p*r^4*v - 2*c^2*kd^3*kz^2*p^3*r^4 - 12*c^2*kd^3*kz^2*p^2*r^4 - 24*c^2*kd^3*kz^2*p*r^4 - 16*c^2*kd^3*kz^2*r^4 - 2*c^2*kd^3*kz*p^3*r^3*v - 12*c^2*kd^3*kz*p^2*r^3*v - 24*c^2*kd^3*kz*p*r^3*v - 16*c^2*kd^3*kz*r^3*v - 4*c^2*kd^2*kz^3*p^3*r^4 - 16*c^2*kd^2*kz^3*p^2*r^4 - 16*c^2*kd^2*kz^3*p*r^4 - 8*c^2*kd^2*kz^2*p^3*r^3*v - 32*c^2*kd^2*kz^2*p^2*r^3*v - 32*c^2*kd^2*kz^2*p*r^3*v - 4*c^2*kd^2*kz*p^3*r^2*v^2 - 4*c^2*kd^2*kz*p^2*r^6 - 16*c^2*kd^2*kz*p^2*r^2*v^2 - 16*c^2*kd^2*kz*p*r^6 - 16*c^2*kd^2*kz*p*r^2*v^2 - 16*c^2*kd^2*kz*r^6 - 4*c^2*kd^2*p^2*r^5*v - 16*c^2*kd^2*p*r^5*v - 16*c^2*kd^2*r^5*v - 4*c^2*kd*kz^2*p^2*r^6 - 8*c^2*kd*kz^2*p*r^6 - 16*c^2*kd*kz*p^2*r^5*v - 32*c^2*kd*kz*p*r^5*v - 12*c^2*kd*p^2*r^4*v^2 - 2*c^2*kd*p*r^8 - 24*c^2*kd*p*r^4*v^2 - 4*c^2*kd*r^8 - c*kd^2*kz^2*p^2*r^7 - 4*c*kd^2*kz^2*p*r^7 - 4*c*kd^2*kz^2*r^7 - 2*c*kd^2*kz*p^2*r^6*v - 8*c*kd^2*kz*p*r^6*v - 8*c*kd^2*kz*r^6*v - c*kd^2*p^2*r^5*v^2 - 4*c*kd^2*p*r^5*v^2 - 4*c*kd^2*r^5*v^2 - 2*c*kd*kz^3*p^2*r^7 - 4*c*kd*kz^3*p*r^7 - 6*c*kd*kz^2*p^2*r^6*v - 12*c*kd*kz^2*p*r^6*v - 6*c*kd*kz*p^2*r^5*v^2 - c*kd*kz*p*r^9 - 12*c*kd*kz*p*r^5*v^2 - 2*c*kd*kz*r^9 - 2*c*kd*p^2*r^4*v^3 - c*kd*p*r^8*v - 4*c*kd*p*r^4*v^3 - 2*c*kd*r^8*v))/(16*p^5*r^5)

D.2.3. Output: S_3 for $q_x = 0$ and $b = 0$

(c*kd*kz*(p + 2)*(2*c + v + kz*r)*(4*c*p + 2*kd*r + 2*p*v + kd*p*r + 2*kz*p*r)*(8*c^2*kd*kz*p^2 + 16*c^2*kd*kz*p + 16*c^2*kz^2*p^2 + 8*c^2*p*r^2 + 2*c*kd^2*kz*p^2*r + 8*c*kd^2*kz*p*r + 8*c*kd^2*kz*r + 4*c*kd*kz^2*p^2*r + 8*c*kd*kz^2*p*r + 4*c*kd*kz*p^2*v + 8*c*kd*kz*p*v + 2*c*kd*p*r^3 + 4*c*kd*r^3 + 8*c*p*r^2*v + kd*kz*p*r^4 + 2*kd*kz*r^4 + kd*p*r^3*v + 2*kd*r^3*v + 2*kz^2*p*r^4 + 4*kz*p*r^3*v + 2*p*r^2*v^2 + r^6))/(16*p^5*r^3)

D.3. Generating and plotting two-dimensional stability curves

D.3.1. Stability boundary function program

```
s1 = sqrt(2); % = 1.4142
%Symbolic Variable Assignment:
%'non-dim0' means division by          [0.5*I_phi]
%'non-dim1' means division by          [0.5*I_phi*wo]
%'non-dim2' means division by          [0.5*I_phi*wo^2]
syms p      % non-dim0 pod inertia      Ip
syms q      % non-dim2 aerodynamic      (h*T0-Q0)/s1      for del=45 deg
syms r      % non-dim0 gyroscopic       Ir
syms kd     % non-dim1 damping coeff    kd
syms kz     % non-dim1 yaw gyro gain    kq        (here,div by I_psi*wo)
syms v      % non-dim2 motor param      v0
syms b      % non-dim2 thrust moment    b*T0
syms c      % non-dim2 torque           Q0
syms X      % plotting abscissa, =      q/r^2
syms Y      % plotting ordinate, =      b/r^2

%Numerical and relationship assignments:
kd = 0.5*r;
kz = 0.5*kd;
p  = 0.10;
c  = 0.25*r^2;
v  = 2.5*r^2;
%q and b put in terms of plotting variables X and Y:
q = X*r^2;
b = Y*r^2;

%Characteristic eqn coefficients:
syms b1;syms b2;syms b3;syms b4;syms b5;syms b6
b1 = (v+2*c)/r;
b2 = b1+kz;
b3 = kd*(0.5+1/p);
b4 = 0.5*(s1*q+r^2/p);
b5 = 2*c*kz/r;
b6 = 0.5*s1*q*r/p;
syms a1; syms a2; syms a3; syms a4; syms a5
a1 = b2 + b3;                          %%
a2 = b2*b3 + b4+ b5;                   %%
a3 = b2*b4 + b5*b3 - b6;               %%
a4 =-b1*b6 + b5*b4 - kz*(b^2/r+b6);    %%
a5 = kz*(b^2-s1*q*c)/p;

%Routh sums:
%S = a1*a2 - a3;                                  %1st condition, S1 > 0
%S = a1*a2*a3 - a3^2 - a1^2*a4 + a1*a5;           %2nd condition, S2 > 0
S = a3*(a1*a4-a5)*(a1*a2-a3)-a1*(a1*a4-a5)^2-a5*(a1*a2-a3)^2;  %3rd, S3

%Output:
```

```
S = expand(S);
S = simplify(S);
simplify(S, 'Steps', 100)
```

D.3.2. Stability boundary functions:

These sample symbolic expressions (using $k_{qz}^{*} = 0.5 \cdot k_{dx}^{*}$) were copied and pasted from the MATLAB command window after execution of the program in D.3.1 Setting each expression equal to zero gives the stability boundary curve Y vs. X (where $X \equiv \frac{q_x}{r_x{}^2}$ and $Y \equiv \frac{bT_0}{r_x{}^2}$) for the corresponding coefficient or sum:

a_1: (17*r)/2 (→ always positive)

a_2: (r^2*(8*2^(1/2)*X + 355))/16 (→ positive when X > - 31.4)

a_3: -(r^3*(108*X - 541))/32 (→ positive when X < + 3.5)

a_4: -(r^4*(4*Y^2 + 259*2^(1/2)*X - 10))/16 (→ see plot in E4.2.2)

a_5: -(5*r^5*(- 4*Y^2 + X))/8 (→ see plot in E4.2.2)

S_1: (r^3*(122*2^(1/2)*X + 2747))/16 (→ positive when X > -15.9)

S_2: (r^6*(- 26352*X^2 + 365414*2^(1/2)*X + 20128*Y^2 + 1463007))/512

S_3: -(17*r^11*(- 6864208*2^(1/2)*X^3 + 50752*X^2*Y^2 + 185533972*X^2 + 14679128*2^(1/2)*X*Y^2 + 355788173*2^(1/2)*X + 175232*Y^4 + 83556748*Y^2 - 14630070))/16384

After their r^<i> terms have been extracted, these expressions are inserted into the function plot program of D.3.3 for subsequent plotting of the stability boundaries in D.3.4.

D.3.3. Function Plot Program:

```
syms X Y

% %p  = 0.1
% %kd = 0.5*r
% %c  = 0.25*r^2
% %v  = 2.5*r^2

%a4:
%kz =  0.5*kd
f = -4*Y^2 - 259*2^(1/2)*X + 10;
figure; h=ezplot(f,[-0.5,0.5,0,3]);set(h,'Color',[0 0 0])

%kz =  5.0*kd
f = -4*Y^2 - 43*2^(1/2)*X + 10;
hold all; h=ezplot(f,[-0.5,0.5,0,3]); set(h,'Color',[0 0 0])


%a5: (boundary loc indep of kz)
f = 4*Y^2 - 2^(1/2)*X;
figure; h=ezplot(f,[-0.5,0.5,0,3]);set(h,'Color',[0 0 0])


%S2:
%kz = 0.5*kd
f = - 26352*X^2 + 365414*2^(1/2)*X + 20128*Y^2 + 1463007;
figure; h=ezplot(f,[-8,0,0,3]); set(h,'Color',[0 0 0])

%kz = 5*kd
f = - 17568*X^2 + 1292972*2^(1/2)*X + 285520*Y^2 + 5621385;
hold all; h=ezplot(f,[-8,0,0,3]); set(h,'Color',[0 0 0])


%S3:
%kz = 0.5*kd
f = 6864208*2^(1/2)*X^3 - 50752*X^2*Y^2 - 185533972*X^2 ...
  - 14679128*2^(1/2)*X*Y^2 - 355788173*2^(1/2)*X - 175232*Y^4 ...
  - 83556748*Y^2 + 14630070;
figure; h=ezplot(f,[-0.5,0.5,0,3]); set(h,'Color',[0 0 0])

%kz = 5*kd
f = 794464*2^(1/2)*X^3 - 85888*X^2*Y^2 - 103975432*X^2 ...
  - 31975328*2^(1/2)*X*Y^2 - 167353175*2^(1/2)*X - 2204480*Y^4 ...
  - 265376980*Y^2 + 56213850;
hold all; h=ezplot(f,[-0.5,0.5,0,3]); set(h,'Color',[0 0 0])
```

D.3.4. Stability boundary plots:

Below are the stability boundary plots based on the characteristic coefficient and Routh sum outputs of Appendix D3.3 and plotted by the MATLAB boundary plot program of Appendix E4.2.1. ($X \equiv \frac{q_x}{{r_x}^2}$ and $Y \equiv \frac{bT_0}{{r_x}^2}$)

The number beside each boundary curve is yaw-gyro gain k_{qz}^* value relative to the damping coefficient k_{dx}^* . For example, $k_{qz}^* = 5k_{dx}^*$. Boundary location for a_5 coefficient is independent of k_{qz}^* (and also of prop-motor coefficient ϑ_{0x}^*). S_1 is not shown since it is always positive for X > -15.9

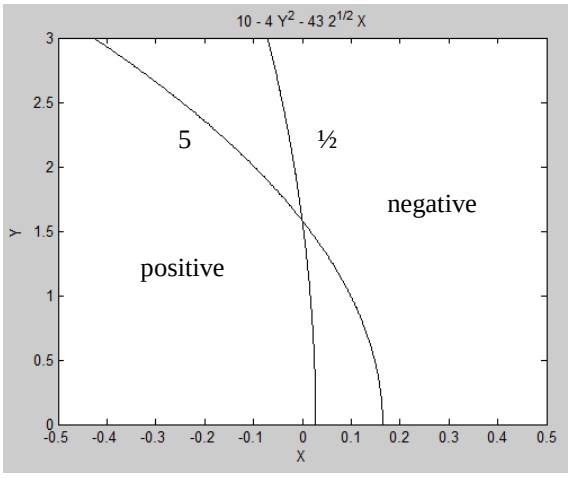

a_4

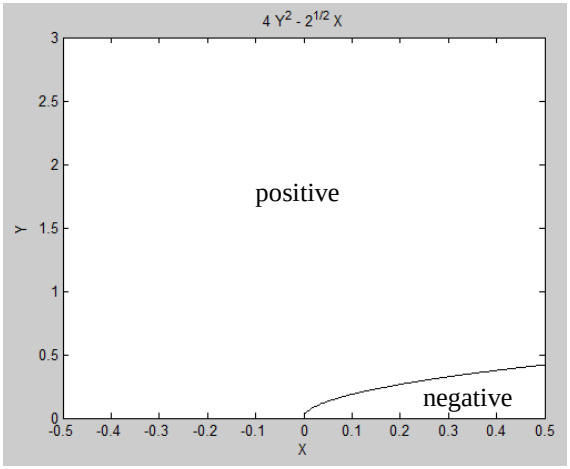

a_5

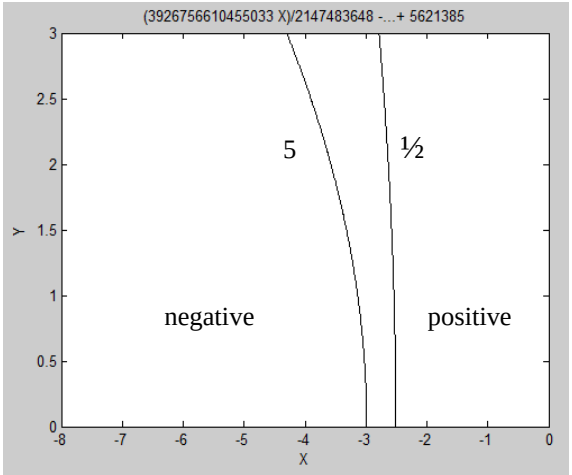

S_2

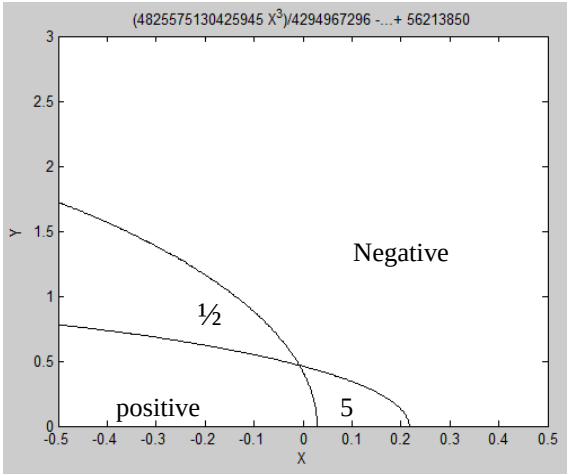

S_3